AWARD NUMBER: W81XWH-19-1-0540

TITLE:
Ex Vivo-Generated Autologous iTregs as a Cell-Based Therapy for Acquired Aplastic Anemia

PRINCIPAL INVESTIGATOR: Lisa M. Minter, PhD

CONTRACTING ORGANIZATION: University of Massachusetts Amherst, Amherst, MA

REPORT DATE: August 2020

TYPE OF REPORT: Annual Report

PREPARED FOR: U.S. Army Medical Research and Materiel Command
Fort Detrick, Maryland 21702-5012

REPORT DOCUMENTATION PAGE

Form Approved OMB No. 0704-0188

PLEASE DO NOT RETURN YOUR FORM TO THE ABOVE ADDRESS.

1. REPORT DATE *(DD-MM-YYYY*	**2. REPORT TYPE**	**3. DATES COVERED** *(From - To)*
August 2020	Annual	01Aug2019-31Jul2020

4. TITLE AND SUBTITLE

Ex vivo-generated iTregs as a cell-based therapy for acquired Aplastic Anemia

5a. CONTRACT NUMBER
W81XWH-19-1-0540

5b. GRANT NUMBER
BM180090

5c. PROGRAM ELEMENT NUMBER
N/A

6. AUTHOR(S)

Lisa M. Minter, PhD

5d. PROJECT NUMBER
0011340318

5e. TASK NUMBER
N/A

5f. WORK UNIT NUMBER
N/A

7. PERFORMING ORGANIZATION NAME(S) AND ADDRESS(ES)

University of Massachusetts Amherst
661 N. Pleasant St.
470Integrated Sciences Building
Amherst, MA 01003

8. PERFORMING ORGANIZATION REPORT NUMBER

Unique Identifier: 153926712

9. SPONSORING/MONITORING AGENCY NAME(S) AND ADDRESS(ES)

University of Massachusetts Amherst
Office of Grant and Contract Administration
Office of Grants and Contracts, Commonwealth Avenue
Amherst, MA 01003

10. SPONSOR/MONITOR'S ACRONYM(S)
OGCA

11. SPONSOR/MONITOR'S REPORT NUMBER(S)
N/A

12. DISTRIBUTION/AVAILABILITY STATEMENT

Approved for public release; distribution is unlimited

13. SUPPLEMENTARY NOTES

None

14. ABSTRACT

Patients with acquired AA show aberrant activation of T effector (Teff) cells and naturally occurring regulatory T cells (nTregs) that are frequently dysfunctional. Immunosuppressive therapies that use Tregs, rely on isolating and expanding rare populations of nTregs from the circulating blood. nTregs with *in vitro* suppressive functions have been successfully expanded from AA patients. However, the extremely low numbers of circulating nTregs, coupled with the long process (up to several months) of expanding these cells in culture, underscores the practical challenges of this approach for AA patients. We have developed a means of using synthetic cell-penetrating peptide mimics (CPPM) to deliver functional antibodies into human CD4 T cells. Delivering anti-pPKCθ into CD4 T cells generates iTregs (anti-pPKCθ-iTregs) with superior *in vitro* and *in vivo* suppressive functions and, in proof-of-concept experiments, provide a significant survival benefit in a humanized mouse model of AA, when given at the time of BMF induction. We determined that inhibiting pPKCθ or the protein repair methyltransferase, PCMT1, alters the cellular location and protein-protein association of key iTreg-destabilizing proteins, increases surface expression of the immune-inhibitory receptor, PD1, and increases demethylation the *FOXP3* promoter. We conclude that these alterations contribute to a more suppressive iTreg phenotype in vitro and in vivo.

15. SUBJECT TERMS

Aplastic anemia; immune-mediated bone marrow failure; intracellular antibody delivery; CPPM; ex vivo-generated iTregs; PKCθ; PCMT1; cell-based therapy

16. SECURITY CLASSIFICATION OF:			17. LIMITATION OF ABSTRACT	18. NUMBER OF PAGES	19a. NAME OF RESPONSIBLE PERSON
a. REPORT	b. ABSTRACT	c. THIS PAGE			USAMRMC
U	U	U	UU	87	19b. TELEPHONE NUMBER *(Include area code)*

TABLE OF CONTENTS

1. INTRODUCTION:

Patients with acquired AA show aberrant activation of T effector (Teff) cells and naturally occurring regulatory T cells (nTregs) that are frequently dysfunctional. Immunosuppressive therapies that use Tregs, rely on isolating and expanding rare populations of nTregs from the circulating blood. nTregs with *in vitro* suppressive functions have been successfully expanded from AA patients. However, the extremely low numbers of circulating nTregs, coupled with the long process (up to several months) of expanding these cells in culture, underscores the practical challenges of this approach for AA patients. We have developed a means of using synthetic cell-penetrating peptide mimics (CPPM) to deliver functional antibodies into human CD4 T cells. Delivering anti-pPKCθ into CD4 T cells generates iTregs (anti-pPKCθ-iTregs) with superior *in vitro* and *in vivo* suppressive functions and, in proof-of-concept experiments, provide a significant survival benefit in a humanized mouse model of AA, when given at the time of BMF induction. We will investigate CPPM-antibody delivery as a therapeutic option to generate AA patient-derived iTregs, *ex vivo*. We will use a humanized mouse model of AA, optimized in our lab, *to test the hypothesis that combined delivery of anti-pPKCθ and anti-PCMT1 will generate iTregs with a "locked" phenotype*, refractory to the inhibitory actions of CsA *in vitro* and *in vivo*, and ask whether administering autologous anti-pPKCθ+anti-PCMT1-iTregs attenuates disease in a patient "avatar" model of AA.

2. KEYWORDS:

Aplastic anemia; immune-mediated bone marrow failure; intracellular antibody delivery; CPPM; ex vivo-generated iTregs; PKCθ; PCMT1; cell-based therapy

3. ACCOMPLISHMENTS:

What were the major goals of the project?

Specific Aim 1 **Determine how inhibiting pPKCθ, PCMT1, or both, using CPPM:antibody delivery influences *ex vivo* iTreg differentiation**	**Time line**	**Site 1**	**Site 2**
Major Task 1 **Generate and characterize iTregs differentiated *ex vivo* under various conditions of CPPM:antibody delivery, with or without the addition of CsA or Rapamycin**			
Subtask 1 HRPO approval for use of commercially available healthy donor PBMCs	1-4	Dr. Minter 100% COMPLETED	
Subtask 2 Local IACUC approval	1-3	Dr. Minter 100% COMPLETED	
Subtask 3 ACURO protocol approval	4-6	Dr. Minter 100% COMPLETED	
Subtask 4 Produce synthetic cell penetrating peptide mimics (CPPMs)	1-18		Dr. Tew ONGOING (75% COMPLETE)
Subtask 5 Complex CPPMs with: IgG, anti-pPKCθ, anti-PCMT1	1-18		Dr. Tew ONGOING (75% COMPLETE)
Subtask 6 Differentiate iTregs in the presence of: CPPM:IgG, CPPM:anti-pPKCθ, CPPM:anti-PCMT1	3-9	Dr. Minter 100% COMPLETED	
Subtask 7 Characterize iTregs differentiated in the presence of: CPPM:IgG, CPPM:anti-pPKCθ, CPPM:anti-PCMT1 (phenotype; suppression assays; FOXP3 methylation)	3-9	Dr. Minter ONGOING 90% COMPLETE	
Subtask 8 Characterize iTregs differentiated in the presence of: CPPM:IgG, CPPM:anti-pPKCθ, CPPM:anti-PCMT1 with CsA or Rapamycin added (phenotype; suppression assays; FOXP3 methylation)	3-12	Dr. Minter ONGOING 50% COMPLETE	

1. Major activities:

a) Obtaining DOD HRPO, DOD ACURO, and University of Massachusetts Amherst IACUC approval for protocols involving the use of human PBMCs and research animals.

b) Confirming continuity of data acquisition by new personnel which included troubleshooting experiments, providing additional training to personnel, titrating reagents.

b) Synthesizing cell penetrating peptide mimics (CPPMs) for use in antibody delivery experiments.

d) Evaluating the effects of differentiating iTregs in the presence of CPPM-IgG, CPPM-anti-pPKCθ, CPPM-anti-PCMT1, combined CPPM-anti-pPKCθ+CPPM-anti-PCMT1

e) Evaluating the suppressive capacity of iTregs differentiated in the presence of CPPM-IgG, CPPM-anti-pPKCθ, CPPM-anti-PCMT1, combined CPPM-anti-pPKCθ+CPPM-anti-PCMT1

f) Evaluating the effects of differentiating iTregs in the presence of CPPM-IgG, CPPM-anti-pPKCθ, CPPM-anti-PCMT1, combined CPPM-anti-pPKCθ+CPPM-anti-PCMT1, when exposed to low (40 ng/ml) and high (400 ng/ml) doses of cyclosporine A.

2. Specific objectives:

a) Acquire all pertinent agency approval.

b) Use CPPMs to deliver anti-pPKCθ, anti-PCMT1, and combined anti-pPKCθ-anti-PCMT1 to iTregs to determine if there are differences in iTreg differentiation, based on antibody target or combination antibody delivery, compared to delivering irrelevant IgG.

c) Use CPPMs to deliver anti-pPKCθ, anti-PCMT1, and combined anti-pPKCθ-anti-PCMT1 to iTregs to determine if there are differences in iTreg suppressive function, based on antibody target or combination antibody delivery, compared to delivering irrelevant IgG.

d) Use CPPMs to deliver anti-pPKCθ, anti-PCMT1, and combined anti-pPKCθ-anti-PCMT1 to iTregs to in the presence of cyclosporine or rapamycin, to determine how these immunosuppressive drugs affect iTreg differentiation *in vitro*, compared to delivering irrelevant IgG.

3. Significant Results (**See Appendix A for data, methodologies, and discussion**):

a) CPPMs were synthesized and purified. Newly synthesized CPPMs provided reproducible antibody delivery and were utilized for *in vitro* iTreg differentiation experiments (Figure 1).

b) Differentiating CD4 T cells with anti-pPKCθ, anti-PCMT1, and combination anti-pPKCθ+anti-PCMT1 generates higher percentages of CD4+CD25+CD127-FOXP3+ iTregs and greater FOXP3+ expression than those differentiated with an irrelevant IgG (Figure 2).

c) Differentiating CD4 T cells with anti-pPKCθ, anti-PCMT1, and combination anti-pPKCθ+anti-PCMT1 increases their suppressive capacity, compared to those differentiated with an irrelevant IgG (Figure 3).

d) Preliminary data show low dose (40ng/ml) CsA exposure enhances iTreg differentiation. Using CPPM to deliver anti-pPKCθ or antiPCMT1 protects FOXP3 expression in iTregs exposed to high doses of (400 ng/ml) CsA (Figure 4).

4. Other Achievements:

a) Completed acquisition of final data sets.

b) Wrote, submitted, revised, and published two manuscripts in a high impact, translational journal (*Molecular Therapy*, impact factor 8.402). Funding from this grant was acknowledged in both articles (Appendices C, D, E).

What opportunities for training and professional development has the project provided?

Nothing to report.

How were the results disseminated to communities of interest?

Data collection for two manuscripts were completed, manuscripts were finalized and submitted for peer review, manuscripts were accepted and published in the journal, *Molecular Therapy* (Ozay et al., Mol. Therapy, May 2020; Ozay et al., Mol. Therapy, June, 2020).

Plans are in place to:
1. Complete *in vitro* characterization of iTregs differentiated with CPPM:anti-pPCKθ, CPPM:anti-PCMT1, CPPM:anti-pPKCθ+anti-PCMT1 (acquire final data sets for suppression assays and FOXP3 promoter methylation).
2. Train additional personnel to assist in the completion of remaining *in vivo* experiments.
3. Characterize patient iTregs differentiated in the presence of CPPM:anti-pPCKθ, CPPM:anti-PCMT1, or CPPM:anti-pPKCθ+anti-PCMT1.
4. Perform *in vivo* therapeutic experiments using a humanized model of bone marrow failure.
5. Create avatar mice and treat with patient iTregs.

4. IMPACT:

What was the impact on the development of the principal discipline(s) of the project?

With funding from this grant, we extended preliminary studies and acquired final data sets that describe the therapeutic potential of converting circulating blood cells, easily obtained from the peripheral blood, into suppressive cells that can control the inflammation associated with immune-mediated bone marrow failure. We documented how we can convert these cells, using a new technology for transporting a neutralizing antibody across the cell membrane, then culturing the cells in a manner that induces them to adopt suppressive functions. We further described how our approach changes the location of several surface-bound and intracellular proteins, which we believe lies at the heart of their increased suppressive capacity. We used an animal model of acute graft-versus-host disease, which causes bone marrow failure, to further demonstrate the efficacy of using these cells to reduce disease severity and increase survival in proof-of-concept experiments. Funding from this grant also allowed us to perform mechanistic studies that provided additional insight as how cells are changed in an epigenetic fashion, following intracellular antibody delivery. We identified a kinase, Protein Kinase C theta, and a protein repair methyltransferase, PCMT1, as being key regulators of cellular genetic stability, by influencing the degree to which the promoter of *FOXP3*, the master transcriptional regulator of regulatory T cells, is methylated. Collectively, funding through this grant has enabled us to optimize and describe the mechanism of action of a potential highly suppressive cell-based therapy that may prove useful in the treatment of immune-mediated bone marrow failure diseases.

What was the impact on other disciplines?

While we feel the progress made during our first year of funding will be beneficial to the field of immune-mediated bone marrow failure directly, we also feel our findings have the potential to indirectly benefit patients with immune-mediated bone marrow failure for whom a bone marrow/hematopoietic stem cell transplant is a curative treatment. However, this procedure frequently leads to an adverse condition known as graft-versus-host disease, in which donor immune cells that are present in the bone marrow/hematopoietic stem cell graft expand and attack the recipient's (host) tissues and organs. Our data suggest that using our new technology for transporting a neutralizing antibody across the cell membrane, then culturing donor cells in a manner that induces them to adopt suppressive functions, has the potential to greatly reduce or prevent destructive graft-versus-host responses, when these cells are given at the same time as a bone marrow/hematopoietic stem cell transplant. Furthermore, we predict that using our approach to generate ex vivo immune-suppressive regulatory T cells may provide therapeutic relief to other autoimmune diseases such as inflammatory bowel disease, rheumatoid arthritis, or multiple sclerosis.

What was the impact on technology transfer?

Nothing to report.

What was the impact on society beyond science and technology?

5. CHANGES/PROBLEMS:

Changes in approach and reasons for change

There are no significant changes in the proposal to report.

Actual or anticipated problems or delays and actions or plans to resolve them

Actual problems:
Two unexpected issues were encountered during the first year of funding for this DOD grant that delayed reaching some experimental goals laid out in the SOW: i) unforeseen technical difficulties that required extensive troubleshooting and re-optimizing experimental protocols; and ii) a major disruption to research progress caused by the Covid-19 pandemic. At this time, these issues have been fully resolved and research progress is gaining momentum.

Actions to resolve them:
1. We provided additional training to new personnel to facilitate “hand-off” of established protocols.
2. We have been successful in trouble shooting the differentiation protocols to identify the source of technical difficulties.
3. We have titrated vital cell dyes to prevent toxicity after cell-loading.
4. We have optimized hPBMC stimulation.
5. We are assessing individual hPBMC donor responses to stimulation to optimize suppression assays.
6. We will reserve samples of specific hPBMC lot numbers to maintain continuity of results.

Changes that had a significant impact on expenditures

Changes that negatively impacted expenditures:
1. Summer salary to pay for 1 graduate student ($9,099) was incurred during this reporting period. The graduate student assisted in trouble shooting differentiation, proliferation, and suppression assays.

Significant changes in use or care of human subjects, vertebrate animals, biohazards, and/or select agents

Significant changes in use or care of human subjects

Nothing to report. IACUC protocol (#1867) was approved on January 3, 2019.

Significant changes in use or care of vertebrate animals

Nothing to report.

Significant changes in use of biohazards and/or select agents

Nothing to report.

6. PRODUCTS:

- **Publications, conference papers, and presentations**

Journal publications.

PUBLISHED:

1. E. Ilker Ozay, Sudarvili Shanthalingam, Heather L. Sherman, Joe A. Torres, Barbara A. Osborne, Gregory N. Tew, Lisa M. Minter. Cell-penetrating anti-Protein Kinase C theta antibodies act intracellularly to generate stable, highly suppressive regulatory T cells. *Molecular Therapy* (2020). https://doi.org/1016/j.mthe.2020.05.020.

Acknowledgement of federal support: YES

2. E. Ilker Ozay, Sudarvili Shanthalingam, Joe A. Torres, Barbara A. Osborne, Gregory N. Tew, Lisa M. Minter. (2020) Protein Kinase C theta modulates PCMT1 through hnRNPL to regulate FOXP3 stability in regulatory T cells. *Molecular Therapy* (2020). https://doi.org/10.1016/j.ymthe.2020.06.012

Acknowledgement of federal support: YES

Books or other non-periodical, one-time publications.

Nothing to report.

Other publications, conference papers and presentations.

Nothing to report.

- **Website(s) or other Internet site(s)**

Nothing to report.

- **Technologies or techniques**

Nothing to report.

- **Inventions, patent applications, and/or licenses**

Nothing to report.

- **Other Products**

Nothing to report.

7. PARTICIPANTS & OTHER COLLABORATING ORGANIZATIONS

What individuals have worked on the project?

Name:	Lisa M. Minter
Project Role:	Principal Investigator
Researcher Identifier (ORCID ID)	0000-0002-1728-6389
Nearest person month worked:	2 (summer)
Contribution to Project:	Dr. Minter analyzed final data sets, wrote two manuscripts that were peer reviewed and published, oversees current experimental plan, execution, data acquisition, analysis, and troubleshooting.
Name:	Gregory N. Tew
Project Role:	Co-Principal Investigator
Researcher Identifier (ORCID ID)	0000-0003-3277-7925
Nearest person month worked:	1 (summer)
Contribution to Project:	Dr. Tew provided critical input on the two published manuscripts and supervised synthesis of cell-penetrating peptide mimic polymers used for antibody delivery.
Name:	Sudarvili Shanthalingam
Project Role:	(Senior Research Fellow)
Researcher Identifier (ORCID ID)	N/A
Nearest person month worked:	12 months
Contribution to Project:	Dr. Shanthalingam assisted in the collection of final data sets needed for manuscripts, provided critical input on manuscripts, performed in vitro differentiation experiments, aided in trouble shooting proliferation and suppression assays.
Name:	Christopher Hango
Project Role:	Graduate Student Research Assistant
Researcher Identifier (ORCID ID)	0000-0002-4066-9548
Nearest person month worked:	5 months
Contribution to Project:	Mr. Hango assisted in the synthesis of cell-penetrating peptide mimic polymers used for antibody delivery.
Name:	Heather Sherman
Project Role:	Graduate Student Research Assistant
Researcher Identifier (ORCID ID)	0000-0002-8303-426X
Nearest person month worked:	2 months
Contribution to Project:	Ms. Sherman assisted in troubleshooting the differentiation, proliferation and suppression assays.

Has there been a change in the active other support of the PD/PI(s) or senior/key personnel since the last reporting period?

The PI is listed as a co-PI on a second, recently funded DOD grant (CDMRP Log Number: PR190722, PI TEW) to explore the use of *ex vivo*-generated iTregs as a cell-based treatment for Irritable Bowel Disease. The PI will decrease compensation from the current DOD BMF grant from 1.8 mo summer salary to 1.5 mo summer salary, to comply with University of Massachusetts Amherst summer salary policy, but the PI will not decrease actual effort on the current funded project.

What other organizations were involved as partners?

Nothing to report.

8. SPECIAL REPORTING REQUIREMENTS

COLLABORATIVE AWARDS:

QUAD CHARTS:

9. APPENDICES:

Appendix A: REVISED Significant Results

Appendix B: REVISED Quad Chart Progress Report
Ex Vivo-Generated Autologous iTregs as a Cell-Based Therapy for Acquired Aplastic Anemia

Appendix C: Journal article
E. Ilker Ozay, Sudarvili Shanthalingam, Heather L. Sherman, Joe A. Torres, Barbara A. Osborne, Gregory N. Tew, Lisa M. Minter. Cell-penetrating anti-Protein Kinase C theta antibodies act intracellularly to generate stable, highly suppressive regulatory T cells. Molecular Therapy (2020). https://doi.org/1016/j.mthe.2020.05.020.

Appendix D: Journal article

E. Ilker Ozay, Sudarvili Shanthalingam, Joe A. Torres, Barbara A. Osborne, Gregory N. Tew, Lisa M. Minter. (2020) Protein Kinase C theta modulates PCMT1 through hnRNPL to regulate FOXP3 stability in regulatory T cells. Molecular Therapy (2020). https://doi.org/10.1016/j.ymthe.2020.06.012

Appendix E: Supplemental Information for journal article

E. Ilker Ozay, Sudarvili Shanthalingam, Joe A. Torres, Barbara A. Osborne, Gregory N. Tew, Lisa M. Minter. (2020) Protein Kinase C theta modulates PCMT1 through hnRNPL to regulate FOXP3 stability in regulatory T cells. Molecular Therapy (2020). https://doi.org/10.1016/j.ymthe.2020.06.012 - SUPPLEMENTAL INFORMATION

REVISED Annual and Technical Report (8/1/2019 – 7/31/2020) MINTER – W81XWH1910540

APPENDIX A

SIGNIFICANT RESULTS

Figure 1

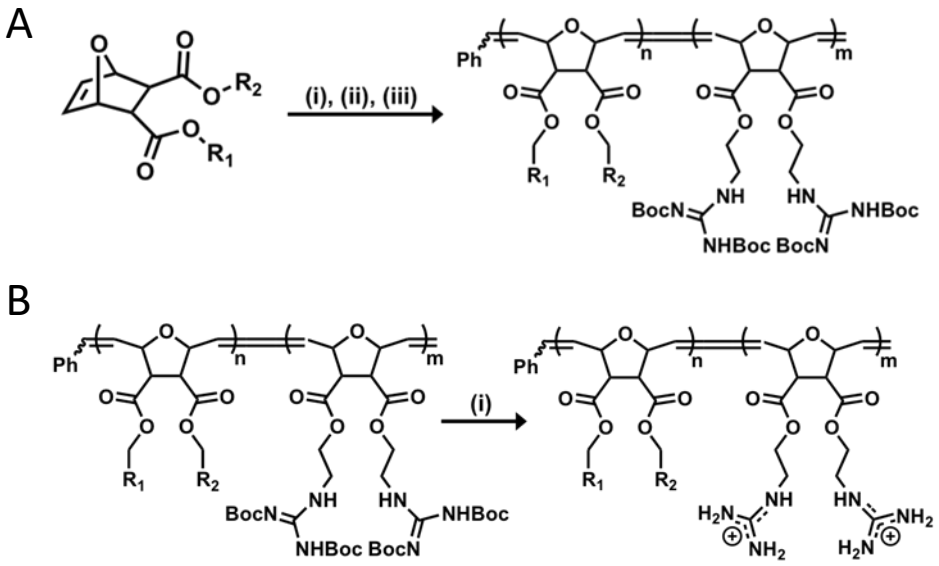

Figure 1. Cell penetrating peptide mimics can be synthesized and purified.
(**A**) Synthesis of Boc-protected block copolymer Cell penetrating peptide mimics (CPPMs). i) Dichloro-di(3-bromopyridino)-*N,N'*-Dimesitylenoimidazolino-Ru=CHPh (G3) catalyst, CH_2Cl_2, RT, 10 min; ii) dG, CH_2Cl_2, RT, 90 min; iii) Ethyl vinyl ether, RT, overnight. (**B**) Deprotection of boc-protected block copolymers to yield CPPMs. i) TFA/CH_2Cl_2 (1:1), RT, overnight. CPPMs further purified by dialysis using membranes with molecular weight cut-off: 100-500 g/mol.

Methodology:
General Block Copolymer Synthesis: 5, 10, 13, 20, or 40 equivalents of hydrophobic monomers; 5, 7, 10, 20, or 40 equivalents of diguanidine monomer; and one equivalent of G3 catalyst were each dissolved in 1.5 mL of dry CH_2Cl_2 in separate schlenk flasks. The catalyst flask also contained a small stir bar. Three freeze-pump-thaw cycles were used to remove air. Following the third thaw step, the flasks containing monomers were kept under nitrogen while the catalyst flask remained under vacuum. Monomer was then cannulated into the vigorously stirring catalyst solution at RT. After 10 min, a small aliquot (0.05 mL) was removed from the solution for analysis and then diguanidine monomer was cannulated into the vigorously stirring polymerization solution at RT reaction. After 1.5 hr, the polymerizations were quenched with 3 mL of ethyl vinyl ether and allowed to stir overnight at RT. The solutions were then transferred to 20 mL scintillation vials and concentrated using rotary evaporation. Polymers were then dissolved in a minimal amount of THF and added drop-wise to 100 mL of cold, stirring pentanes to precipitate the polymers. After 5-10 minutes of stirring, polymers were isolated using vacuum filtration with fine sinter funnels. Polymers were dried under vacuum at RT overnight.
Boc-group Deprotection: Polymers were dissolved in 2 mL of CH_2Cl_2 and allowed to stir. 2 mL of TFA was then added drop-wise to the solution and allowed to stir overnight at RT. Excess TFA was removed by azeotropic distillation with MeOH. During this process, 5-7 mL of MeOH was added and then the sample was concentrated using rotary evaporation. This process was repeated 7-9 times to ensure complete TFA removal. Following this, samples were dissolved in a water/MeOH mixture, transferred to Biotech CE dialysis tubing membranes with a MWCO 100-500 g/mol and dialyzed against RO water until the conductivity of the water remained < 0.2 µS (2-3 days on dialysis). Polymers were then aqueous filtered and isolated from water by lyophilization.

Figure 2

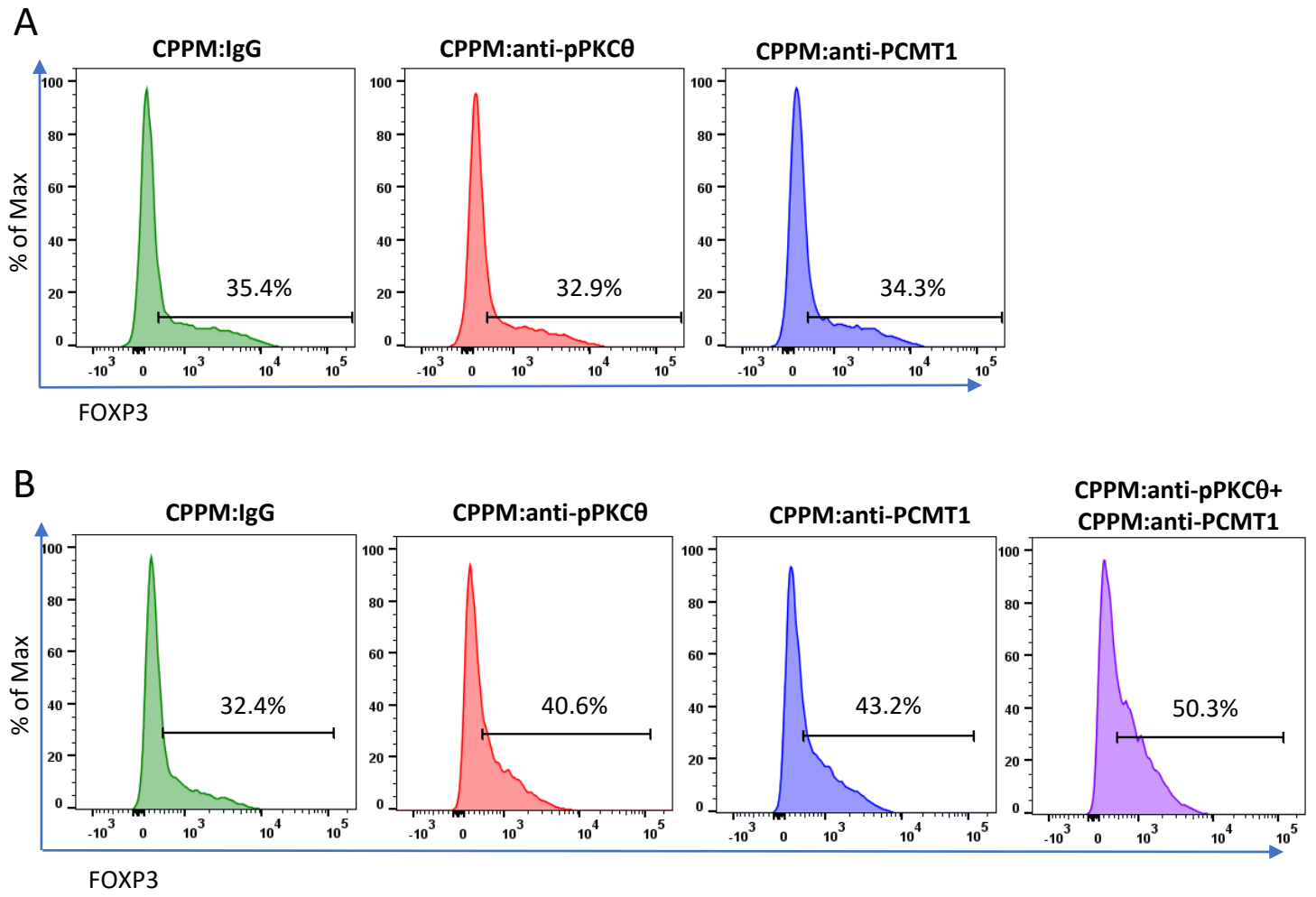
A
CPPM:IgG
CPPM:anti-pPKCθ
CPPM:anti-PCMT1
% of Max
35.4%
32.9%
34.3%
FOXP3
B
CPPM:IgG
CPPM:anti-pPKCθ
CPPM:anti-PCMT1
CPPM:anti-pPKCθ+
CPPM:anti-PCMT1
% of Max
32.4%
40.6%
43.2%
50.3%
FOXP3
C
CPPM:IgG
CPPM:anti-pPKCθ
CPPM:anti-PCMT1
CPPM:anti-pPKCθ+
CPPM:anti-PCMT1
% of Max
54.6%
66.2%
70.6%
70.5%
FOXP3

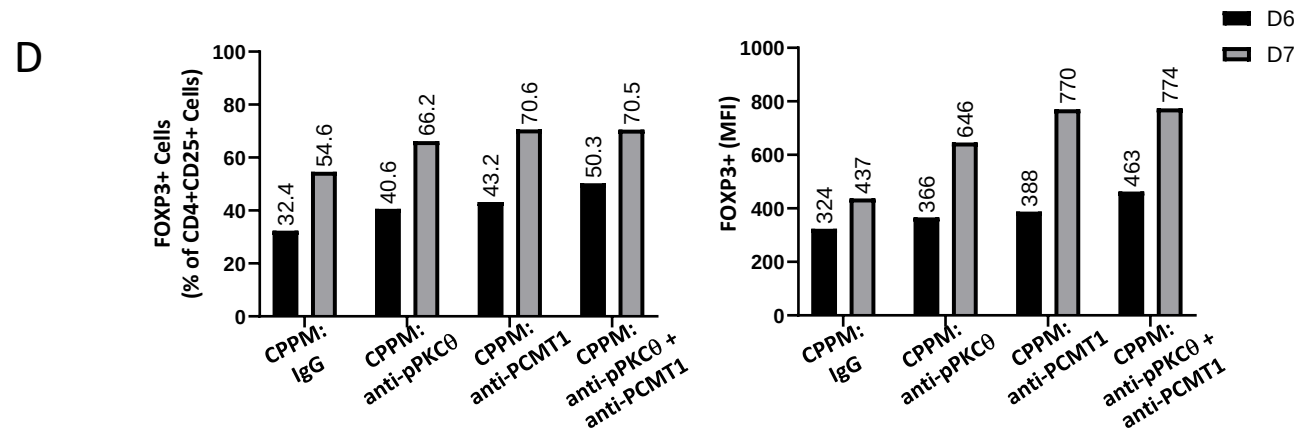
D
D6
D7
FOXP3+ Cells
(% of CD4+CD25+ Cells)
32.4
54.6
40.6
66.2
43.2
70.6
50.3
70.5
CPPM: IgG
CPPM: anti-pPKCθ
CPPM: anti-PCMT1
CPPM: anti-pPKCθ + anti-PCMT1
FOXP3+ (MFI)
324
437
366
646
388
770
463
774

Figure 2

Figure 2. CD4 T cells differentiated in the presence of CPPM:antibodies generate highly suppressive iTregs
Human CD4 T cells were isolated from Peripheral Blood Mononuclear Cells (PBMCs) obtained form healthy donors. Cells were pre-incubated with CPPM:IgG (green tracings), CPPM:anti-pPKCq (red tracings); CPPM:anti-PCMT1 (blue tracings), or both CPPM:anti-pPKCq and anti-PCMT1 (purple tracings). Cells were cultured for (**A**) five, (**B**) six, or (**C**) seven days before staining and analyzing by flow cytometry. Data for day 6 and day 7 cultures are are presented graphically as (**D**) percent CD4+CD25+CD127-FOXP3+ cells (left panel) and FOXP3 median fluorescent intensity (MFI; right panel). Data are representative of two independent replicates that showed similar results.

Methodology:
Human PBMCs were thawed, plated in media, and rested overnight at 37C. On the next day CD4 T cells were positively isolated using anti-CD4 magnetic beads. CPPM was complexed for 30 minutes at RT with antibodies (anti-pPKCθ, anti-PCMT1, or both), or with isotype control Rabbit IgG, at a molar ratio of 40:1 (1μM $P_{13}D_5$ CPPM + 25nM antibody). CPPM:antibody complexes (100μl) were added drop-wise to CD4 T cells (1x10^6/900μl media) and incubated for 4 hours at 37C, after which cells were washed twice with ice cold heparin (20U/ml) to remove surface-bound CPPM:antibody complexes. CD4 T cells (1x10^6/ml media) were plated in iTreg differentiation media in single wells of a 12-well plate that had been pre-coated with anti-human CD3 (5μg/ml) plus anti-human CD28 (2.5μg/ml). Cells were split 1:1 on day 4 and fresh iTreg media was added to plates. iTregs were harvested on day 5, day 6, or day 7 of culture and analyzed by flow cytometry. Zombie-BV421 was used for live/dead staining; iTreg cells were stained for CD4 (FITC), CD25 (PECy7), CD127 (AF700) and FoxP3 (PE). Compensation was set using fluorescent beads and negative gates were set using a Fluorescence Minus One (FMO) approach.

Figure 3

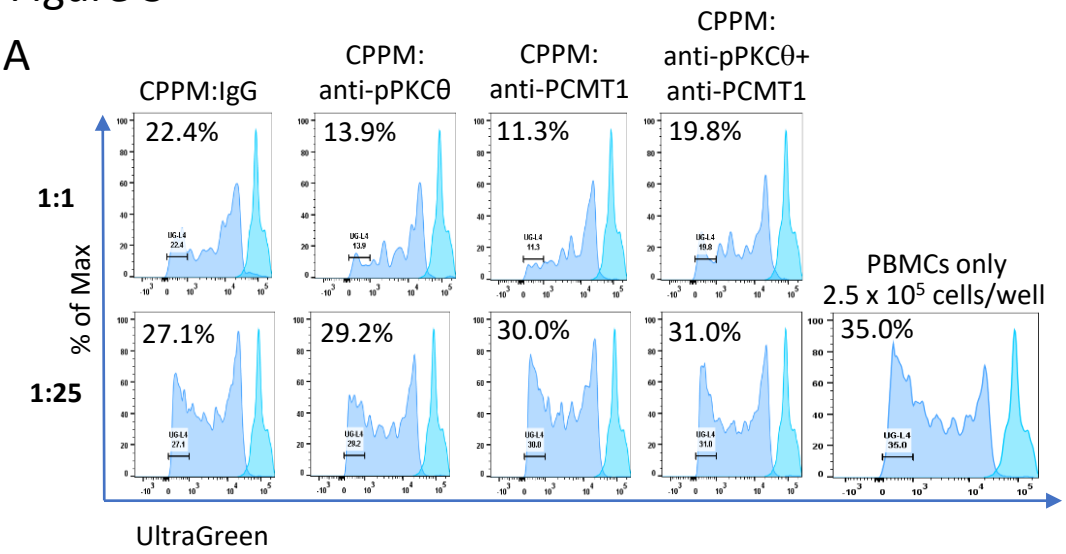
A
CPPM:IgG
CPPM: anti-pPKCθ
CPPM: anti-PCMT1
CPPM: anti-pPKCθ+ anti-PCMT1
1:1
1:25
% of Max
22.4%
13.9%
11.3%
19.8%
27.1%
29.2%
30.0%
31.0%
PBMCs only
2.5 x 10^5 cells/well
35.0%
UltraGreen

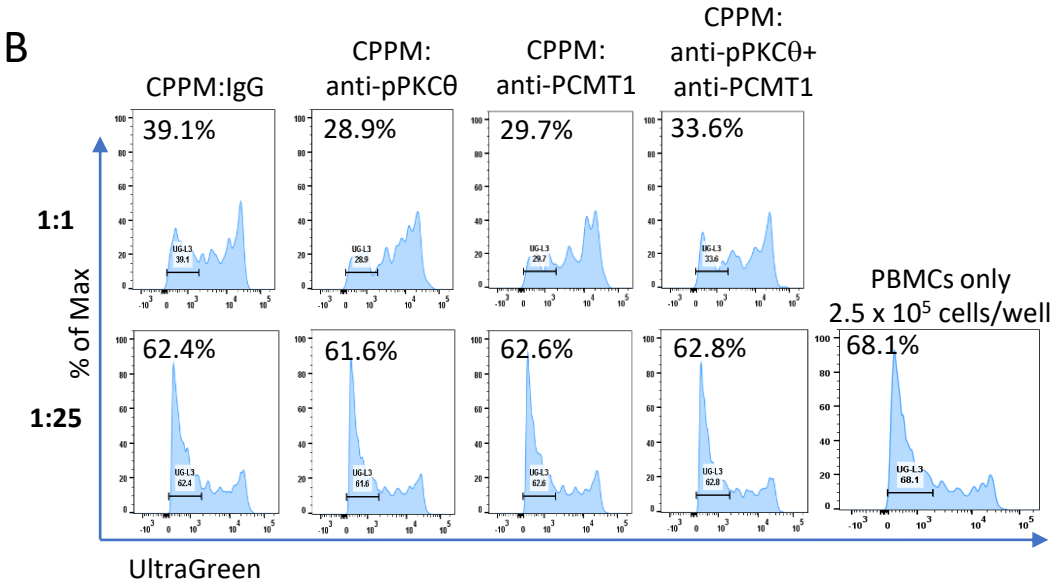
B
CPPM:IgG
CPPM: anti-pPKCθ
CPPM: anti-PCMT1
CPPM: anti-pPKCθ+ anti-PCMT1
1:1
1:25
% of Max
39.1%
28.9%
29.7%
33.6%
62.4%
61.6%
62.6%
62.8%
PBMCs only
2.5 x 10^5 cells/well
68.1%
UltraGreen

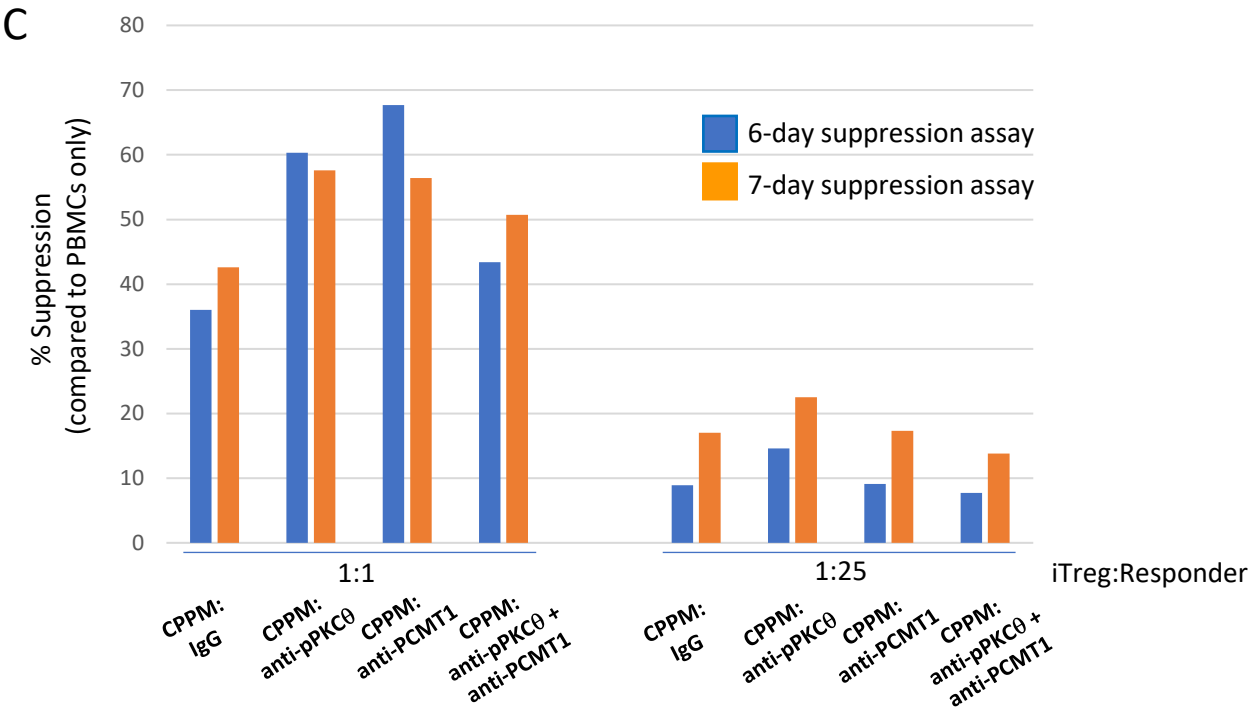
C
% Suppression (compared to PBMCs only)
80
70
60
50
40
30
20
10
0
6-day suppression assay
7-day suppression assay
1:1
1:25
iTreg:Responder
CPPM: IgG
CPPM: anti-pPKCθ
CPPM: anti-PCMT1
CPPM: anti-pPKCθ + anti-PCMT1

Figure 3

Figure 3. CD4 T cells differentiated in the presence of CPPM:antibodies generate highly suppressive iTregs
Human CD4 T cells were isolated from Peripheral Blood Mononuclear Cells (PBMCs) obtained form healthy donors. Cells were pre-incubated with CPPM:IgG), CPPM:anti-pPKCθ, CPPM:anti-PCMT1, or both CPPM:anti-pPKCθ and anti-PCMT1. iTregs were cultured for seven days, labeled with Red650 cell tracker dye, then mixed with (responder) PBMCs that were stimulated with soluble anti-human CD3 plus anti-human CD28, cross-linked with anti-mouse IgG, and labeled with UltraGreen cell tracker dye. Cells were mixed at ratios of 1:1 and 1:25 iTreg:Responder cells, respectively, and co-cultured for (**A**) 6 or (**B**) 7 days. At the indicated timepoints cells were harvested and Ultragreen fluorescence was measured by flow cytometry. Percent of highly proliferated cells are indicated by inserts in the flow cytometry histograms.(**C**) Percent suppression was calculated and is presented graphically for co-cultures of cells mixed at ratios of 1:1 and 1:25 iTreg:Responder cells, respectively. Data are representative of at two independent replicates that showed similar results.

Methodology:
iTreg differentiation: Human PBMCs were thawed, plated in media, and rested overnight at 37C. On the next day CD4 T cells were positively isolated using anti-CD4 magnetic beads. CPPM was complexed for 30 minutes at RT with antibodies (anti-pPKCθ, anti-PCMT1, or both), or with isotype control Rabbit IgG, at a molar ratio of 40:1 (1μM $P_{13}D_5$ CPPM + 25nM antibody). CPPM:antibody complexes (100μl) were added drop-wise to CD4 T cells ($1x10^6$/900μl media) and incubated for 4 hours at 37C, after which cells were washed twice with ice cold heparin (20U/ml) to remove surface-bound CPPM:antibody complexes. CD4 T cells ($1x10^6$/ml media) were plated in iTreg differentiation media in single wells of a 12-well plate that had been pre-coated with anti-human CD3 (5μg/ml) plus anti-human CD28 (2.5μg/ml). Cells were split 1:1 on day 4 and fresh iTreg media was added to plates. iTregs were harvested on day 7 of culture. A small sample was analyzed by flow cytometry to confirm iTreg differentiation. Zombie-BV421 was used for live/dead staining; iTreg cells were stained for CD4 (FITC), CD25 (PECy7), CD127 (AF700) and FoxP3 (PE). Compensation was set using fluorescent beads and negative gates were set using a Fluorescence Minus One (FMO) approach.

Suppression Assay: Human PBMCs (responder cells) were thawed and rested for 1 hour at 37C. Cells were stimulated with soluble anti-human CD3 (5μg/ml) plus anti-human CD28 (2.5 μg/ml) at 4C for 30 minutes. Antibodies were cross-linked by incubating cells with anti-mouse IgG (5μg/ml) at RT for 30 minutes. Cells were washed once in cold PBS and labeled for 37C for 20 minutes with CytoTell UltraGreen cell tracker dye ($1x10^6$ cells were stained 1:1500 in 1500μl of PBS). Cells were washed twice with cold PBS and counted. iTregs, differentiated as described above, were labeled for 20 minutes at 37C with CytoTell Red 650 cell tracker dye ($1x10^6$ cells were stained 1:2000 in 2000μl of PBS). Cells were washed Cells were washed twice with cold PBS and counted. Responder cells were added to wells of a 48-well plate; then iTregs were added at the following ratios:

1:1 = $1.25 x10^5 : 1.25 x10^5$
1:25 = $0.10 x10^5 : 2.5 x10^5$

A proliferation control well was set up containing $2.5x10^5$ cells, but no iTregs; 30U/ml IL-2 was addd to all wells at time of plating. After 6 and 7 days of co-culture, cells were harvested and cell proliferation was measured by flow cytometry as determined by loss of UltraGreen fluorescence. Persent suppression was calculated as follows:

$$100 - \left[\frac{\text{Percent proliferation in treated sample}}{\text{Percent proliferation in untreated control}} \right] \times 100$$

Figure 4

A

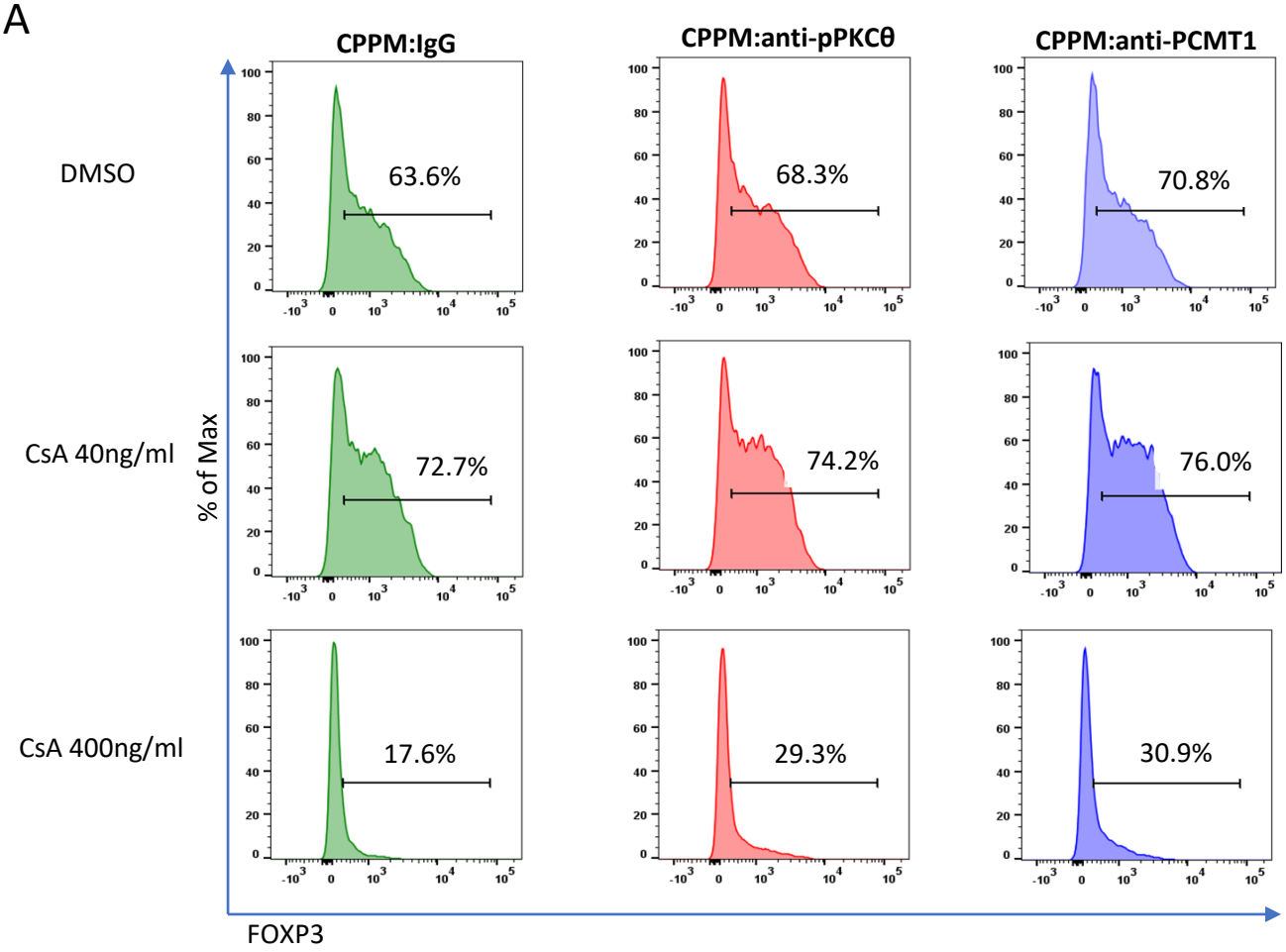
CPPM:IgG
CPPM:anti-pPKCθ
CPPM:anti-PCMT1
DMSO
CsA 40ng/ml
CsA 400ng/ml
63.6%
68.3%
70.8%
72.7%
74.2%
76.0%
17.6%
29.3%
30.9%
% of Max
FOXP3

B

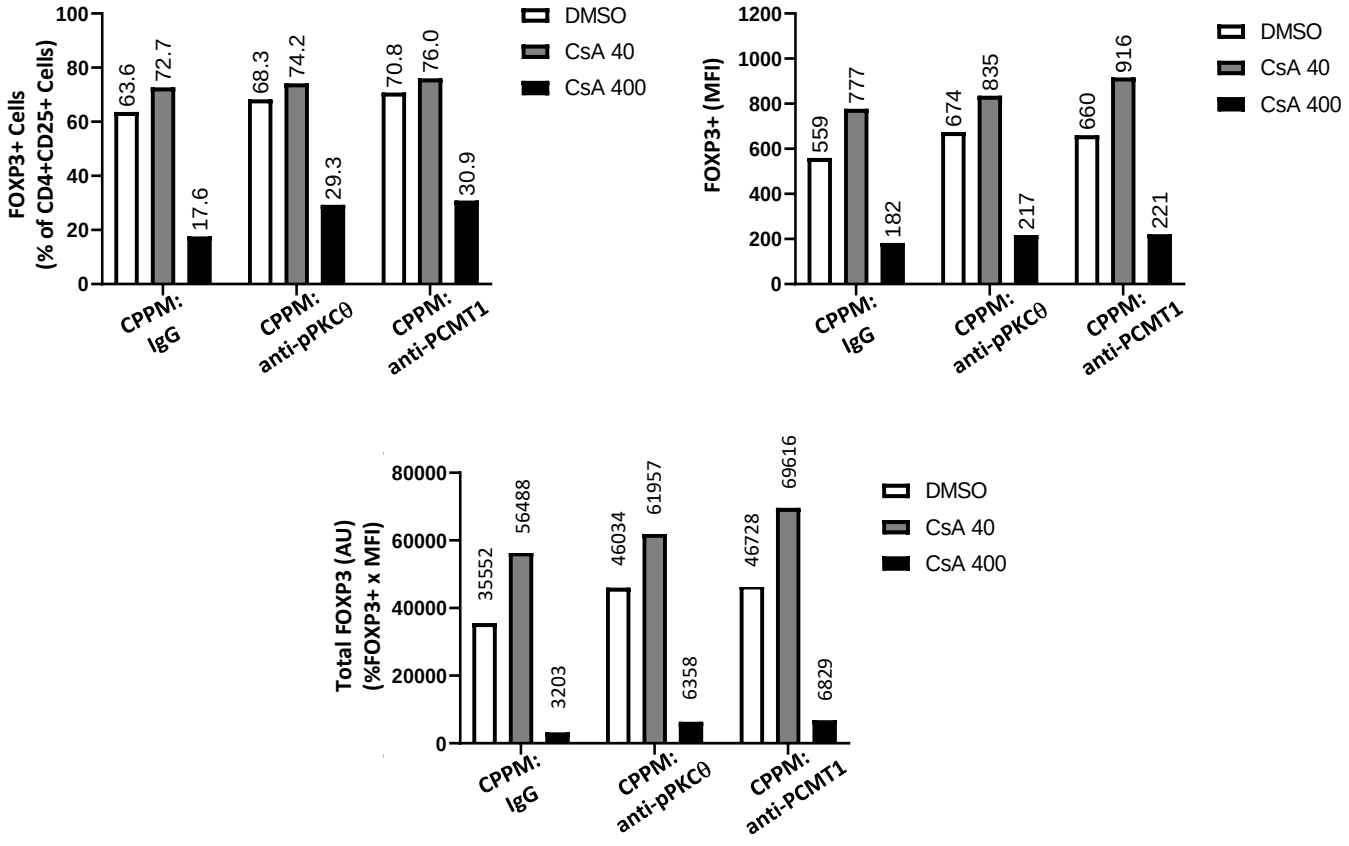
FOXP3+ Cells (% of CD4+CD25+ Cells)
63.6
72.7
17.6
68.3
74.2
29.3
70.8
76.0
30.9
DMSO
CsA 40
CsA 400
CPPM: IgG
CPPM: anti-pPKCθ
CPPM: anti-PCMT1
FOXP3+ (MFI)
559
777
182
674
835
217
660
916
221
Total FOXP3 (AU) (%FOXP3+ x MFI)
35552
56488
3203
46034
61957
6358
46728
69616
6829

Figure 4

Figure 4. Low dose cyclosporine A enhances iTreg differentiation, while CPPM:antibody delivery protects FOXP3 expression in iTregs exposed to high dose cyclosporine A.

(**A**) Human CD4 T cells were isolated from Peripheral Blood Mononuclear Cells (PBMCs) obtained form healthy donors. Cells were pre-incubated with CPPM:IgG (green tracings), CPPM:anti-pPKCθ (red tracings), or CPPM:anti-PCMT1 (blue tracings). Cells were cultured 7 days in iTreg differentiation media to which DMSO (1μl/ml; top row), low dose cyclosporine A (40ng/ml; middle row) or high dose cyclosporine A (400ng/ml; bottom row) was added. On day 4 cells were split 1:1 and fresh iTreg media containing DMSO or cyclosporine A, as described, was added. After 7 days, cells were harvested, stained, and analyzed by flow cytometry. Percent CD4+CD25+CD127-FOXP3+ cells (panel inserts) are shown. (**B**) Data are represented graphically as percent CD4+CD25+CD127-FOXP3+ cells cultured under various treatment condition (upper left-hand graph); as FOXP3 median fluorescent intensity (MFI) of cells cultured under various treatment condition (upper right-hand graph); and as total FOXP3 expressed in AU and calculated by multiplying %FOXP3+ x MFI (lower center graph) for cells cultured under various treatment conditions. Data are representative of two independent replicates that showed similar results.

Methodology:

Human PBMCs were thawed, plated in media, and rested overnight at 37C. On the next day CD4 T cells were positively isolated using anti-CD4 magnetic beads. CPPM was complexed for 30 minutes at RT with antibodies (anti-pPKCθ, anti-PCMT1, or both), or with isotype control Rabbit IgG, at a molar ratio of 40:1 (1μM $P_{13}D_5$ CPPM + 25nM antibody). CPPM:antibody complexes (100μl) were added drop-wise to CD4 T cells ($1x10^6$/900μl media) and incubated for 4 hours at 37C, after which cells were washed twice with ice cold heparin (20U/ml) to remove surface-bound CPPM:antibody complexes. CD4 T cells ($1x10^6$/ml media) were plated in iTreg differentiation media containing DMSO (1μl/ml as vehicle control), 40ng/ml cyclosporine A, or 400ng/ml cyclosporine A in single wells of a 12-well plate that had been pre-coated with anti-human CD3 (5μg/ml) plus anti-human CD28 (2.5μg/ml). Cells were split 1:1 on day 4 and fresh iTreg media with DMSO, 40 ng/ml cyclosporine A, or 400ng/ml cyclosporine A was added to plates. iTregs were harvested on day 7 of culture and analyzed by flow cytometry. Zombie-BV421 was used for live/dead staining; iTreg cells were stained for CD4 (FITC), CD25 (PECy7), CD127 (AF700) and FoxP3 (PE). Compensation was set using fluorescent beads and negative gates were set using a Fluorescence Minus One (FMO) approach.

Discussion of stated goals not met

Two unexpected issues were encountered during the first year of funding for this DOD grant that delayed reaching some experimental goals laid out in the SOW: i) unforeseen technical difficulties that required extensive troubleshooting and re-optimizing experimental protocols; and ii) a major disruption to research progress caused by the Covid-19 pandemic. At this time, these issues have been fully resolved and research progress is gaining momentum.

Regarding the first issue, in the hand off of our experimental protocols to new personnel, we encountered some unanticipated reproducibility issues. To address these, we provided additional training for new personnel, re-titrated experimental reagents, and re-optimized experimental conditions. As a result, we now have robust protocols that are producing compelling and reproducible data. Specifically, we have increased the length of time we are differentiating human iTregs, and find that culturing human CD4 T cells for 7 days under iTreg polarizing conditions shows that CPPM:anti-PCMT1-treated iTregs exhibit the highest level of FOXP3 expression (Figure 2), show the greatest suppressive capacity, especially at a 1:1 ratio of iTregs:responder cells (Figure 3), and provide a high level of FOXP3 protection when iTregs are differentiated in the presence of high levels (400ng/ml) of cyclosporine A (Figure 4). Given that many patients with aplastic anemia receive cyclosporine A as an immunosuppressive therapy, this is an important preliminary observation.

No doubt, having to re-optimize our protocols caused a delay in our research progress; however, we also lost considerable time due to the Covid-19 pandemic. Our university halted all laboratory research from mid-March through July, effectively shuttering our lab for 4-plus months – a full one third of research time during our first year of funding! This set-back, which was completely beyond our control, had the greatest impact on our ability to complete our data sets once all experimental optimizing had been implemented. Thus, we have for Major Task 1, subtask 7 is approximately 90% completed, while subtask 8 is approximately 50% completed. Due to the convergence of unexpected issues, we had to delay beginning Major Task 3, subtask 2 - which requires the use of archived patient samples. Due to their precious nature, we did not want to use these samples experimentally before all protocols were fully optimized.

Barring any future lab shutdowns due to the present surge in Covid-19 infections we expect to be able to complete our data sets and catch up quickly with the timeline laid out in our SOW.

Ex Vivo-Generated Autologous iTregs as a Cell-Based Therapy for Acquired Aplastic Anemia

(W81XWH1910540)

PI: MINTER, Lisa M. **Org:** University of Massachusetts Amherst **Award Amount:** $509,356.00

Study/Product Aim(s)

- Produce synthetic cell penetrating peptide mimics (CPPM)
- Complex CPPMs with: IgG, anti-pPKCθ, anti-PCMT1
- Differentiate iTregs in the presence of: CPPM:IgG, CPPM:anti-pPKCθ, CPPM:anti-PCMT1, and combination of CPPM:anti-pPKCθ + CPPM:anti-PCMT1
- Characterize iTregs differentiated in the presence of: CPPM:IgG, CPPM:anti-pPKCθ, CPPM:anti-PCMT1 (phenotype; suppression assays; FOXP3 methylation)
- Characterize iTregs differentiated in the presence of: CPPM:IgG, CPPM:anti-pPKCθ, CPPM:anti-PCMT1 with CsA or Rapamycin added (phenotype suppression assays; FOXP3 methylation)

Approach

CPPM synthesis: Dichloro-di(3-bromopyridino)-*N,N'*-Dimesitylenoimidazolino-Ru=CHPh (G3) catalyst, CH_2Cl_2, RT, 10 min; ii) dG, CH_2Cl_2, RT, 90 min; iii) Ethyl vinyl ether, RT, overnight. Deprotection to yield CPPMs: I) TFA/CH_2Cl_2 (1:1), RT, overnight, then dialysis-purified using membranes with molecular weight cut-off:100-500 g/mol.

Human CD4 T cells isolated from PBMCs were differentiated into iTregs for 5-7 days following addition of different CPPM:antibody combinations, or IgG as control, then characterized by flow cytometry. In some experiments, iTreg cells were exposed to Csa or loaded with a red fluorescent tracking dye, then mixed with stimulated human PBMCs (loaded with a fluorescent green tracking dye) to evaluate suppressive capabilities.

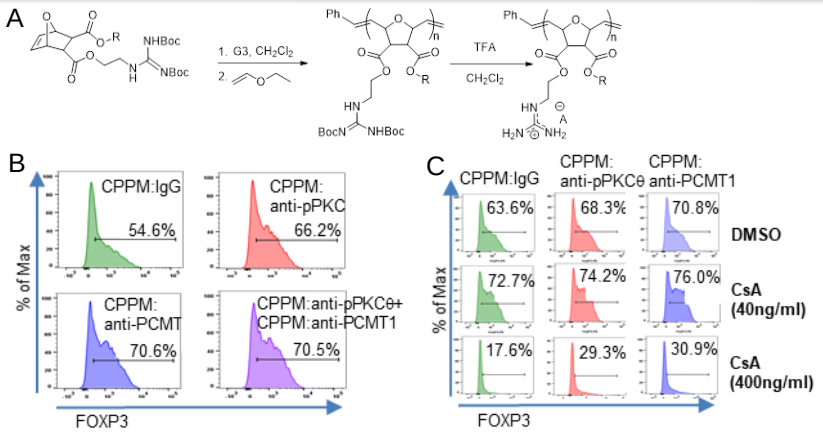

Accomplishments: (**A**) Cell Penetrating Peptide Mimics (CPPMs) were synthesized as bloc-co-polymers comprised of a 13-phenyl, 5-di-guanidinium backbone. (**B**) CPPM-antibody delivery into human CD4 T cells increases the percent of CD4+CD25+DC127-FOXP3+ iTregs. (**C**). Low dose (40ng/ml) CsA treatment enhances iTreg differentiation, while CPPM:antibody treatment protects FOXP3 expression in iTregs exposed to high doses (400ng/ml) of CsA.

Timeline and Cost

Activities CY	2019	2020	2021
Major Task 1 (sub tasks 1-3)			
Major Task 1 (sub tasks 4-5)			
Major Task 1 (sub tasks 6-7)			
Major Task 1 (sub tasks 8)			
Estimated Budget ($K)	**$80K**	**$160K**	**$85K**

Updated: (8/31/2020 – revised 11/30/2020)

Goals/Milestones

CY 2019/CY 2020 Goals – *In vitro* testing and characterization studies

Completed

- ☑ Obtain necessary IACUC and ACURO approval
- ☑ Synthesize Cell Penetrating Peptide Mimics
- ☑ Submit research proposal to NMDP for approval of sample release
- ☑ Differentiate iTregs with CPPM:antibodies

Ongoing (>75% complete)

- ☐ Functional assays for iTregs differentiated with CPPM:antibodies
- ☐ Characterize iTregs differentiated with CsA or Rapamycin

Comments/Challenges/Issues/Concerns

- Mandatory 4-month, full-lab shut down due to the pandemic
- Pandemic caused major disruption in research progress including a
- significant delay in shipping of patient samples
- Differentiation and suppression assays required some optimization.

Budget Expenditure to Date

Projected Expenditure: Y1 = $159,953.00

Actual Expenditure: Y1 = $192,447.11 (10% over Y1 budgeted expenditures)

Please cite this article in press as: Ozay et al., Cell-Penetrating Anti-Protein Kinase C Theta Antibodies Act Intracellularly to Generate Stable, Highly Suppressive Regulatory T Cells, Molecular Therapy (2020), https://doi.org/10.1016/j.ymthe.2020.05.020

Molecular Therapy
Original Article

Cell-Penetrating Anti-Protein Kinase C Theta Antibodies Act Intracellularly to Generate Stable, Highly Suppressive Regulatory T Cells

E. Ilker Ozay,[1,4] Sudarvili Shanthalingam,[2] Heather L. Sherman,[1] Joe A. Torres,[1] Barbara A. Osborne,[1,2] Gregory N. Tew,[1,2,3] and Lisa M. Minter[1,2]

[1]Graduate Program in Molecular and Cellular Biology, University of Massachusetts Amherst, Amherst, MA 01003, USA; [2]Department of Veterinary and Animal Sciences, University of Massachusetts Amherst, Amherst, MA 01003, USA; [3]Department of Polymer Science and Engineering, University of Massachusetts Amherst, Amherst, MA 01003, USA

Regulatory T cells maintain immunological tolerance and dampen inflammatory responses. Administering regulatory T cells can prevent the immune-mediated tissue destruction of graft-versus-host disease, which frequently accompanies hematopoietic stem cell transfer. Neutralizing the T cell-specific kinase, protein kinase C theta, which promotes T cell effector functions and represses regulatory T cell differentiation, augments regulatory T cell immunosuppression and stability. We used a synthetic, cell-penetrating peptide mimic to deliver antibodies recognizing protein kinase C theta into primary human CD4 T cells. When differentiated *ex vivo* into induced regulatory T cells, treated cells expressed elevated levels of the regulatory T cell transcriptional regulator forkhead box P3, the surface-bound immune checkpoint receptor programmed death receptor-1, and pro-inflammatory interferon gamma, previously ascribed to a specific population of stable, highly suppressive human induced regulatory T cells. The *in vitro* suppressive capacity of these induced regulatory T cells was 10-fold greater than that of T cells differentiated without antibody delivery. When administered at the time of graft-versus-host disease induction, using a humanized mouse model, antibody-treated regulatory T cells were superior to non-treated T cells in attenuating lethal outcomes. This antibody delivery approach may overcome obstacles currently encountered using patient-derived regulatory T cells as a cell-based therapy for immune modulation.

INTRODUCTION

Naive CD4 T cells differentiate into unique T helper (Th) subsets in response to specific signals generated in peripheral tissues. Regulatory T cells (Tregs) are a subset of differentiated Th cells that function to mitigate immune responses and maintain immunological tolerance.[1] In humans, Tregs are characterized *in vivo* as $CD4^+CD25^+CD127^-FOXP3^+$ cells, and are consistently suppressive across species and in multiple disease models.[2–8] Treg function is critical for attenuating autoimmune responses, controlling tumor and microbial immunity, preventing graft rejection in mice and humans, and suppressing the immune-mediated tissue destruction of graft-versus-host disease (GvHD), which frequently accompanies hematopoietic stem cell transplantation (HSCT).[9–13] In autoimmune conditions, Treg function can be negatively regulated by the inflammatory cytokine milieu.[14] Appropriate migration to secondary lymphoid organs and subsequent expansion are necessary prior to Treg trafficking to sites of inflammation where they exert their suppressive functions *in vivo*.[15]

The immunological synapse (IS) is a supramolecular signaling complex that coalesces in an ordered fashion at the contact point between naive T cells and antigen-loaded dendritic cells (DCs). Following stimulation through the T cell receptor (TCR), the T cell-specific kinase protein kinase C theta (PKCθ) is phosphorylated at threonine 538 and translocates to the centermost region of the IS. Here, it links activation signals from the TCR with costimulatory signals provided by CD28, culminating in transcription of immune-responsive genes.[16–18] Interestingly, PKCθ is the only PKC isoform recruited to the center of the IS. However, unlike in effector T cells, in Tregs PKCθ is sequestered away from the central domain of the IS.[19,20] Through this differential positioning in the IS, PKCθ promotes activation of effector T cell functions at the expense of Treg programs.[21–23] Inhibiting the actions of PKCθ with small-molecule inhibitors or using small interfering RNA (siRNA) approaches enhances the suppressive capacity of Tregs, restores impaired function of Tregs from rheumatoid arthritis patients, and blocks the autoimmune response in a mouse model of colitis.[24] Therefore, attenuating PKCθ activity in Tregs may be a valuable component in Treg adoptive immunotherapy when used to treat autoimmune conditions or GvHD.[25]

Received 8 January 2020; accepted 19 May 2020;
https://doi.org/10.1016/j.ymthe.2020.05.020.

[4]Present address: SQZ Biotechnologies, 200 Arsenal Yards Boulevard, Watertown, MA 02472, USA

Correspondence: Lisa M. Minter, Department of Veterinary and Animal Sciences, University of Massachusetts Amherst, 661 North Pleasant Street, 427K ISB, Amherst, MA 01003, USA.
E-mail: lminter@vasci.umass.edu

Please cite this article in press as: Ozay et al., Cell-Penetrating Anti-Protein Kinase C Theta Antibodies Act Intracellularly to Generate Stable, Highly Suppressive Regulatory T Cells, Molecular Therapy (2020), https://doi.org/10.1016/j.ymthe.2020.05.020

Initial evidence shows that PKCθ is required in fully functional mature, but not immature, T cell responses by bridging stimuli received through the TCR to downstream gene transcription, including those generated by nuclear factor-κB (NF-κB), nuclear factor of activated T cells (NFAT), and activator protein 1 (AP1) transcriptional regulators.[18,26] More recent work demonstrated that immune cells from PKCθ-deficient mice, transplanted together with T cell-depleted bone marrow (BM) stem cells from wild-type mice, did not induce GvHD in recipients. This is in contrast to the majority of recipient mice that died from GvHD when wild-type immune cells were transferred together with BM stem cells.[27] PKCθ-deficient immune cells did not confer GvHD. They did, however, retain their ability to protect recipient mice from bacterial and viral infections, as well as mediate immune depletion of residual leukemia cells. These and follow-up studies reinforce the notion that inhibiting PKCθ activity during BM transplantation may constitute a beneficial approach to limiting the severity of GvHD, while maintaining important anti-tumor surveillance.

Effectively and specifically blocking PKCθ function is challenging, due to the high structural homology it shares with eight, more broadly expressed family members. As a result, many existing small-molecule PKCθ inhibitors have toxic or off-target effects and show suboptimal penetration into T cells.[28] In contrast, using antibodies to modulate cell surface receptor function, either positively or negatively, is now a widely accepted immunotherapeutic approach. However, because of its intracellular residence PKCθ is not a suitable candidate for antibody-targeting strategies. Recently, we developed and reported on a successful and highly specific strategy for routine and effective intracellular antibody delivery using cell-penetrating peptide mimics (CPPMs) and demonstrated its powerful application by targeting a phosphorylated threonine residue (Thr538) of activated PKCθ (phosphorylated PKCθ [pPKCθ]) in the context of T cell immunomodulation.[29] Manipulating primary T cells *ex vivo* using intracellular anti-pPKCθ delivery constrained pPKCθ in the cytosol and reduced the capacity of these cells to adopt a pro-inflammatory Th type 1 (Th1) cell fate.[29]

Naive CD4 T cells can be induced to differentiate *ex vivo* into Tregs (iTregs). In an allogeneic mouse model of BM transplantation, adoptively transferring iTregs provided beneficial relief from disease by suppressing immune-mediated, acute GvHD.[30] This approach has now entered the clinic where cellular immunotherapy using adoptively transferred iTregs is recognized as a feasible and efficacious option to treat immune-mediated conditions.[9] The first in-human trial of adoptive iTreg therapy delivered encouraging outcomes for preventing GvHD associated with allogeneic HSCT, and it offers great promise for treating immune-mediated diseases and allograft rejection.[30–32]

Herein, we report that *ex vivo* CPPM delivery of an antibody specific for pPKCθ enhances the differentiation and expansion of iTregs in culture. Moreover, anti-pPKCθ-treated iTregs exhibited increased suppressive properties *in vitro*, as characterized by increased surface expression of the co-inhibitory receptor programmed cell death 1 (PD-1). Anti-pPKCθ iTregs could be detected *in vivo* up to 17 days after their administration into recipient mice and, compared to control iTregs, were highly efficacious in preventing GvHD in a humanized mouse model. Therefore, CPPM delivery of anti-pPKCθ into human CD4 T cells represents an approach that overcomes obstacles associated with *ex vivo* expansion and sustained *in vivo* stability, and it provides a powerful, reproducible, and effective means of generating iTregs for therapeutic application.

RESULTS

Intracellular Anti-pPKCθ Delivery Prevents Nuclear Accumulation of pPKCθ in iTregs

In fully activated CD4 T cells, PKCθ is phosphorylated on Thr538 by germinal center kinase-like kinase (GLK) downstream of co-stimulatory signals provided by CD28 engagement on the cell surface.[33] This activated form of PKCθ is important for negatively regulating Treg function, and it may mediate these effects through an AKT/Foxo1/3 pathway.[34] Additionally, PKCθ in Tregs is sequestered away from the IS, suggesting that Thr538 both phosphorylation and recruitment to the IS may be important for PKCθ to exert its inhibitory actions on iTreg formation. We previously demonstrated we could utilize a synthetic CPPM to achieve highly efficient intracellular antibody delivery into human primary T cells *ex vivo*.[29] Non-covalently complexing the CPPM, comprised of 13 U of phenyl-containing moiety and 5 U of diguanidine moiety, with anti-pPKCθ reduced nuclear translocation of pPKCθ, attenuated downstream signaling and compromised Th1 differentiation.[29] In the present study, we predicted that delivering anti-pPKCθ prior to iTreg polarization would similarly alter pPKCθ function to enhance iTreg differentiation. To confirm intracellular antibody uptake, we isolated CD4 T cells from human peripheral blood mononuclear cells (hPBMCs) and incubated them with CPPM-immunoglobulin G (IgG) only or CPPM-anti-pPKCθ, followed by staining with a fluorescently conjugated secondary antibody. We found that the delivery efficiency of CPPM-anti-pPKCθ (or CPPM-anti-rabbit IgG as a non-specific control) into CD4 T cells was approximately 90%, with high intracellular delivery detected for both antibodies (Figure S1A). Incubating CD4 T cells with CPPM alone, or with uncomplexed anti-pPKCθ, showed no detectable uptake of anti-pPKCθ (Figure S1A). We subsequently incubated CD4 T cells with anti-pPKCθ only, CPPM only, CPPM-anti-IgG only, DMSO only (as a vehicle control for CPPM-antibody complexing), or CPPM-anti-pPKCθ and then differentiated the cells into iTregs over 5 days of culture using commercially available iTreg-polarizing reagents (Figure 1A). We deviated from the manufacturer's directions, which suggested stimulating cells only with anti-CD3, by also cross-linking the CD28 receptor to provide the co-stimulatory signals needed to phosphorylate PKCθ on Thr538 and, thus, generate the target epitope recognized by anti-pPKCθ. At the end of the 5-day differentiation period, the percent of $CD4^+CD25^+FOXP3^+$ iTregs was greater than 90% regardless of pre-treatment conditions (Figure S1B). Human CD4 T cells did not tolerate CPPM-IgG delivery well, showing increased levels of cell death by the end of the differentiation period. Therefore, based on the nearly identical staining patterns of CD25, CD127, and FOXP3 exhibited by DMSO-treated

Please cite this article in press as: Ozay et al., Cell-Penetrating Anti-Protein Kinase C Theta Antibodies Act Intracellularly to Generate Stable, Highly Suppressive Regulatory T Cells, Molecular Therapy (2020), https://doi.org/10.1016/j.ymthe.2020.05.020

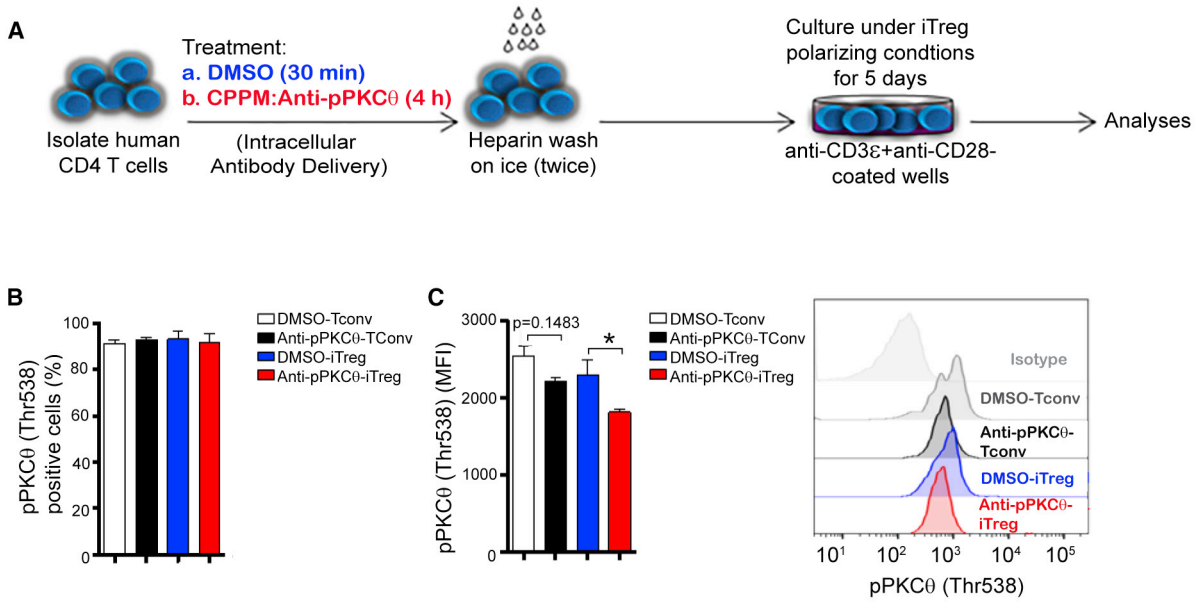

(legend on next page)

Please cite this article in press as: Ozay et al., Cell-Penetrating Anti-Protein Kinase C Theta Antibodies Act Intracellularly to Generate Stable, Highly Suppressive Regulatory T Cells, Molecular Therapy (2020), https://doi.org/10.1016/j.ymthe.2020.05.020

(DMSO-iTregs) and CPPM-anti-pPKCθ-treated (anti-pPKCθ-iTregs) iTregs (Figure S1C), we chose these two populations to further compare differences in iTreg functions *in vitro* and *in vivo*.

We used flow cytometry to quantify total pPKCθ in stimulated DMSO- and anti-pPKCθ-treated conventional T cells (Tconvs) and in iTregs. We observed similar percentages of pPKCθ-positive cells in Tconv and iTreg populations (Figure 1B). However, when we assessed the abundance of pPKCθ on a per cell basis, as measured by median fluorescence intensity (MFI; Figure 1C), we found that anti-pPKCθ-iTregs expressed lower levels of pPKCθ, compared to DMSO-iTregs. Although it did not differ significantly in iTregs, regardless of pre-treatment, *PRKCQ* gene expression was significantly reduced in anti-pPKCθ-Tconvs (Figure 1D). These data are consistent with a previous report in which we describe that anti-pPKCθ delivery into T cells, prior to their *in vitro* differentiation into Th1 cells, diminishes PKCθ activity, including driving its own expression.[29] PKCθ can function both in the nucleus and the cytosol;[35] therefore, we further quantified PKCθ cytoplasmic and nuclear distribution in Tconvs and iTregs. We detected strong cytosolic expression of the 82-kDa protein, as expected, in Tconvs and in DMSO-iTregs. Consistent with the flow cytometric assessment of pPKCθ, there was much less of this isoform in the cytosol of anti-PKCθ-iTregs (Figure 1E). We next used imaging flow cytometry to quantify the abundance of pPKCθ in the nucleus of iTregs. Nuclear pPKCθ protein was significantly reduced in anti-pPKCθ-iTregs, compared to DMSO-iTregs (Figure 1F). Collectively, these data demonstrate that CPPM-mediated delivery of anti-pPKCθ into CD4 T cells alters the cellular distribution of pPKCθ within *ex vivo*-differentiated iTregs.

Ex Vivo CPPM-Anti-pPKCθ Delivery Generates a Unique Population of $CD4^+CD25^{high}FOXP3^{high}$ iTregs That also Produces Interferon γ (IFNγ)

Reduced nuclear accumulation of PKCθ in anti-pPKCθ-iTregs is consistent with the reported nuclear role for PKCθ in pro-inflammatory gene regulation in human CD4 T cells.[35] In complementary studies, Zanin-Zhorov et al.[21] provided compelling evidence that using a small-molecule inhibitor to block PKCθ activity in CD4 T cells enhanced their regulatory phenotype. However, cell toxicity and off-target effects constitute two major obstacles to using small-molecule inhibitors to intervene in signaling pathways. We predicted that inhibiting the actions of PKCθ using anti-pPKCθ, delivered *ex vivo* into the cytosol of human CD4 T cells, would enhance the *ex vivo* differentiation of functional, stable iTregs. High surface expression of CD25, the high-affinity subunit of the interleukin 2 (IL-2) receptor, is a hallmark of Tregs. More than 90% of differentiated iTregs exhibited high surface CD25, including those treated with CPPM-anti-pPKCθ (Figure 2A). On a per cell basis, the concentration of surface CD25 on anti-pPKCθ-iTregs was increased more than that expressed on DMSO-iTregs or on Tconvs (Figure 2B). We further stratified iTregs phenotypically using flow cytometry to quantify the percent of $CD4^+CD25^{high}$ cells that also expressed the signature iTreg master transcriptional regulator, FOXP3. When we applied this gating strategy, we found anti-pPKCθ delivery enhanced the percentage of FOXP3-expressing $CD4^+CD25^{high}$ cells following iTreg polarization (Figures 2C and 2D). In comparison, nearly 50% of $CD4^+CD25^{high}$ DMSO-iTregs remained $FOXP3^-$ (Figure 2D). We also assessed whether FOXP3 abundance varied between treatments. In parallel to increased CD25 expression on anti-pPKCθ-iTregs, we observed significantly more FOXP3 protein in anti-pPKCθ-iTregs, compared to DMSO-iTregs (Figure 2E). This was notable, because *FOXP3* gene expression in iTregs did not differ between the treatments (Figure 2F) and suggests that anti-pPKCθ treatment may act to increase the stability of FOXP3.

Co-inhibitory receptor-ligand engagement increases cell-cell contact time and leads to decreased cytokine production by effector T cells.[36] However, these receptors are effective in cell-cell suppression only when they are expressed on the cell surface.[37–39] For instance, freshly isolated, naturally occurring (n)Tregs retain PD-1 in intracellular compartments and upon TCR signaling will translocate PD-1 to the cell surface and, subsequently, become more suppressive.[39] We detected higher levels of *PDCD1*, as well as higher surface PD-1 expression, in anti-pPKCθ-iTregs (Figure 2G). Of note, we observed that *ex vivo*-generated anti-pPKCθ-iTregs also expressed increased amounts of *IFNG* transcripts and produced more IFNγ than did DMSO-iTregs (Figure 2H), which is consistent with unique populations of highly suppressive Tregs previously described.[40,41] These results demonstrate that when peripheral CD4 T cells are activated *ex vivo*, using methods that mimic physiological activation and co-stimulatory signals, and then cultured with a defined polarizing cocktail, these cells can be successfully differentiated into iTregs. However, delivering anti-pPKCθ across the cell membrane prior to differentiating CD4 T cells generated a greater percentage of $CD4^+CD25^{high}FOXP3^{high}$ iTregs, increased the concentration of FOXP3 and surface PD-1 expressed by these iTregs, and induced IFNγ production.

Anti-pPKCθ-iTregs Exhibit Superior Suppressive Capabilities *In Vitro*

Tregs function to suppress the activation of nearby T cells, through mechanisms that are both direct, i.e., cell-cell contact, and indirect,

Figure 1. Intracellular Anti-pPKCθ Delivery Prevents Nuclear Accumulation of pPKCθ in iTregs

(A) Schematic of *in vitro* iTreg differentiation protocol in the presence of cell-penetrating anti-pPKCθ (CPPM-anti-pPKCθ). (B and C) Percent $pPKC\theta^+$ cells (B) and median fluorescent intensity (MFI) (C) of pPKCθ expression, with representative histogram of pPKCθ-positive cells following CPPM-anti-pPKCθ delivery in non-differentiated conventional T cells (Tconvs) and iTreg-differentiated cells. (D) Quantification of *PRKCQ* expression in non-differentiated and iTreg-differentiated cells. (E) Representative immunoblot of cytosolic and nuclear distribution of total PKCθ in non-differentiated and iTregs without or with CPPM-anti-pPKCθ delivery. (F) Nuclear localization score distribution of pPKCθ-expressing cells, quantification of nuclear similarity scores for pPKCθ, and representative image showing nuclear pPKCθ in iTregs determined by AMNIS imaging flow cytometry analysis of 1,000 iTregs differentiated without or with CPPM-anti-pPKCθ. Data represent the mean ± SEM three independent experiments. $^*p < 0.05$, $^{**}p < 0.01$, by unpaired, two-tailed Student's t test.

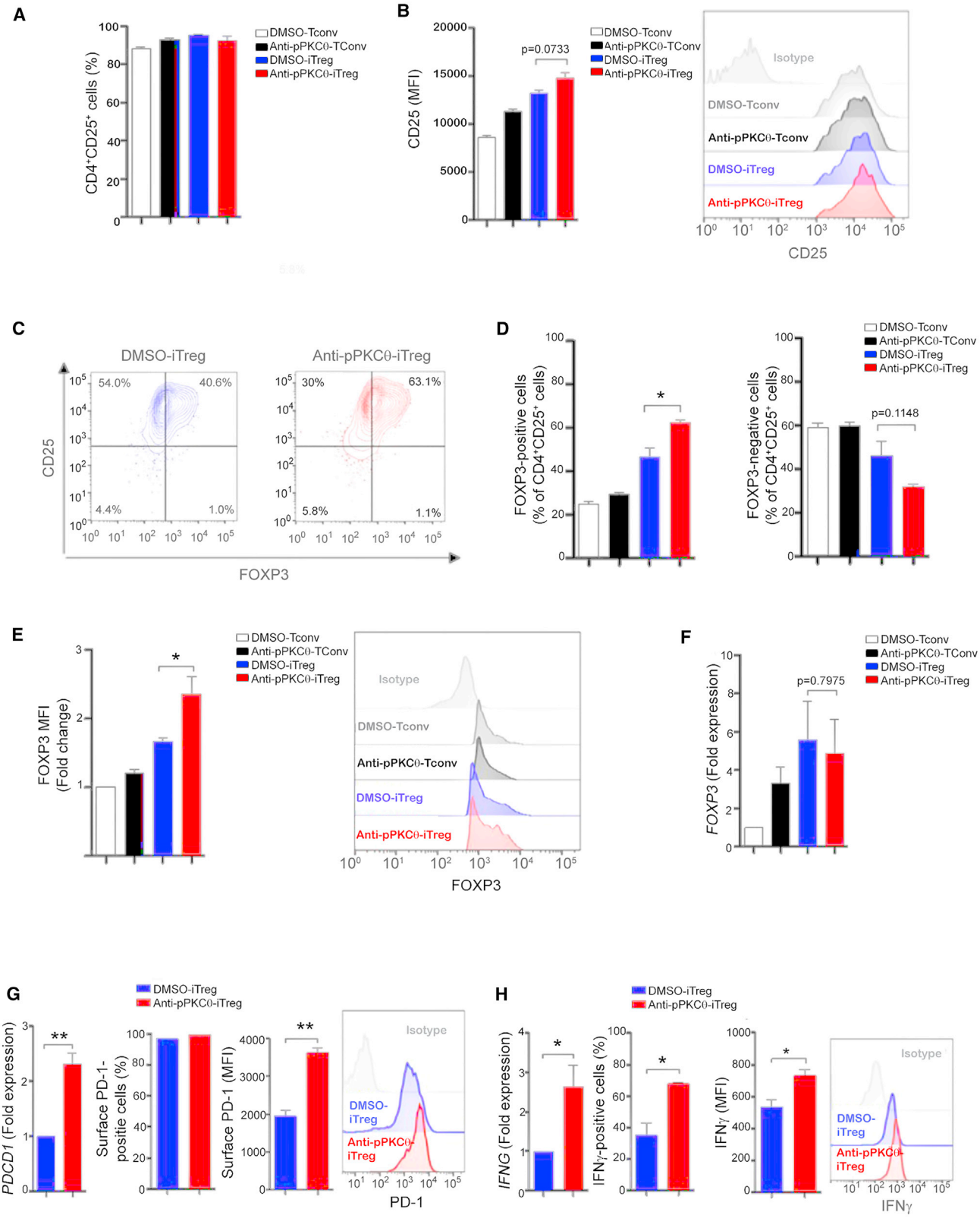

(legend on next page)

Please cite this article in press as: Ozay et al., Cell-Penetrating Anti-Protein Kinase C Theta Antibodies Act Intracellularly to Generate Stable, Highly Suppressive Regulatory T Cells, Molecular Therapy (2020), https://doi.org/10.1016/j.ymthe.2020.05.020

i.e., release of anti-inflammatory cytokines.[42] Tregs that are defined by the $CD4^+CD25^{high}FOXP3^{high}$ phenotype, and which were increased in the iTreg population following anti-pPKCθ delivery, are presumed to possess potent suppressive capabilities. However, an iTreg phenotype alone does not demonstrate functional suppression. Therefore, we utilized a standard *in vitro* suppression assay to determine whether anti-pPKCθ delivery generated iTregs with superior suppressive activity, compared to their DMSO-iTreg counterparts. We activated hPBMCs, mimicking physiological conditions by stimulating them with soluble anti-CD3 and anti-CD28. We labeled these responder T cells (T_{resp}s) with the vital dye UltraGreen and mixed them in culture at three different ratios with *ex vivo*-differentiated suppressor iTregs (T_{supp}s). We used a second vital dye, Red650, which emits fluorescence at a longer wavelength, to label the T_{supp}s (Figure 3A). We used flow cytometry to track the proliferative responses of T_{resp}s and T_{supp}s at the end of the 4-day suppression assay. When we cultured anti-pPKCθ-iTregs with responder cells at a 1:10 ratio, and the suppression we observed was as strong as when DMSO-treated iTregs were mixed with responder cells at a 1:1 ratio, suggesting that anti-pPKCθ-iTregs potently suppress T cell proliferation in standard suppression assays (Figure 3B). Furthermore, anti-pPKCθ-iTregs proliferated in culture more extensively than did DMSO-iTregs, as indicated by the loss of Red650 fluorescence (Figure 3C). This was also reflected in the overall percentages of iTregs at the end of the co-culture period, when we detected significantly higher percentages of $CD4^+CD25^{high}FOXP3^{high}$ cells in co-cultures containing anti-pPKCθ-iTregs compared to those with DMSO-iTregs (Figure 3D).

Following activation, both $CD4^+CD25^-$ Tconvs and $CD4^+CD25^+$ iTregs increase expression of FOXP3. However, FOXP3 in Tconvs remains mostly in the cytosol, whereas in iTregs, FOXP3 is localized primarily to the nucleus.[43] Furthermore, when a mutant, nuclear-translocating form of FOXP3 was expressed in Jurkat T cells, it endowed these transfected cells with suppressive capabilities.[43] To ask whether there were differences in the cellular distribution of FOXP3 in DMSO-Tregs and anti-pPKCθ-iTregs, we again used imaging flow cytometry to assess FOXP3 localization. As indicated by the increased positive nuclear similarity score, we detected significantly more nuclear FOXP3 in anti-pPKCθ-iTregs than in DMSO-iTregs, consistent with their enhanced suppressive capacity (Figure 3E). PD-1 expression in Tregs has been associated with increased FOXP3 stability,[42] and IFNγ signaling upregulates the co-inhibitory ligand for PD-1, PD-L1, on activated T cells.[42] Thus, it is likely that anti-pPKCθ delivery modulates several key iTreg signaling pathways to convey superior *in vitro* suppression.

Adoptively Transferring Anti-pPKCθ-iTregs Attenuates Disease and Prolongs Survival in a Humanized Mouse Model of GvHD

Using Treg adoptive immunotherapy in mouse models of GvHD represents a viable strategy for understanding T cell biology, as well as Treg-mediated suppression.[44] iTreg abundance correlated with attenuated GvHD severity and increased long-term graft tolerance, without the need for drug-induced immunosuppression.[32,45] Therefore, we assessed the translational potential of anti-pPKCθ-iTregs using a preclinical mouse model of acute GvHD.[29] In this humanized mouse model, PBMCs (graft) are transferred, via the tail vein, into lightly irradiated recipient (host) NOD-*scid IL2rγ*^{null} (NSG) mice. The BM is the target of immune-mediated destruction, with symptoms peaking approximately 17 days after PBMCs are transferred. This model is uniformly fatal, and mice succumb to lethal BM failure approximately 3 weeks after disease induction.[29] To test the translational potential of administering anti-pPKCθ-treated iTregs as a cell-based prophylaxis for GvHD, we differentiated iTregs from a single donor *ex vivo* without or with anti-pPKCθ delivery. We used PBMCs from the same donor to induce GvHD in host mice (Figure 4A). Our rationale for this approach stems from the understanding that immune-competent T cells residing in the graft are activated and expand in the host as the result of conditioning regimens that produce a pro-inflammatory setting. We reasoned that if peripheral blood CD4 T cells from the donor were differentiated into iTregs *ex vivo*, before administering to the host at the time of BM transplantation, they would prevent expansion of alloreactive T cells in the host and attenuate acute GvHD. To test this hypothesis, we transferred *ex vivo*-differentiated iTregs, together with disease-inducing PBMCs, at a ratio of 1:3 into NSG mice. We chose this "responder/suppressor" ratio guided by our *in vitro* suppression results (Figure 3). On day 17, we analyzed BM, peripheral blood, and spleens of diseased animals to evaluate the efficacy of iTreg treatment.

To confirm equivalent disease induction across all of the cohorts, we evaluated the extent to which the transferred PBMCs expanded *in vivo*. We collected samples from the peripheral blood and spleens from mice with GvHD that received no iTregs, that received DMSO-iTregs, or that received anti-pPKCθ-iTregs, and evaluated the percentage of cells that expressed the human leukocyte antigen CD45 as a measure of cellular expansion after transfer. The percentages of human $CD45^+$ cells detected in the peripheral blood and spleens of GvHD mice did not differ greatly, regardless of whether they also received iTregs, and the overall cellularity of the spleens also appeared similar when stained with hematoxylin and eosin (Figures S2A and S2B), indicating comparable disease induction across all treatment cohorts. When we refined our analyses of cells by subsets and noted fewer circulating CD4 T cells in mice treated with anti-pPKCθ-iTregs, but otherwise there were no

Figure 2. *Ex Vivo* CPPM-Anti-pPKCθ Delivery Generates a Unique Population of $CD4^+CD25^{high}FOXP3^{high}$ iTregs That Also Produce IFNγ

(A and B) Percentage of total $CD4^+CD25^+$ T cells (A) and MFI and representative histograms of CD25 expression within $CD4^+CD25^+$ T cell gate of non-differentiated and iTreg-differentiated cells (B). (C) Representative FACS clouds showing percent of $CD25^+FOXP3^+$ cells within $CD4^+CD25^+$ T cell gate. (D) Percent $FOXP3^+$ and $FOXP3^-$ cells within the $CD4^+CD25^+$ T cell gate. (E) Fold increase in FOXP3 MFI and representative histogram in non-differentiated and iTreg-differentiated cells. (F) *FOXP3* expression, shown relative to untreated, non-differentiated T cells. (G and H) Gene expression, percent positive, MFI, and representative histograms of (G) PD-1- and (H) IFNγ-expressing iTregs differentiated without or with CPPM-anti-pPKCθ are shown. Data represent the mean ± SEM of three independent experiments. *$p < 0.05$, **$p < 0.01$, by unpaired, two-tailed Student's t test.

Please cite this article in press as: Ozay et al., Cell-Penetrating Anti-Protein Kinase C Theta Antibodies Act Intracellularly to Generate Stable, Highly Suppressive Regulatory T Cells, Molecular Therapy (2020), https://doi.org/10.1016/j.ymthe.2020.05.020

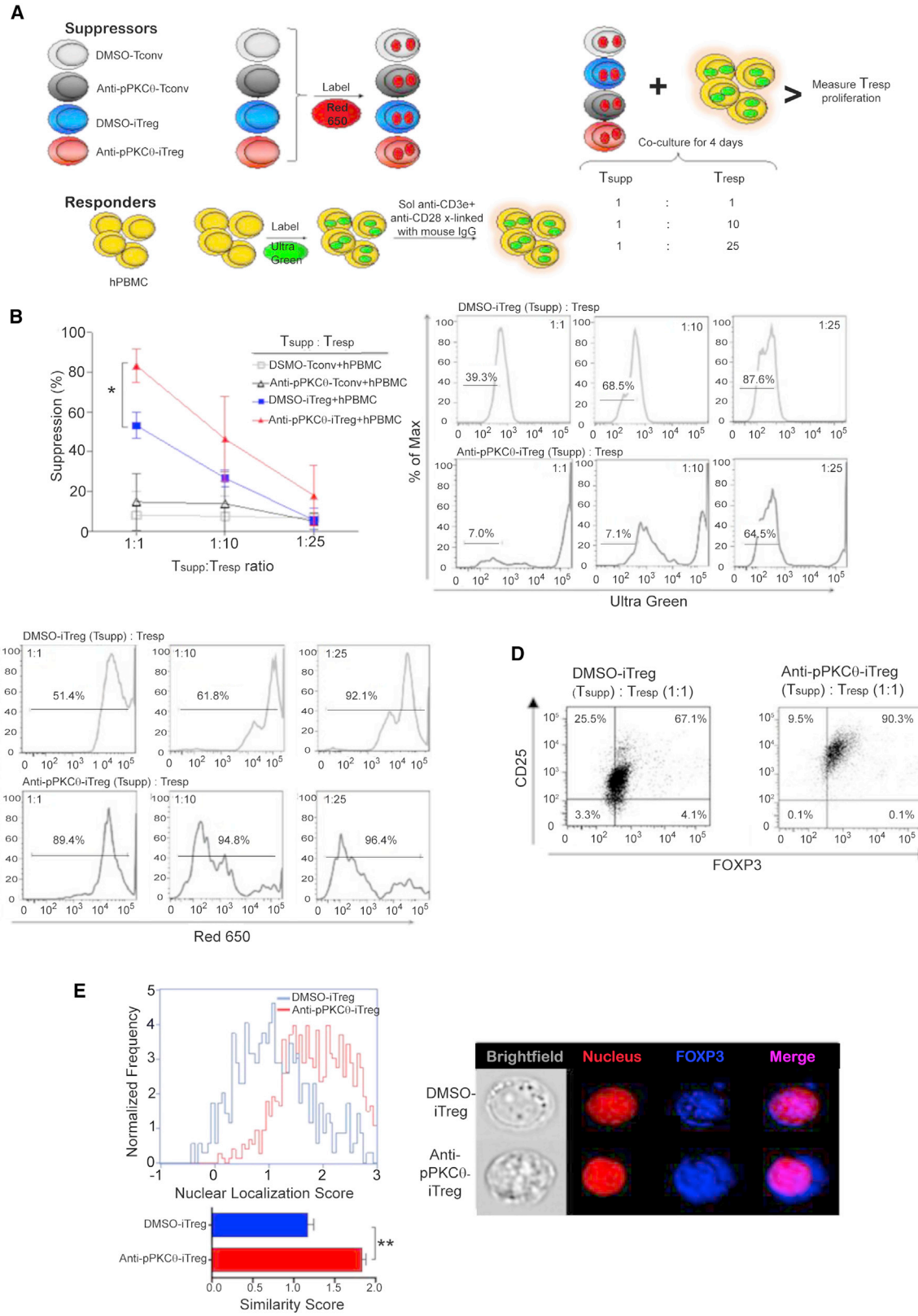

(legend on next page)

Please cite this article in press as: Ozay et al., Cell-Penetrating Anti-Protein Kinase C Theta Antibodies Act Intracellularly to Generate Stable, Highly Suppressive Regulatory T Cells, Molecular Therapy (2020), https://doi.org/10.1016/j.ymthe.2020.05.020

significant differences in the percentages of human CD4 or CD8 T cells between treated or untreated animals (Figure S2C).

Hematopoiesis in the BM gives rise to circulating white and red blood cells. Pancytopenia is a hallmark of the GvH-mediated BM failure that accompanies this model. Transferring DMSO-iTregs when GvHD was induced afforded discernable protection to circulating white and red blood cells, and this protection was significantly enhanced in mice that received anti-pPKCθ-iTregs (Figure 4B). Similarly, when we evaluated BM cellularity, either by counting nucleated cells in the BM or by histological assessment (Figure 4C), it was evident that administering anti-pPKCθ-iTregs at the time of disease induction provided robust protection of the BM compartment. This was likely due to differences in the percentages, as well as in absolute numbers, of PBMCs that had infiltrated the BM by day 17 (Figure 4D). However, the distribution of T cells recruited to the BM by this time was similar in mice that received iTregs, regardless of how these cells were differentiated prior to infusion (Figure 4E). These results led us to conclude that treating mice with anti-pPKCθ-iTregs may alter the kinetics of T cell migration into the BM, rather than the percentages of BM-infiltrating CD4 and CD8 T cells.

We next evaluated whether administering iTregs attenuated disease severity in a humanized mouse model of GvHD. Treating diseased mice with DMSO-iTregs reduced their cumulative GvHD clinical score, and nearly doubled their median survival time, compared to untreated mice with GvHD (38 days versus 21 days, respectively; Figures 4F and 4G). More remarkable was the impact on GvHD that co-administering anti-pPKCθ-iTregs had in this model. As a cohort, mice that received anti-pPKCθ-iTregs had less severe symptoms of disease, as compared to mice that received DMSO-iTregs or no treatment, respectively (Figure 4F). Predictably, mice that exhibited less severe symptoms also lived longer. The median length of survival for mice treated with anti-pPKCθ-iTregs was twice that of DMSO-iTreg-treated mice, and nearly 4-fold that of untreated mice (78 days versus 38 days versus 21 days, respectively; Figure 4G). Quite unexpectedly, one of the five mice treated with anti-pPKCθ-iTregs exhibited full rescue from lethal GvHD, surviving a full 100 days after disease induction. Overall, these *in vivo* results demonstrated that anti-pPKCθ-iTregs were highly efficacious as a cell-based therapy in a humanized mouse model of GvHD, when infused at the time of disease induction.

Ex Vivo-Generated Anti-pPKCθ-iTregs Exhibit a Stable, Unique FOXP3^{high}PD-1^{+}IFNγ^{high} Phenotype *In Vivo*

In this pre-clinical model of GvHD, BM destruction is mediated by Th1 responses resulting from an imbalanced Th1/Th2 response.[29] When we measured circulating cytokines in mice treated with anti-pPKCθ-iTregs, we detected significantly increased IL-2 and IL-10, both of which enhance the immunosuppressive functions of Tregs *in vivo*. Signature Th2 cytokines, IL-4 and IL-13, which can counteract Th1 responses, were also increased in the plasma of anti-pPKCθ-iTreg-treated mice (Figure 5A), suggesting that anti-pPKCθ-iTregs alter Th cell responses *in vivo*.

Administering anti-pPKCθ-iTregs proved superior in reducing the severity of GvHD and extending survival in the humanized mouse model. Accumulating evidence suggests that *in vitro*-expanded Tregs have unstable FOXP3 expression and may lose their suppressive properties when encountering proinflammatory conditions, such as those that characterize the GvHD milieu *in vivo*.[46] Therefore, we sought to better evaluate the *in vivo* stability of anti-pPKCθ-iTregs, compared to iTregs generated without anti-pPKCθ delivery. We identified iTregs based on CD4, CD25, and FOXP3 expression, as described previously,[32,45] and used magnetic beads to sort iTreg (CD4^{+}CD127^{-}CD25^{+}) populations recovered from the BM, peripheral blood, and spleens of iTreg-treated mice on day 17 after GvHD induction. We noted significantly higher percentages, as well as total numbers, of CD4^{+}CD25^{+}FOXP3^{+} iTregs in the BM of mice that received anti-pPKCθ-iTregs, compared to animals that received DMSO-iTregs (Figures 5B and 5C). The percentage of FOXP3^{high} cells among BM-infiltrating iTregs was also significantly greater in mice that received anti-pPKCθ-iTregs (Figure 5D). Furthermore, *FOXP3* expression in anti-pPKCθ-iTregs isolated from the BM was greater than its expression in DMSO-iTregs, although it did not reach significance (Figure 5D). The percentages of iTregs in peripheral blood and spleen did not differ greatly between treatments (Figures S3A and S4A). However, the FOXP3^{high} iTreg population was consistently and significantly greater in peripheral blood and spleens of anti-pPKCθ-iTreg-treated mice (Figures S3B and S4B). When we further analyzed the CD4^{+}CD25^{+}FOXP3^{+} iTreg population recovered from the BM of mice treated with anti-pPKCθ-iTregs, we found a significantly lower percentage of cells that stained positively for pPKCθ, compared to mice treated with DMSO-iTregs (Figure 5E). In addition, pPKCθ^{low} iTregs were significantly higher in peripheral blood, but not in spleen, of anti-pPKCθ-iTreg-treated mice (Figures S3C and S4C). Consistent with decreased percentages of pPKCθ-expressing Tregs in the BM, we also noted that BM-infiltrating anti-pPKCθ-iTregs tended to express less total pPKCθ, as indicated by a higher percentage of pPKCθ^{low} iTregs, as well as less nuclear pPKCθ, than did DMSO-iTregs, although these data did not reach statistical significance (Figures 5E and 5F). We

Figure 3. Anti-pPKCθ iTregs Exhibit Superior Suppressive Capabilities *In Vitro*

(A) Experimental setup for *in vitro* suppression assay with UltraGreen-labeled responder cells and Red650-labeled suppressor cells mixed in three different ratios. (B) Percent of suppression efficiency of suppressor iTregs and representative histograms of proliferating, UltraGreen-labeled responder cells (indicted by gates and percentages) on day 4 of suppression assay. (C) Flow cytometric analysis of proliferating Red650-labeled iTregs (indicated by gates and percentages) on day 4 of suppression assay (D) Representative FACS plots of CD25^{+}FOXP3^{+} Red650-labled iTregs. (E) Nuclear localization score distribution of FOXP3-expressing iTregs, quantification of nuclear localization similarity scores for FOXP3, and representative image showing nuclear FOXP3 in iTregs determined by AMNIS imaging flow cytometry analysis of 1,000 iTregs differentiated without or with CPPM-anti-pPKCθ. Data represent the mean ± SEM of three independent experiments. *$p < 0.05$, **$p < 0.01$, by unpaired, two-tailed Student's t test.

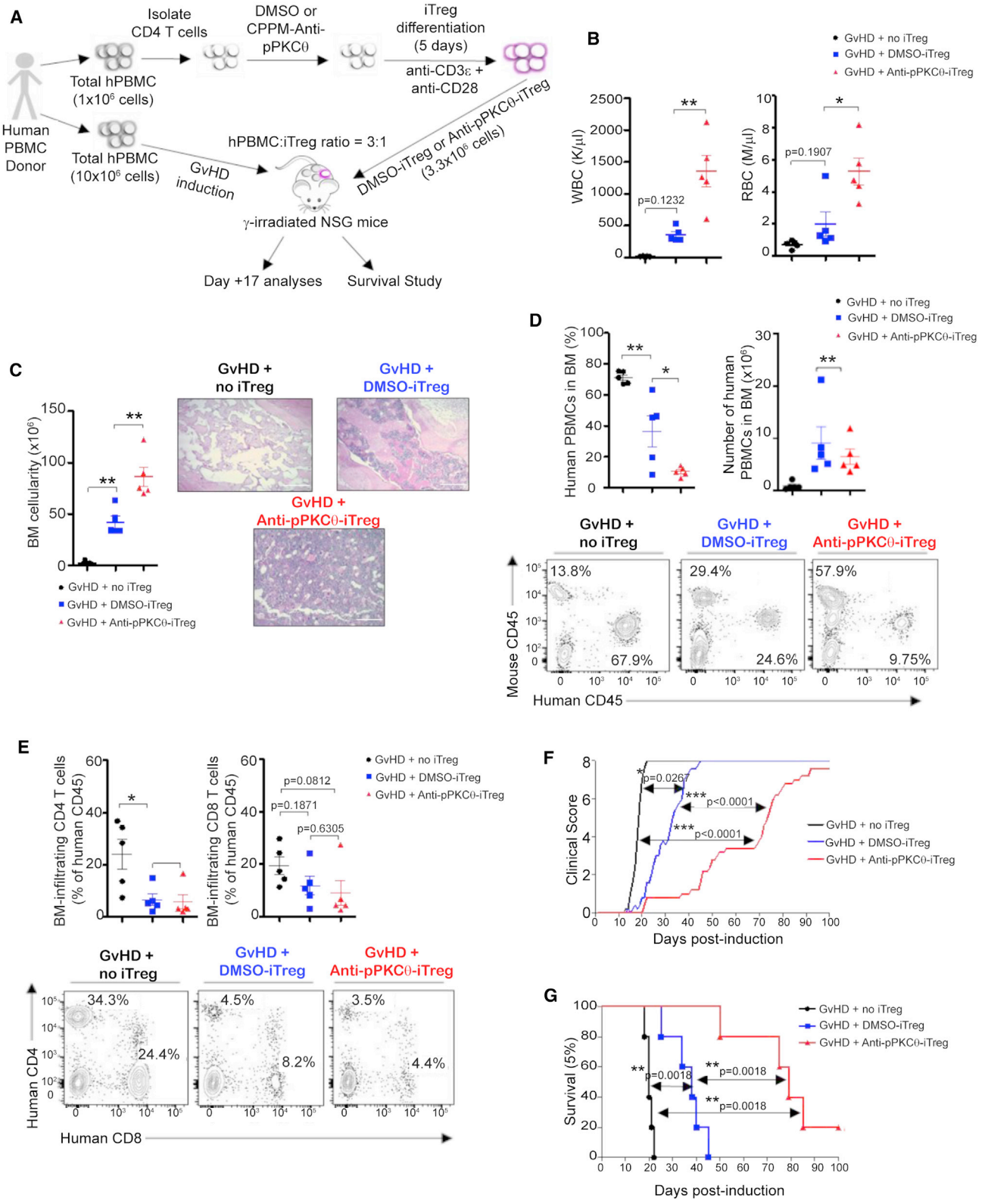

(legend on next page)

Please cite this article in press as: Ozay et al., Cell-Penetrating Anti-Protein Kinase C Theta Antibodies Act Intracellularly to Generate Stable, Highly Suppressive Regulatory T Cells, Molecular Therapy (2020), https://doi.org/10.1016/j.ymthe.2020.05.020

did not observe differences in pPKCθ nuclear localization among iTregs circulating in the peripheral blood or that had trafficked to the spleen (Figures S3D and S4D).

One means by which iTregs can suppress activated T cells is through cell contact-dependent mechanisms, specifically by upregulating the immune-inhibitory receptor PD-1, which will engage its cognate ligand, PD-L1, on activated T cells.[47] Percentages of PD-1-expressing iTregs in BM were similar in mice regardless of iTreg treatment (Figure 5G). Both the percentage of PD-1^{high}-expressing iTregs, as well as total intracellular and surface-expressed PD-1 (MFI), trended higher in anti-pPKCθ-iTregs, and we could detect a population of PD-1^{high}-expressing anti-pPKCθ-iTregs that was not present within the DMSO-iTreg population (Figure 5G). We did not observe differences in PD-1^{high} iTregs isolated from peripheral blood or spleen of mice from either cohort (Figures S3E and S4E).

We also investigated changes in gene expression in iTregs. Specifically, there were significantly higher levels of *PDCD1* and *IFNG* transcripts in anti-pPKCθ-iTregs isolated from the BM, compared to DMSO-iTregs (Figures 5H and 5I, respectively). These findings led us to evaluate plasma levels of IFNγ in iTreg-treated mice. In contrast to DMSO-iTreg-treated mice, we measured significantly greater levels of circulating IFNγ in mice that received anti-pPKCθ-iTregs (Figure 5J). This contrasted with splenic iTregs, which showed no difference in *PDCD1* and significantly lower *IFNG* mRNA levels (Figures S4F and S4G). Altogether, these results indicate that compared to DMSO-iTregs, and even up to 17 days after *in vivo* administration, anti-pPKCθ-iTregs display an increased ability to traffic to sites of inflammation (here the BM) and express high levels of PD-1, and they can produce large quantities of IFNγ, suggesting that the combination of these unique characteristics contributes to reducing disease severity.

Ex Vivo-Generated Anti-pPKCθ-iTregs Show Increased PD-1 Co-localization with PKCθ and NFATc1

Consistent with reports in the literature, we observed increased surface PD-1 on anti-pPKCθ-iTregs, compared to DMSO-iTregs, and this correlated with their higher expression of *PDCD1* (Figure 2G). Anti-pPKCθ-iTregs also expressed more IFNγ than did DMSO-iTregs (Figure 2H). Therefore, we sought to further characterize DMSO-iTregs and anti-pPKCθ-iTregs to increase our understanding of their functional differences. We used imaging flow cytometry to ask whether surface PD-1 association with other signaling proteins differed between DMSO-iTregs and anti-pPKCθ-iTregs differentiated *ex vivo*. We detected higher PD-1-pPKCθ co-localization in anti-pPKCθ-iTregs (Figure 6A), even though pPKCθ is significantly reduced in these cells (Figure 2), suggesting that the much of the pPKCθ that is expressed in anti-pPKCθ-iTregs may be associated with surface PD-1. Downstream of CD28 signaling, NFATc1 is dephosphorylated on specific residues by the calcium-dependent phosphatase calcineurin, mediated by the enzymatic activity of the calcineurin B (CnB) subunit.[48] Dephosphorylating NFATc1 unmasks a nuclear localization signal that allows its nuclear import. Once in the nucleus, NFATc1 differentially associates with various transcription partners to regulate context-specific gene expression, including *IFNG*, *FOXP3*, and *PDCD1*.[49–51] Compared to DMSO-iTregs, we found that PD-1 colocalized with NFATc1 to a much greater extent in anti-pPKCθ-iTregs (Figure 6B). As a result, nuclear NFATc1 levels were significantly reduced in anti-pPKCθ-iTregs, although NFATc1 cytosolic levels were comparable regardless of iTreg treatment (Figure 6C). As with NFATc1, cytosolic CnB levels were comparable in DMSO-iTregs and anti-pPKCθ-iTregs, but DMSO-iTregs expressed significantly more nuclear CnB (Figure 6D). We determined that CnB functioned similarly in DMSO-iTregs and anti-pPKCθ-iTregs, since treating either with the CnB inhibitor, tacrolimus, equivalently reduced nuclear NFATc1 localization and concomitantly increased its cytosolic levels (Figure 6C). We also noted that tacrolimus treatment decreased the amount of nuclear CnB in DMSO-iTregs suggesting, perhaps, that NFATc1 and CnB are both imported into the nucleus of DMSO-iTregs (Figure 6D). This does not appear to be the case in anti-pPKCθ-iTregs, and it is possible that the increased association of NFATc1 with PD-1 in these cells makes it less accessible to dephosphorylation by CnB. Nuclear CnB has not been previously reported in T cells, and additional investigation is needed to determine whether CnB acts similarly in the nucleus to maintain a pool of dephosphorylated and, therefore, nuclear-resident NFATc1 in DMSO-iTregs.

NFATc1 and CnB Subcellular Localization in iTregs Is Associated with Signaling through IFNγ and PD-1

We next investigated whether NFATc1 or CnB localization was linked to PD-1 or IFNγ signaling in *ex vivo*-generated iTregs. During differentiation, we treated DMSO-iTregs and anti-pPKCθ-iTregs with antibodies to neutralize either IFNγ- or PD-1-initiated signaling, then used imaging flow cytometry to ask how modulating these cell-extrinsic signals affected NFATc1 and CnB localization. In DMSO-iTregs, both anti-IFNγ and anti-PD-1 treatment reduced nuclear NFATc1, while nuclear CnB was reduced following anti-IFNγ treatment only (Figures 7A and 7C). In stark contrast, in anti-pPKCθ-treated iTregs, only anti-IFNγ treatment increased nuclear NFATc1, while higher amounts of nuclear CnB were detected following anti-IFNγ or anti-PD-1 treatment (Figures 7B and 7D). These results clearly indicate that signaling downstream of PD-1 and IFNγ

Figure 4. Adoptively Transferring Anti-pPKCθ-iTregs Attenuates Disease and Prolongs Survival in a Humanized Mouse Model of GvHD

(A) Schematic representation of adoptive transfer of *ex vivo*-differentiated iTregs used in a humanized mouse model of GvHD. (B and C) Circulating white blood cells (WBCs), red blood cells (RBCs) (B), and bone marrow (BM) cellularity (C), with hematoxylin and eosin staining of sterna from untreated and iTreg-treated mice harvested 17 days after GvHD induction. Scale bars, 200 μm. (D and E) Percent (left) and absolute number (right) of human CD45$^+$ cells (D), and percent of human CD4 and CD8 T cells (E) in BM of untreated and iTreg-treated mice harvested 17 days after GvHD-induction. (F and G) Clinical scores (F) and Kaplan-Meier survival curves (G) for untreated and iTreg-treated mice; n = 5 mice per group. Data were pooled from and represent the mean ± SEM of three independent experiments. Kaplan-Meier statistical analysis was used to determine survival benefit. *$p < 0.05$, **$p < 0.01$, *** $p < 0.001$, by unpaired, two-tailed Student's t test.

Please cite this article in press as: Ozay et al., Cell-Penetrating Anti-Protein Kinase C Theta Antibodies Act Intracellularly to Generate Stable, Highly Suppressive Regulatory T Cells, Molecular Therapy (2020), https://doi.org/10.1016/j.ymthe.2020.05.020

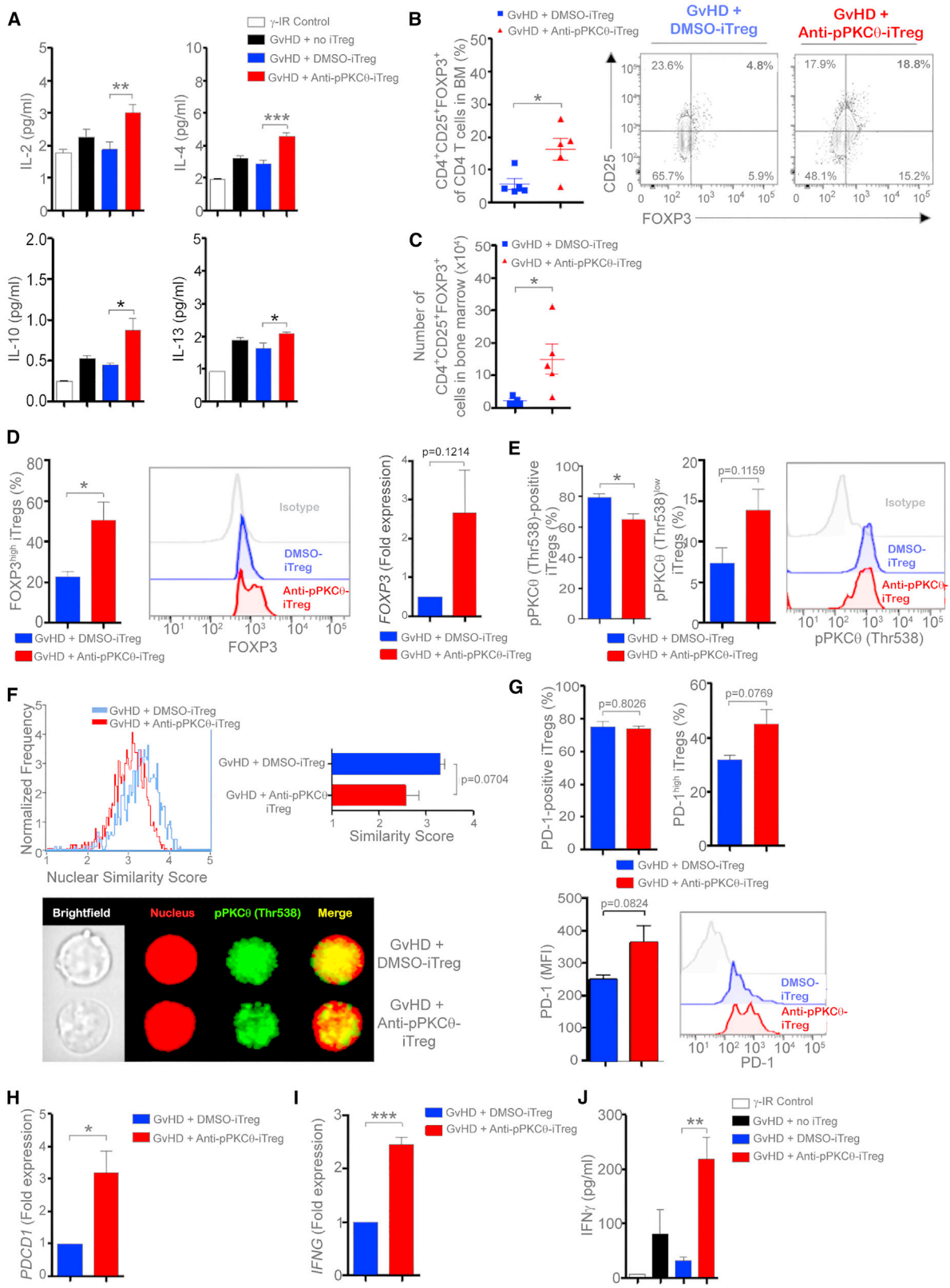

(legend on next page)

Please cite this article in press as: Ozay et al., Cell-Penetrating Anti-Protein Kinase C Theta Antibodies Act Intracellularly to Generate Stable, Highly Suppressive Regulatory T Cells, Molecular Therapy (2020), https://doi.org/10.1016/j.ymthe.2020.05.020

converges at the level of NFATc1 and CnB subcellular localization in iTregs, and this is further modulated when iTregs are treated with anti-pPKCθ during *ex vivo* differentiation.

DISCUSSION

In this study, we demonstrate that targeting pPKCθ using a cell-penetrating antibody enhanced *ex vivo* iTreg differentiation and expansion. Anti-pPKCθ-treated iTregs showed increased expression of FOXP3, the co-inhibitory receptor PD-1, and IFNγ. iTregs differentiated in the presence of anti-pPKCθ displayed a stable phenotype *in vivo* when examined 17 days after transfer into mice, using a humanized mouse model of GvHD, and were highly efficacious in attenuating symptoms and prolonging survival.

Cell-based therapies are being actively investigated within the developing field of personalized medicine, the use of which can minimize side effects and provide long-term management of immunological diseases.[44,52] T cells are highly specific, adaptable, "smart" therapeutic agents that selectively target tissues by tuning their activities in response to inflammatory microenvironments. Freshly isolated Tregs, administered together with BM allograft, can ameliorate GvHD and enhance HST engraftment.[53,54] Following *in vivo* administration, Tregs can exert their suppressive function by inhibiting effector T cell activation and altering cytokine production and migration. Tregs can downregulate DC maturation in a cell contact-dependent manner, inhibit monocyte and macrophage survival through Fas-FasL signaling, and constrain neutrophil activity by promoting their apoptosis.[55–58] Recent studies showed that, rather than isolating nTregs from patients and expanding them in culture, *ex vivo* conversion of $CD4^+CD25^-$ T cells into iTregs by culturing them with polarizing factors such as transforming growth factor β (TGF-β), IL-2, all-*trans* retinoic acid, DNA methyltransferase (DNMT) inhibitors, histone deacetylase (HDAC) inhibitors, butyrate, and/or rapamycin conveys greater immunosuppressive functions, making iTregs more attractive for immunotherapy.[59,60] In our study, we found that intracellular anti-PKCθ delivery, coupled with a standard differentiation protocol and anti-CD3 plus anti-CD28 stimulation, enhanced *ex vivo* iTreg differentiation. This strategy appears to be highly efficient for *ex vivo* iTreg generation, since anti-PKCθ-treated iTregs expressed higher levels of nuclear FOXP3, surface PD-1, and IFNγ, compared to DMSO-treated iTregs.

Additional obstacles to successful Treg-based immunotherapy involve maintaining Treg stability and reducing plasticity by sustaining FOXP3 expression, as well as proper trafficking to target organs, following adoptive transfer *in vivo*.[1,61,62] In our study, we utilized a humanized mouse model of GvHD that targets the BM for immune-mediated destruction. Our results demonstrated that mice treated with anti-pPKCθ-iTregs had significantly more $FOXP3^{high}$-expressing iTregs in the BM and experienced a greater reduction in the severity of GvHD, compared to mice treated with DMSO-iTregs. Furthermore, anti-pPKCθ-iTregs recovered from the BM of treated mice displayed an immunophenotype very similar to *ex vivo*-differentiated anti-pPKCθ-iTregs, suggesting these cells remain stable *in vivo*, even several weeks after transfer.

PKCθ has been implicated as a driver protein of aberrant T cell activation in the context of GvHD progression.[27,29] PKCθ is phosphorylated on Thr538 to complete its activation and facilitate its translocation both to the IS and to the nucleus.[19,35,63] Studies suggest that inhibiting PKCθ may constitute an effective therapy for T cell-mediated diseases,[22,25,26,64] and inhibiting PKCθ function in Tregs enhances their suppressive function both *in vitro* and *in vivo*.[21,23] However, these studies utilized small-molecule inhibitors that lacked the ability to specifically target PKCθ actions, potentially affecting closely related PKC family members, such as PKCα and PKCδ. Considering the greater specificity of antibody binding, we showed that we could modify PKCθ function in iTregs, using a highly specific cell-penetrating antibody-delivery strategy.

Molecular mechanisms that link reduced PKCθ signaling with transcriptional changes, as well as co-inhibitory receptor expression on the cell surface, remain to be fully elucidated. We observed near complete loss of nuclear pPKCθ and significantly reduced cytosolic anti-pPKCθ-iTregs. Studies suggest that PKCθ can be found in close proximity to PD-1 in the cytosol.[65,66] Indeed, PKCθ-PD1 co-localization was increased in anti-pPKCθ-iTregs, compared to DMSO-iTregs, potentially stabilizing PD-1 and enhancing iTreg PD-1-PD-L1-mediated suppression, which has been shown to be an important mechanism by which Tregs negatively regulate the immune response.[67]

Interestingly, anti-pPKCθ-iTregs exhibited high IFNγ expression both *in vitro* and *in vivo*. The actions of IFNγ in immune responses and inflammatory processes are paradoxical. IFNγ can facilitate Th1 differentiation and T cell migration to sites of inflammation and initiate proinflammatory signaling events. However, IFNγ-producing Th1 cells can also trigger the immune system to initiate control

Figure 5. *Ex Vivo* Generated Anti-pPKCθ-iTregs Exhibit a Stable, Unique $FOXP3^{high}PD\text{-}1^+IFN\gamma^{high}$ Phenotype *In Vivo*

(A) Plasma cytokine levels from control, untreated, and iTreg-treated mice 17 days after GvHD induction. (B and C) Percent and representative FACS plots (B) and total $CD4^+CD127^{-/low}CD25^+FOXP3^+$ iTregs (C) recovered from BM 17 days after GvHD induction. (D) Percent, representative histograms, and *FOXP3* expression in $CD4^+CD127^{-/low}CD25^+FOXP3^{high}$ iTregs recovered from BM 17 days after GvHD induction. (E) Percent $pPKC\theta^+$ and $pPKC\theta^{low}$ cells with representative histograms within the $CD4^+CD127^{-/low}CD25^+FOXP3^{high}$ iTregs recovered from BM 17 days after GvHD induction. (F) Nuclear localization score of pPKCθ-expressing cells, quantification of nuclear similarity scores for pPKCθ, and representative image showing nuclear pPKCθ in iTregs determined by AMNIS imaging flow cytometry analysis of 1,000 $CD4^+CD127^{-/low}CD25^+FOXP3^+$ iTregs recovered from BM 17 days after GvHD induction. (G) Percent $PD\text{-}1^+$ and $PD\text{-}1^{high}$ cells, with representative histograms of $CD4^+CD25^+FOXP3^+$ iTregs recovered from BM 17 days after GvHD-induction. (H and I) qPCR analysis of (H) *PDCD1* and (I) *IFNG* gene expression in $CD4^+CD25^+CD127^-$ iTregs recovered from BM 17 days after GvHD induction. (J) Plasma IFNγ levels from control, untreated, and iTreg-treated mice 17 days after GvHD induction. Data were pooled from four mice/treatment and represent the mean ± SEM of three independent experiments. $^*p < 0.05$, $^{**}p < 0.01$, $^{***}p < 0.001$, by unpaired, two-tailed Student's t test.

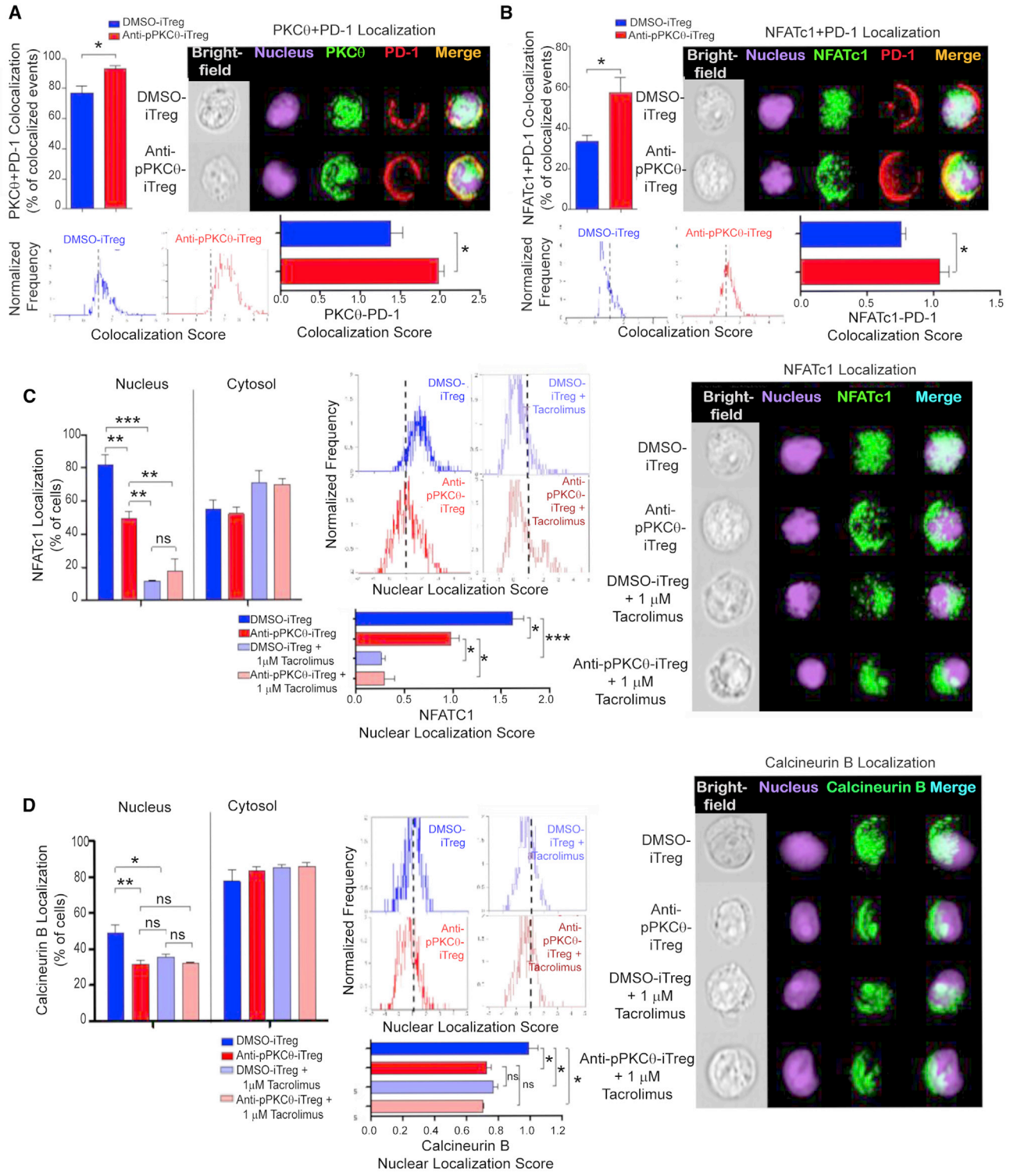

Figure 6. *Ex Vivo* Generated Anti-pPKCθ-iTregs Show Increased PD-1 Co-localization with PKCθ and NFATc1

(A and B) Percent of co-localized events, representative images, co-localization score distributions, and quantification of co-localization similarity scores for (A) PD-1-PKCθ and (B) PD-1-NFATc1 co-localization as determined by AMNIS imaging flow cytometry analysis of 1,000 iTregs differentiated without or with CPPM-anti-pPKCθ. (C and D) Percent of cells positive for nuclear and cytosolic (C) NFATc1 and (D) calcineurin B, together with representative nuclear localization score distributions, quantification of

(legend continued on next page)

Please cite this article in press as: Ozay et al., Cell-Penetrating Anti-Protein Kinase C Theta Antibodies Act Intracellularly to Generate Stable, Highly Suppressive Regulatory T Cells, Molecular Therapy (2020), https://doi.org/10.1016/j.ymthe.2020.05.020

mechanisms.[68] T cells require three signals for full activation: signal 1 is received through the TCR, signal 2 is a co-stimulatory signal (i.e., though the CD28 co-receptor), while signal 3 is mediated by cytokine receptors.[69] When naive T cells encounter elevated IFNγ, in the absence of signaling through the TCR and CD28, activation of multiple cellular and molecular events leads to peripheral conversion of $CD4^+CD25^-$ T cells to $CD4^+CD25^+$ Tregs, to regulate overt inflammation and suppress autoimmune responses.[68] It has been argued that the source of IFNγ is critical to driving either pro-inflammatory or anti-inflammatory responses in GvHD.[70,71] However, functional consequences of IFNγ production by Tregs in GvHD remain unexplored. It has been suggested that IFNγ produced by Tregs is advantageous in preventing allogeneic skin graft rejection.[40,41] Moreover, allogeneic donor FOXP3-expressing Tregs appeared to express IFNγ upon bone marrow transplantation (BMT) and prevented the development of lethal GvHD.[53,54] However, donor Tregs treated with neutralizing anti-IFNγ monoclonal antibody or Tregs from IFNγ-knockout donor mice failed to prevent the lethal GvHD.[40,70] Furthermore, STAT1, an important mediator in IFNγ signaling, was found to be critical to the induction of $CD4^+CD25^+$ Tregs.[72] Anti-pPKCθ delivery into iTregs leads to increased IFNγ. This finding is consistent with recent studies that showed perturbing the CARMA1-Bcl10-MALT-1 (CBM) complex in Tregs generates IFNγ-producing Tregs.[73,74] We previously showed that PKCθ interacts with the CBM complex.[75] Furthermore, delivering anti-pPKCθ into CD4 T cells prior to *in vitro* Th1 polarization reduces phosphorylation of the PKCθ substrate, CARMA1.[29] Thus, it is possible that in anti-pPKCθ-iTregs, we are similarly perturbing the CBM complex, leading to increased IFNγ production by these cells. Additional studies are needed to fully elucidate the mechanism driving this phenomenon. Anti-pPKCθ-iTregs produced significantly more IFNγ *in vitro* and *in vivo*, resulting in higher levels of IFNγ in the plasma from the mice that received anti-pPKCθ-iTregs. These findings, coupled with the presence of more $CD4^+CD25^+FOXP3^+$ iTregs in the BM of anti-pPKCθ-iTreg-treated mice, led us to conclude that IFNγ may act as both an extrinsic and intrinsic factor to promote iTreg differentiation and enhance their suppressive function in this humanized mouse model of GvHD.

The transcription factor NFATc1 functions to link extracellular stimuli to gene transcription, through its association with other transcriptional partners, including but not limited to AP-1, NF-κB, and the various Th master transcriptional regulators. Through selective pairing, NFATc1 can regulate both pro-inflammatory, i.e., cytokine production, and anti-inflammatory, i.e., PD-1 expression, genetic programs.[49,51] To generate anti-pPKCθ-iTregs, we provided co-stimulation though CD28 in the context of iTreg differentiation, together with anti-pPKCθ delivery. Therefore, it is entirely possible that we have altered NFATc1 availability for binding to its nuclear partners, thus generating unique regulation of iTreg genes, including regulation of FOXP3, PD-1, and IFNγ. Our data showing increased co-localization between NFATc1 and PD-1 in anti-pPKθ-iTregs supports this notion, in that its increased association with PD-1 may physically prevent CnB from accessing and dephosphorylating NFATc1, thus impeding its nuclear translocation. However, additional studies are needed to confirm this model.

Dephosphorylation by CnB is necessary to facilitate NFATc1 nuclear translocation.[76] Once in the nucleus it may be re-phosphorylated by one of several kinases, including GSK3β and casein kinase 1/2, promoting its export to the cytosol.[77] Compared to anti-pPKCθ-iTregs, DMSO-iTregs expressed higher amounts of nuclear NFATc1, and of nuclear CnB as well. This raises the intriguing possibility that a pool of nuclear CnB may function to keep NFATc1 dephosphorylated and, thus, nuclear-resident, in DMSO-iTregs. Reduced PKCθ activity is known to enhance GSK3β function.[78] Thus, it is equally intriguing to speculate that GSK3β may be acting to re-phosphorylate nuclear NFATc1 in anti-pPKCθ-iTregs to facilitate its nuclear export, accounting for the reduced amount of nuclear NFATc1 expressed in these cells. Further investigation would be required to determine whether this is, indeed, a mechanism that supports our observations.

Our results, together with supporting evidence from the literature, demonstrate that modulating PKCθ function in iTregs reprograms their cell fate and enhances their immunosuppressive capacity both *in vitro* and *in vivo*. Intracellular anti-pPKCθ delivery using cell-penetrating peptide mimics is a promising strategy to fine-tune iTreg differentiation to favor generating and expanding a unique and highly suppressive population, characterized by increased expression of FOXP3, PD-1, and IFNγ. More importantly, using a humanized model of GvHD, we show that adoptively transferring anti-pPKCθ-iTregs into mice is highly efficacious in attenuating the severity of GvHD *in vivo* when transferred at the time of disease induction. In humans, this would correlate to giving anti-pPKCθ-iTregs at the time of HSCT, with the prediction that the transferred iTregs would effectively suppress the rapidly expanding donor T cell population within the stem cell graft. Our data suggest that anti-pPKCθ-iTregs, generated from PBMCs of the stem cell donor, may have prophylactic value when given to recipients at the time of HSCT. However, note that all animal models have limitations, and extrapolating results from murine models to humans must be done with care. Further study is needed to answer remaining questions regarding optimal *ex vivo* differentiation conditions, optimal concentration and timing of doses, and the potential need for adjuvant immunosuppressive therapy that will enhance and not counteract iTreg administration. Nonetheless, our study constitutes a compelling argument to further explore the use of CPPM-antibody delivery as a means of programming immune cells *ex vivo* to generate readily available, stable, efficacious, and personalized cell-based therapeutics.

nuclear localization similarity scores, and representative images, as determined by AMNIS imaging flow cytometry analysis of 1,000 iTregs differentiated without or with CPPM-anti-pPKCθ, and without or with tacrolimus added during differentiation. Data represent the mean ± SEM of three independent experiments. *$p < 0.05$, **$p < 0.01$, ***$p < 0.001$, by unpaired, two-tailed Student's t test.

Please cite this article in press as: Ozay et al., Cell-Penetrating Anti-Protein Kinase C Theta Antibodies Act Intracellularly to Generate Stable, Highly Suppressive Regulatory T Cells, Molecular Therapy (2020), https://doi.org/10.1016/j.ymthe.2020.05.020

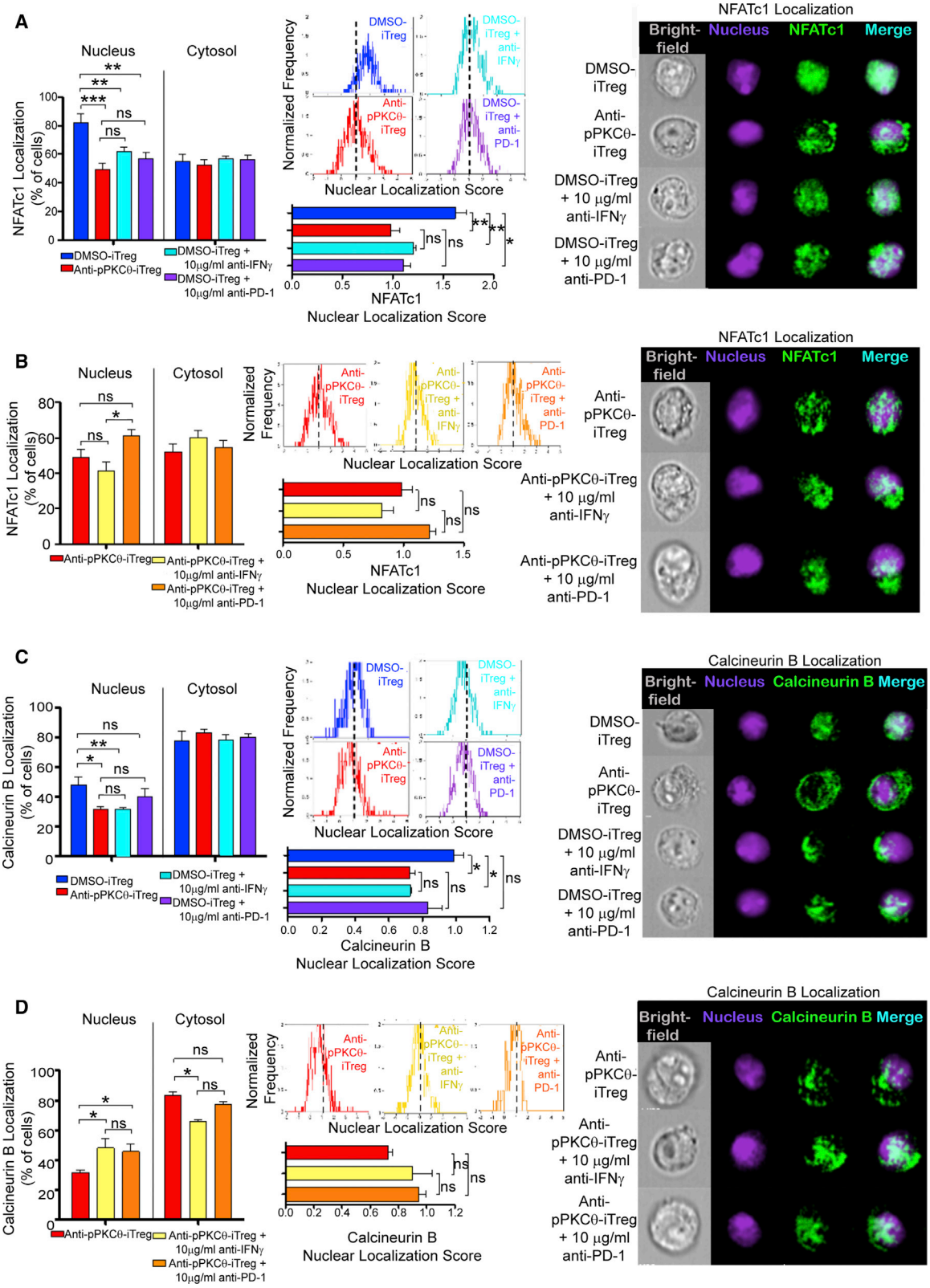

(legend on next page)

Please cite this article in press as: Ozay et al., Cell-Penetrating Anti-Protein Kinase C Theta Antibodies Act Intracellularly to Generate Stable, Highly Suppressive Regulatory T Cells, Molecular Therapy (2020), https://doi.org/10.1016/j.ymthe.2020.05.020

MATERIALS AND METHODS

Animals

All animal studies were approved by, and conducted under oversight of, the Institutional Animal Care and Use Committee of the University of Massachusetts, Amherst. Seven-week-old female NOD.Cg-*Prkdc*^{scid} *Il2rg*^{tm1Wjl}/SzJ (NSG) mice were purchased from The Jackson Laboratories (Bar Harbor, ME, USA). Mice were rested 1 week prior to use, housed under pathogen-free conditions in micro-isolator cages, and received acidified water (pH 3.0) supplemented with trimethoprim + sulfamethoxazole throughout the duration of the experimental procedures.

Antibodies and Reagents

Antibodies used in this study were as follows: CD3ε (clone UCHT1), CD28 (clone CD28.2), CD4 (clone RPA-T4), CD8 (clone RPA-T8), CD25 (clone BC96), CD25 (clone BC96), CD25 (clone BC96), CD45RA (clone HI100), CD45RO (clone UCHL1), CD127 (clone A019D5), CD127 (clone A019D5), PD-1 (clone EH12.2H7), and NFATc1 (clone7A6), all from BioLegend (San Diego, CA, USA); CD4/CD8 cocktail (clones RPA-T4 and RPA-T8) and human CD45 (clone 2D1) from eBioscience (Santa Clara, CA, USA); mouse CD45 (clone 30-F11) and IFNγ (clone B27) from BD Biosciences (Billerica, MA, USA); histone H3 (clone 96C10), pPKCθ (Thr538), and total PKCθ (clone E1I7Y) from Cell Signaling Technology (Danvers, MA, USA); anti-PP2B-B1/2 (CnB; clone D-1) from Santa Cruz Biotechnology (Santa Cruz, CA, USA); α-Tubulin (clone B-5-1-2) from Sigma-Aldrich (St. Louis, MO, USA); and pPKCθ (Thr538; clone F4H4L1) and F(ab′)$_2$-goat anti-rabbit IgG (H+L) secondary antibody (Qdot625, polyclonal) from Life Technologies (Carlsbad, CA, USA). For nuclear staining, DRAQ5^{TM} was obtained from Thermo Fisher Scientific (Waltham, MA, USA). Live/dead staining was performed utilizing either Zombie Aqua or Zombie Violet fixable viability kit (BioLegend). For *in vitro* suppression assay, cells were tracked using labeling with CytoTell UltraGreen or CytoTell Red650 (AAT Bioquest, Sunnyvale, CA, USA). Tacrolimus was obtained from Thermo Fisher Scientific (Agawam, MA, USA).

Human iTreg Differentiation Coupled with Intracellular CPPM-Anti-pPKCθ Delivery

1 μM CPPM ($P_{13}D_5$) and 25 nM of anti-pPKCθ (Thr538, clone F4H4L1) were complexed in PBS (phosphate-buffered saline, pH 7.2) at a 40:1 ratio (CPPM/anti-pPKCθ) for 30 min at room temperature (RT). CD4 T cells were isolated from human PBMCs (STEMCELL Technologies, Vancouver, BC, Canada) using a MojoSort human T cell isolation kit (BioLegend). Isolated human CD4 T cells were treated with the CPPM-antibody complex for 4 h at 37°C or DMSO as vehicle control. Cells were harvested and washed with PBS, then washed twice with 20 U/mL heparin in PBS for 5 min on ice to remove cell surface-bound complexes. For iTreg differentiation, a CellXVivo human Treg differentiation kit (R&D Systems, Minneapolis, MN, USA) was used and iTreg differentiation media were prepared using X-VIVO 15 chemically defined, serum-free hematopoietic cell medium according to the manufacturer's instructions. Treated cell pellets were resuspended in iTreg differentiation media and seeded onto wells of a 12-well tissue culture plate precoated with 5 μg/mL anti-CD3ε plus 2.5 μg/mL anti-CD28, and stimulated for 5 days at 37°C.

Immunoblotting

iTregs were harvested on day 5 of differentiation. Nuclear and cytosolic extracts were prepared using NE-PER nuclear and cytosolic extraction kit (Thermo Scientific). 1× SDS Laemmli buffer was added to samples, which were separated on 8% gels using SDS-PAGE. Blots were probed with anti-pPKCθ (Thr538) and anti-total PKCθ, then reprobed using anti-α-tubulin and anti-histone H3 as cytosolic and nuclear loading controls, respectively.

Protein Subcellular Localization Using AMNIS Imaging Flow Cytometry

For *ex vivo* analysis, iTregs were harvested on day 5 of differentiation. For *in vivo* analysis, BM, spleen, and peripheral blood were collected on day 17 and single-cell suspensions were prepared from each sample. Cells were surface stained for CD4 and CD25. Each sample was then fixed and permeabilized according to the manufacturer's directions using the Foxp3 staining buffer kit (BD Biosciences) and stained for FOXP3, NFATc1, CnB, and pPKCθ (Thr538) followed by Qdot625-labeled secondary antibody. Nuclei were stained using the cell-permeable DRAQ5 fluorescent probe (Thermo Fisher Scientific). Cells were visualized and quantified using an ImageStream^{X} Mk II imaging flow cytometer (EMD Millipore, Billerica, MA, USA). Subcellular localization and nuclear similarity scores for FOXP3, pPKCθ (Thr538), NFATc1, and CnB proteins were determined using the nuclear localization wizard and the IDEAS software following masking of nuclear and non-nuclear regions to quantify proteins localized out of and within the nucleus, respectively.

In Vitro Suppression Assay

On day 0, human CD4 T cells were plated onto anti-CD3+anti-CD28-coated wells and differentiated for 5 days in iTreg differentiation media. On day 5, iTregs (suppressors) were loaded with the cell tracker dye Red650 (allophycocyanin [APC] fluorescence). Total hPBMCs (responders) were thawed and stimulated with soluble anti-CD3+anti-CD28 and crosslinked using mouse IgG. Responder cells were then loaded with a different cell tracker dye, UltraGreen

Figure 7. NFATc1 and Calcineurin B Subcellular Localization in iTregs Is Associated with Signaling through IFNγ and PD-1

(A–D) Percent of cells positive for nuclear and cytosolic (A and B) NFATc1 and (C and D) calcineurin B, together with representative nuclear localization score distributions, quantification of nuclear localization similarity scores, and representative images, as determined by AMNIS imaging flow cytometry analysis of 1,000 iTregs differentiated without or with CPPM-anti-pPKCθ. (A and C) DMSO-iTregs and (A–D) anti-pPKCθ-iTregs were treated with or without anti-IFNγ or anti-PD-1 during iTreg differentiation. Data represent the mean ± SEM of three independent experiments. *$p < 0.05$, **$p < 0.01$, ***$p < 0.001$, by unpaired, two-tailed Student's t test.

Please cite this article in press as: Ozay et al., Cell-Penetrating Anti-Protein Kinase C Theta Antibodies Act Intracellularly to Generate Stable, Highly Suppressive Regulatory T Cells, Molecular Therapy (2020), https://doi.org/10.1016/j.ymthe.2020.05.020

(fluorescein isothiocyanate [FITC] fluorescence). Responder cells were seeded onto tissue culture plates and suppressors were added to responders at the indicated ratio. Cells were co-cultured for 4 days and proliferation of responder and suppressor cells was determined. Percent suppression was calculated as follows: Suppression (%) = 100% − FITC-negative cells (%).

Surface versus Intracellular Expression of Co-inhibitory Receptors

iTregs were harvested on day 5 of differentiation. Cells were stained with Zombie Aqua viability dye. For surface-only expression, cells were directly stained using PD-1. For surface+intracellular expression, cells were surface stained, then fixed and permeabilized according to the manufacturer's directions using the Foxp3 staining buffer kit, followed by staining with anti-PD-1. Samples were acquired using a BD LSRFortessa flow cytometer (Becton Dickinson) and MFIs were calculated. For intracellular-only expression, MFI of surface staining was subtracted from MFI of surface+intracellular staining.

Quantitative Real-Time PCR

Total RNA was isolated from samples using a Quick-RNA isolation kit (Zymo Research, Irvine, CA, USA) according to the manufacturer's protocol. 1 μg of total RNA was reverse-transcribed to cDNA using dNTP (2′-deoxynucleoside 5′-triphosphate) (New England Biolabs, Ipswich, MA, USA), Moloney murine leukemia virus (M-MuLV) reverse transcription buffer (New England Biolabs), oligo(dT) (Promega, Madison, WI, USA), RNase inhibitor (Promega), and M-MuLV reverse transcriptase (New England Biolabs) on a Mastercycler gradient thermal cycler (Eppendorf, Hamburg, Germany). Quantitative real-time PCR primers used in this study are listed in Table S1. Quantitative real-time PCR was performed in duplicate with 2× SYBR Green qPCR master mix (BioTool, Houston, TX, USA) using the RealPlex2 system (Eppendorf). Quantitative real-time PCR conditions were as follows: 95°C for 1 min, 95°C for 25 s, 62°C for 25 s (40 cycles), 95°C for 1 min, 62°C for 1 min, and 95°C for 30 s. Relative gene expression was determined using the ΔΔCt method. The results are presented as fold gene expression normalized to the housekeeping gene β-actin and relative to Tconv+DMSO samples for *ex vivo* experiments and relative to naive+DMSO for *in vivo* experiments.

In Vivo Suppression Analysis Using Adoptive Transfer of iTregs in a Humanized GvHD Model

CD4 T cells were isolated from healthy donor hPBMCs, subsequently treated with the CPPM-anti-pPKCθ complex, and differentiated for 5 days into iTregs, as described. On day 4, total hPBMCs from the same donor were thawed and rested overnight in fresh RPMI 1640 complete media (10% fetal bovine serum, 100 U/mL penicillin-streptomycin, 1 mM sodium pyruvate, 2 mM L-glutamine) at 37°C in 5% CO_2 incubator. On day 5, NOD.Cg-*Prkdc*^{scid} *Il2rg*^{tm1WjI}/SzJ (NSG) mice were conditioned with 2 Gy of total body irradiation using a ^{137}Cs source and then rested for 4–6 h. 10×10^6 hPBMCs were mixed with 3.3×10^6 iTregs and adoptively transferred into irradiated NSG mice via the tail vein. Body weight and disease symptoms were observed daily. On day 17, some animals were sacrificed for tissue analysis. After CO_2 asphyxiation, peripheral blood was obtained using cardiac puncture. Sterna and spleens were collected for histology. BM cells were recovered from the tibias and femurs of both legs by flushing the bones with complete RPMI 1640 media. Splenocytes were isolated by manipulation through a 40-μm filter. Red blood cells were lysed in ACK lysis buffer, and the remaining white blood cells were enumerated using trypan blue exclusion. White and red cell counts were performed using a scil Vet abc hematology analyzer (scil Animal Care, Gurnee, IL, USA). BM, spleen, and peripheral blood were assessed for percent engraftment of hPBMCs [% positive human CD45/(% positive human CD45 cells + % positive mouse CD45 cells)] and infiltration of human CD4 and CD8 T cells. Human CD4 T cells were also analyzed for CD25, CD127, FOXP3, PD-1, and pPKCθ (Thr538) expression.

GvHD Clinical Scoring

GvHD severity was assessed using a standardized scoring system, as previously described,[36] which included five different criteria (weight loss, posture, activity, fur texture, and skin integrity). Mice were weighed, evaluated daily, and graded from 0 (least severe) to 2 (most severe) for each criterion, beginning day 12 after disease induction. Daily clinical scores were generated by adding the grades for the five criteria. When a clinical score of 8 was reached, mice were removed from the study and humanely euthanized. The day animals were from the study was recorded as the day of lethal GvHD induction.

Magnetic Sorting of *In Vivo* iTregs for mRNA Analysis

BM and spleens were collected from NSG mice 17 days after GvHD induction. BM cells were recovered from the tibias and femurs. Splenocytes were isolated by manipulation through a 40-μm filter. Red blood cells were lysed in ACK lysis buffer, and the remaining white blood cells were enumerated using trypan blue exclusion. Cells were incubated with human CD4 T lymphocyte enrichment cocktail (BD Biosciences) followed by incubation with BD IMag streptavidin particles plus (BD Biosciences) to deplete the non-CD4 T cell fraction. Biotinylated anti-CD127 antibody and biotinylated anti-CD25 antibody, followed by an incubation with BD IMag streptavidin particles plus, were applied sequentially to obtain the iTreg fraction ($CD127^-CD25^+$) and naive T cell fraction ($CD127^+CD25^-$). Total RNA was obtained from isolated cells as described.

Histology

Sterna and spleens harvested on day 17 were fixed overnight in 10% neutral buffered formalin (NBF) (VWR, Radnor, PA, USA), decalcified 48 h (Cal-Rite; Richard Allen Scientific, San Diego, CA, USA), preserved in 70% ethanol at 4°C until processed, paraffin embedded, sectioned, and stained with hematoxylin and eosin.

LEGENDPlex Bead-Based Immunoassay

Peripheral blood for cytokine analysis was obtained in heparin-coated syringes from animals via cardiac puncture, immediately after humane euthanasia on day 17. The LEGENDPlex Human Th1/Th2 panel (8-plex; BioLegend) was used to determine the level of IFNγ, IL-2, IL-4, and IL-10. Data were acquired using a BD LSRFortessa

flow cytometer and analyzed using LEGENDPlex software, version 7.0 (BioLegend).

Statistical Analysis

The results shown are the mean ± SEM; all *ex vivo* experimental replicates were repeated at least three times. All *in vivo* experimental replicates were repeated in three separate experiments. An unpaired, two-tailed Student's t test using Prism 5 (GraphPad, San Diego, CA, USA) was used for statistical comparison of two groups, with Welch's correction applied when variances were significantly different. Survival benefit was determined using Kaplan-Meier analysis with an applied log rank test. p values of ≤ 0.05 were considered significantly different.

SUPPLEMENTAL INFORMATION

Supplemental Information can be found online at https://doi.org/10.1016/j.ymthe.2020.05.020.

AUTHOR CONTRIBUTIONS

Conceptualizations: E.I.O. and L.M.M. Methodology: E.I.O., S.S., and L.M.M. Investigations: E.I.O., S.S., H.L.S., and J.A.T. Writing – Original Draft: E.I.O. and L.M.M. Writing – Review & Editing: E.I.O., B.A.O., and L.M.M. Project Administration: G.N.T. and L.M.M. Funding Acquisition: B.A.O. and L.M.M. Supervision: B.A.O., G.N.T., and L.M.M.

CONFLICTS OF INTEREST

The authors declare no competing interests.

ACKNOWLEDGMENTS

The authors thank A.S. Burnside, Director of the Flow Cytometry Core Facility at the Institute for Applied Life Sciences, University of Massachusetts Amherst, Amherst, MA, for guidance, the University of Massachusetts Amherst Animal Care staff for excellent care of research animals, and R.A. Goldsby for critical assessment of the manuscript. This work was supported in part by the National Institutes of Health in the form of a Fellowship from the University of Massachusetts to H.L.S. as part of the Biotechnology Training Program (National Research Service Award T GM108556), by the National Institutes of Health (NIH 5P01CA16600 to B.A.O.), and by the Department of Defense (W81XWH1910540 to L.M.M.).

REFERENCES

1. Ohkura, N., Kitagawa, Y., and Sakaguchi, S. (2013). Development and maintenance of regulatory T cells. Immunity *38*, 414–423.
2. Hori, S., Nomura, T., and Sakaguchi, S. (2003). Control of regulatory T cell development by the transcription factor Foxp3. Science *299*, 1057–1061.
3. Khattri, R., Cox, T., Yasayko, S.A., and Ramsdell, F. (2003). An essential role for Scurfin in $CD4^+CD25^+$ T regulatory cells. Nat. Immunol. *4*, 337–342.
4. Sakaguchi, S., Miyara, M., Costantino, C.M., and Hafler, D.A. (2010). $FOXP3^+$ regulatory T cells in the human immune system. Nat. Rev. Immunol. *10*, 490–500.
5. Brunkow, M.E., Jeffery, E.W., Hjerrild, K.A., Paeper, B., Clark, L.B., Yasayko, S.A., Wilkinson, J.E., Galas, D., Ziegler, S.F., and Ramsdell, F. (2001). Disruption of a new forkhead/winged-helix protein, scurfin, results in the fatal lymphoproliferative disorder of the scurfy mouse. Nat. Genet. *27*, 68–73.
6. Fontenot, J.D., Rasmussen, J.P., Williams, L.M., Dooley, J.L., Farr, A.G., and Rudensky, A.Y. (2005). Regulatory T cell lineage specification by the forkhead transcription factor Foxp3. Immunity *22*, 329–341.
7. Liu, W., Putnam, A.L., Xu-Yu, Z., Szot, G.L., Lee, M.R., Zhu, S., Gottlieb, P.A., Kapranov, P., Gingeras, T.R., Fazekas de St Groth, B., et al. (2006). CD127 expression inversely correlates with FoxP3 and suppressive function of human $CD4^+$ T reg cells. J. Exp. Med. *203*, 1701–1711.
8. Simonetta, F., Chiali, A., Cordier, C., Urrutia, A., Girault, I., Bloquet, S., Tanchot, C., and Bourgeois, C. (2010). Increased CD127 expression on activated $FOXP3^+CD4^+$ regulatory T cells. Eur. J. Immunol. *40*, 2528–2538.
9. Ganguly, S., Ross, D.B., Panoskaltsis-Mortari, A., Kanakry, C.G., Blazar, B.R., Levy, R.B., and Luznik, L. (2014). Donor $CD4^+$ $Foxp3^+$ regulatory T cells are necessary for posttransplantation cyclophosphamide-mediated protection against GVHD in mice. Blood *124*, 2131–2141.
10. Lee, E.S., Lim, J.-Y., Im, K.-I., Kim, N., Nam, Y.-S., Jeon, Y.-W., and Cho, S.-G. (2015). Adoptive transfer of Treg cells combined with mesenchymal stem cells facilitates repopulation of endogenous Treg cells in a murine acute GVHD model. PLoS ONE *10*, e0138846.
11. Komanduri, K.V., and Champlin, R.E. (2011). Can Treg therapy prevent GVHD? Blood *117*, 751–752.
12. Lu, S.Y., Huang, X.J., Liu, K.Y., Liu, D.H., and Xu, L.P. (2012). High frequency of $CD4^+$ $CD25^-$ $CD69^+$ T cells is correlated with a low risk of acute graft-versus-host disease in allotransplants. Clin. Transplant. *26*, E158–E167.
13. Pankratz, S., Bittner, S., Herrmann, A.M., Schuhmann, M.K., Ruck, T., Meuth, S.G., and Wiendl, H. (2014). Human $CD4^+$ HLA-G^+ regulatory T cells are potent suppressors of graft-versus-host disease in vivo. FASEB J. *28*, 3435–3445.
14. Shevach, E.M. (2009). Mechanisms of $Foxp3^+$ T regulatory cell-mediated suppression. Immunity *30*, 636–645.
15. Nguyen, V.H., Zeiser, R., Dasilva, D.L., Chang, D.S., Beilhack, A., Contag, C.H., and Negrin, R.S. (2007). In vivo dynamics of regulatory T-cell trafficking and survival predict effective strategies to control graft-versus-host disease following allogeneic transplantation. Blood *109*, 2649–2656.
16. Isakov, N., and Altman, A. (2002). Protein kinase Cθ in T cell activation. Annu. Rev. Immunol. *20*, 761–794.
17. Gupta, S., Manicassamy, S., Vasu, C., Kumar, A., Shang, W., and Sun, Z. (2008). Differential requirement of PKC-θ in the development and function of natural regulatory T cells. Mol. Immunol. *46*, 213–224.
18. Sun, Z., Arendt, C.W., Ellmeier, W., Schaeffer, E.M., Sunshine, M.J., Gandhi, L., Annes, J., Petrzilka, D., Kupfer, A., Schwartzberg, P.L., and Littman, D.R. (2000). PKC-θ is required for TCR-induced NF-κB activation in mature but not immature T lymphocytes. Nature *404*, 402–407.
19. Isakov, N., and Altman, A. (2012). PKC-theta-mediated signal delivery from the TCR/CD28 surface receptors. Front. Immunol. *3*, 273.
20. Sumoza-Toledo, A., Eaton, A.D., and Sarukhan, A. (2006). Regulatory T cells inhibit protein kinase Cθ recruitment to the immune synapse of naive T cells with the same antigen specificity. J. Immunol. *176*, 5779–5787.
21. Zanin-Zhorov, A., Ding, Y., Kumari, S., Attur, M., Hippen, K.L., Brown, M., Blazar, B.R., Abramson, S.B., Lafaille, J.J., and Dustin, M.L. (2010). Protein kinase C-θ mediates negative feedback on regulatory T cell function. Science *328*, 372–376.
22. Zhang, E.Y., Kong, K.F., and Altman, A. (2013). The yin and yang of protein kinase C-theta (PKCθ): a novel drug target for selective immunosuppression. Adv. Pharmacol. *66*, 267–312.
23. Roybal, K.T., and Wülfing, C. (2010). Inhibiting the inhibitor of the inhibitor: blocking PKC-θ to enhance regulatory T cell function. Sci. Signal. *3*, pe24.
24. Boschelli, D.H. (2009). Small molecule inhibitors of PKCθ as potential antiinflammatory therapeutics. Curr. Top. Med. Chem. *9*, 640–654.
25. Sun, Z. (2012). Intervention of PKC-θ as an immunosuppressive regimen. Front. Immunol. *3*, 225.
26. Isakov, N. (2012). PKCθ is a key regulator of T-cell behavior and a drug target for T cell- mediated diseases. J. Clin. Cell. Immunol. *S12*, 008.

27. Valenzuela, J.O., Iclozan, C., Hossain, M.S., Prlic, M., Hopewell, E., Bronk, C.C., Wang, J., Celis, E., Engelman, R.W., Blazar, B.R., et al. (2009). PKCθ is required for alloreactivity and GVHD but not for immune responses toward leukemia and infection in mice. J. Clin. Invest. *119*, 3774–3786.

28. Mochly-Rosen, D., Das, K., and Grimes, K.V. (2012). Protein kinase C, an elusive therapeutic target? Nat. Rev. Drug Discov. *11*, 937–957.

29. Ozay, E.I., Gonzalez-Perez, G., Torres, J.A., Vijayaraghavan, J., Lawlor, R., Sherman, H.L., Garrigan, D.T., Jr., Burnside, A.S., Osborne, B.A., Tew, G.N., and Minter, L.M. (2016). Intracellular delivery of Anti-pPKCθ (Thr538) via protein transduction domain mimics for immunomodulation. Mol. Ther. *24*, 2118–2130.

30. Joffre, O., Gorsse, N., Romagnoli, P., Hudrisier, D., and van Meerwijk, J.P.M. (2004). Induction of antigen-specific tolerance to bone marrow allografts with $CD4^+CD25^+$ T lymphocytes. Blood *103*, 4216–4221.

31. Taylor, P.A., Panoskaltsis-Mortari, A., Swedin, J.M., Lucas, P.J., Gress, R.E., Levine, B.L., June, C.H., Serody, J.S., and Blazar, B.R. (2004). L-Selectin^{hi} but not the L-selectin^{lo} $CD4^+25^+$ T-regulatory cells are potent inhibitors of GVHD and BM graft rejection. Blood *104*, 3804–3812.

32. Trzonkowski, P., Bieniaszewska, M., Juścińska, J., Dobyszuk, A., Krzystyniak, A., Marek, N., Myśliwska, J., and Hellmann, A. (2009). First-in-man clinical results of the treatment of patients with graft versus host disease with human ex vivo expanded $CD4^+CD25^+CD127^-$ T regulatory cells. Clin. Immunol. *133*, 22–26.

33. Chuang, H.C., Lan, J.L., Chen, D.Y., Yang, C.Y., Chen, Y.M., Li, J.P., Huang, C.Y., Liu, P.E., Wang, X., and Tan, T.H. (2011). The kinase GLK controls autoimmunity and NF-κB signaling by activating the kinase PKC-θ in T cells. Nat. Immunol. *12*, 1113–1118.

34. Du, X., Shi, H., Li, J., Dong, Y., Liang, J., Ye, J., Kong, S., Zhang, S., Zhong, T., Yuan, Z., et al. (2014). *Mst1*/*Mst2* regulate development and function of regulatory T cells through modulation of Foxo1/Foxo3 stability in autoimmune disease. J. Immunol. *192*, 1525–1535.

35. Sutcliffe, E.L., Bunting, K.L., He, Y.Q., Li, J., Phetsouphanh, C., Seddiki, N., Zafar, A., Hindmarsh, E.J., Parish, C.R., Kelleher, A.D., et al. (2011). Chromatin-associated protein kinase C-θ regulates an inducible gene expression program and microRNAs in human T lymphocytes. Mol. Cell *41*, 704–719.

36. Thaventhiran, T., Sethu, S., Yeang, H.X.A., Al-Huseini, L., Hamdam, J., and Sathish, J.G. (2013). T cell co-inhibitory receptors-functions and signalling mechanisms. J. Clin. Cell. Immunol. *S12*, 004.

37. Wang, X.B., Zheng, C.Y., Giscombe, R., and Lefvert, A.K. (2001). Regulation of surface and intracellular expression of CTLA-4 on human peripheral T cells. Scand. J. Immunol. *54*, 453–458.

38. Woo, S.R., Li, N., Bruno, T.C., Forbes, K., Brown, S., Workman, C., Drake, C.G., and Vignali, D.A. (2010). Differential subcellular localization of the regulatory T-cell protein LAG-3 and the coreceptor CD4. Eur. J. Immunol. *40*, 1768–1777.

39. Raimondi, G., Shufesky, W.J., Tokita, D., Morelli, A.E., and Thomson, A.W. (2006). Regulated compartmentalization of programmed cell death-1 discriminates $CD4^+CD25^+$ resting regulatory T cells from activated T cells. J. Immunol. *176*, 2808–2816.

40. Koenecke, C., Lee, C.-W., Thamm, K., Föhse, L., Schafferus, M., Mittrücker, H.-W., Floess, S., Huehn, J., Ganser, A., Förster, R., and Prinz, I. (2012). IFN-γ production by allogeneic $Foxp3^+$ regulatory T cells is essential for preventing experimental graft-versus-host disease. J. Immunol. *189*, 2890–2896.

41. Sawitzki, B., Kingsley, C.I., Oliveira, V., Karim, M., Herber, M., and Wood, K.J. (2005). IFN-γ production by alloantigen-reactive regulatory T cells is important for their regulatory function in vivo. J. Exp. Med. *201*, 1925–1935.

42. Francisco, L.M., Sage, P.T., and Sharpe, A.H. (2010). The PD-1 pathway in tolerance and autoimmunity. Immunol. Rev. *236*, 219–242.

43. Magg, T., Mannert, J., Ellwart, J.W., Schmid, I., and Albert, M.H. (2012). Subcellular localization of FOXP3 in human regulatory and nonregulatory T cells. Eur. J. Immunol. *42*, 1627–1638.

44. Hahn, S.A., Bellinghausen, I., Trinschek, B., and Becker, C. (2015). Translating Treg therapy in humanized mice. Front. Immunol. *6*, 623.

45. Fang, Z., Hua, Z., Changying, L., Jianmin, W., Chengjuan, L., Kangli, X., and Jing, C. (2013). High level of $CD4^+CD25^+CD127^-$ Treg cells in donor graft is associated with a low risk of aGVHD after allo-HSCT for children with hematologic malignancies. J. Cell Sci. Ther. *4*, 148.

46. Beres, A.J., and Drobyski, W.R. (2013). The role of regulatory T cells in the biology of graft versus host disease. Front. Immunol. *4*, 163.

47. Kinter, A.L., Godbout, E.J., McNally, J.P., Sereti, I., Roby, G.A., O'Shea, M.A., and Fauci, A.S. (2008). The common γ-chain cytokines IL-2, IL-7, IL-15, and IL-21 induce the expression of programmed death-1 and its ligands. J. Immunol. *181*, 6738–6746.

48. Hogan, P.G., Chen, L., Nardone, J., and Rao, A. (2003). Transcriptional regulation by calcium, calcineurin, and NFAT. Genes Dev. *17*, 2205–2232.

49. Kiani, A., García-Cózar, F.J., Habermann, I., Laforsch, S., Aebischer, T., Ehninger, G., and Rao, A. (2001). Regulation of interferon-γ gene expression by nuclear factor of activated T cells. Blood *98*, 1480–1488.

50. Vaeth, M., Schliesser, U., Müller, G., Reissig, S., Satoh, K., Tuettenberg, A., Jonuleit, H., Waisman, A., Müller, M.R., Serfling, E., et al. (2012). Dependence on nuclear factor of activated T-cells (NFAT) levels discriminates conventional T cells from $Foxp3^+$ regulatory T cells. Proc. Natl. Acad. Sci. USA *109*, 16258–16263.

51. Bally, A.P.R., Austin, J.W., and Boss, J.M. (2016). Genetic and epigenetic regulation of PD-1 expression. J. Immunol. *196*, 2431–2437.

52. Fishbach, M.A., Bluestone, J.A., and Lim, W.A. (2013). Cell-based therapeutics: the next pillar of medicine. Sci. Transl. Med *5*, 179ps7.

53. Taylor, P.A., Lees, C.J., and Blazar, B.R. (2002). The infusion of ex vivo activated and expanded $CD4^+CD25^+$ immune regulatory cells inhibits graft-versus-host disease lethality. Blood *99*, 3493–3499.

54. Hoffmann, P., Ermann, J., Edinger, M., Fathman, C.G., and Strober, S. (2002). Donor-type $CD4^+CD25^+$ regulatory T cells suppress lethal acute graft-versus-host disease after allogeneic bone marrow transplantation. J. Exp. Med. *196*, 389–399.

55. Misra, N., Bayry, J., Lacroix-Desmazes, S., Kazatchkine, M.D., and Kaveri, S.V. (2004). Cutting edge: human $CD4^+CD25^+$ T cells restrain the maturation and antigen-presenting function of dendritic cells. J. Immunol. *172*, 4676–4680.

56. Taams, L.S., van Amelsfort, J.M., Tiemessen, M.M., Jacobs, K.M., de Jong, E.C., Akbar, A.N., Bijlsma, J.W., and Lafeber, F.P. (2005). Modulation of monocyte/macrophage function by human $CD4^+CD25^+$ regulatory T cells. Hum. Immunol. *66*, 222–230.

57. Venet, F., Pachot, A., Debard, A.L., Bohe, J., Bienvenu, J., Lepape, A., Powell, W.S., and Monneret, G. (2006). Human $CD4^+CD25^+$ regulatory T lymphocytes inhibit lipopolysaccharide-induced monocyte survival through a Fas/Fas ligand-dependent mechanism. J. Immunol. *177*, 6540–6547.

58. Lewkowicz, P., Lewkowicz, N., Sasiak, A., and Tchórzewski, H. (2006). Lipopolysaccharide-activated $CD4^+CD25^+$ T regulatory cells inhibit neutrophil function and promote their apoptosis and death. J. Immunol. *177*, 7155–7163.

59. Lu, L., Lan, Q., Li, Z., Zhou, X., Gu, J., Li, Q., Wang, J., Chen, M., Liu, Y., Shen, Y., et al. (2014). Critical role of all-trans retinoic acid in stabilizing human natural regulatory T cells under inflammatory conditions. Proc. Natl. Acad. Sci. USA *111*, E3432–E3440.

60. Schmidt, A., Éliás, S., Joshi, R.N., and Tegnér, J. (2016). In vitro differentiation of human CD4+FOXP3+ induced regulatory T cells (iTregs) from naïve $CD4^+$ T cells using a TGF-β-containing protocol. J. Vis. Exp. *30*, 55015.

61. Li, X., Liang, Y., LeBlanc, M., Benner, C., and Zheng, Y. (2014). Function of a Foxp3 *cis*-element in protecting regulatory T cell identity. Cell *158*, 734–748.

62. Booth, N.J., McQuaid, A.J., Sobande, T., Kissane, S., Agius, E., Jackson, S.E., Salmon, M., Falciani, F., Yong, K., Rustin, M.H., et al. (2010). Different proliferative potential and migratory characteristics of human $CD4^+$ regulatory T cells that express either CD45RA or CD45RO. J. Immunol. *184*, 4317–4326.

63. Bi, K., Tanaka, Y., Coudronniere, N., Sugie, K., Hong, S., van Stipdonk, M.J., and Altman, A. (2001). Antigen-induced translocation of PKC-theta to membrane rafts is required for T cell activation. Nat. Immunol. *2*, 556–563.

64. Chand, S., Mehta, N., Bahia, M.S., Dixit, A., and Silakari, O. (2012). Protein kinase C-θ inhibitors: a novel therapy for inflammatory disorders. Curr. Pharm. Des. *18*, 4725–4746.

65. Yokosuka, T., Takamatsu, M., Kobayashi-Imanishi, W., Hashimoto-Tane, A., Azuma, M., and Saito, T. (2012). Programmed cell death 1 forms negative

costimulatory microclusters that directly inhibit T cell receptor signaling by recruiting phosphatase SHP2. J. Exp. Med. *209*, 1201–1217.

66. Sheppard, K.A., Fitz, L.J., Lee, J.M., Benander, C., George, J.A., Wooters, J., Qiu, Y., Jussif, J.M., Carter, L.L., Wood, C.R., and Chaudhary, D. (2004). PD-1 inhibits T-cell receptor induced phosphorylation of the ZAP70/CD3ζ signalosome and downstream signaling to PKCθ. FEBS Lett. *574*, 37–41.

67. Gianchecchi, E., and Fierabracci, A. (2018). Inhibitory receptors and pathways of lymphocytes: The role of PD-1 in Treg development and their involvement in autoimmunity onset and cancer progression. Front. Immunol. *9*, 2374.

68. Wang, Z., Hong, J., Sun, W., Xu, G., Li, N., Chen, X., Liu, A., Xu, L., Sun, B., and Zhang, J.Z. (2006). Role of IFN-γ in induction of Foxp3 and conversion of $CD4^+$ $CD25^-$ T cells to $CD4^+$ Tregs. J. Clin. Invest. *116*, 2434–2441.

69. Corthay, A. (2006). A three-cell model for activation of naïve T helper cells. Scand. J. Immunol. *64*, 93–96.

70. Wood, K.J., and Sawitzki, B. (2006). Interferon γ: a crucial role in the function of induced regulatory T cells in vivo. Trends Immunol. *27*, 183–187.

71. Lu, Y., and Waller, E.K. (2009). Dichotomous role of interferon-γ in allogeneic bone marrow transplant. Biol. Blood Marrow Transplant. *15*, 1347–1353.

72. Nishibori, T., Tanabe, Y., Su, L., and David, M. (2004). Impaired development of $CD4^+$ $CD25^+$ regulatory T cells in the absence of STAT1: increased susceptibility to autoimmune disease. J. Exp. Med. *199*, 25–34.

73. Yang, D., Zhao, X., and Lin, X. (2019). Bcl10 is required for the development of suppressive function of $Foxp3^+$ regulatory T cells. Cell. Mol. Immunol. Published online October 8, 2019, 1038/s41423-019-0297-y.

74. Di Pilato, M., Kim, E.Y., Cadilha, B.L., Prüßmann, J.N., Nasrallah, M.N., Seruggia, D., Usmani, S.M., Misale, S., Zappulli, V., Carrizosa, E., et al. (2019). Targeting the CBM complex causes T_{reg} cells to prime tumours for immune checkpoint therapy. Nature *570*, 112–116.

75. Shin, H.M., Tilahun, M.E., Cho, O.H., Chandiran, K., Kuksin, C.A., Keerthivasan, S., Fauq, A.H., Miele, L., Thome, M., Osborne, B.A., and Minter, L.M. (2014). NOTCH1 can initiate NF-κB activation via cytosolic interactions with components of the T cell signalosome. Front. Immunol. *26*, 249.

76. Hogan, P.G. (2017). Calcium-NFAT transcriptional signalling in T cell activation and T cell exhaustion. Cell Calcium *63*, 66–69.

77. Shen, T., Cseresnyés, Z., Liu, Y., Randall, W.R., and Schneider, M.F. (2007). Regulation of the nuclear export of the transcription factor NFATc1 by protein kinases after slow fibre type electrical stimulation of adult mouse skeletal muscle fibres. J. Physiol. *579*, 535–551.

78. Goode, N., Hughes, K., Woodgett, J.R., and Parker, P.J. (1992). Differential regulation of glycogen synthase kinase-3β by protein kinase C isotypes. J. Biol. Chem. *267*, 16878–16882.

YMTHE, Volume *28*

Supplemental Information

Cell-Penetrating Anti-Protein Kinase C Theta Antibodies Act Intracellularly to Generate Stable, Highly Suppressive Regulatory T Cells

E. Ilker Ozay, Sudarvili Shanthalingam, Heather L. Sherman, Joe A. Torres, Barbara A. Osborne, Gregory N. Tew, and Lisa M. Minter

Cell-penetrating anti-Protein Kinase C theta antibodies act intracellularly to generate stable, highly suppressive regulatory T cells

E. Ilker Ozay[1#], Sudarvili Shanthalingam[2], Heather L. Sherman[1], Joe A. Torres[1], Barbara A. Osborne[1,2], Gregory N. Tew[1,2,3], Lisa M. Minter[1,2*]

[1]Graduate Program in Molecular and Cellular Biology, [2]Department of Veterinary and Animal Sciences, [3]Department of Polymer Science and Engineering, University of Massachusetts Amherst, Amherst, MA, 01003, United States.

#Current address: SQZ Biotechnologies, 200 Arsenal Yards Boulevard, Watertown, MA, 02472

Figure S1

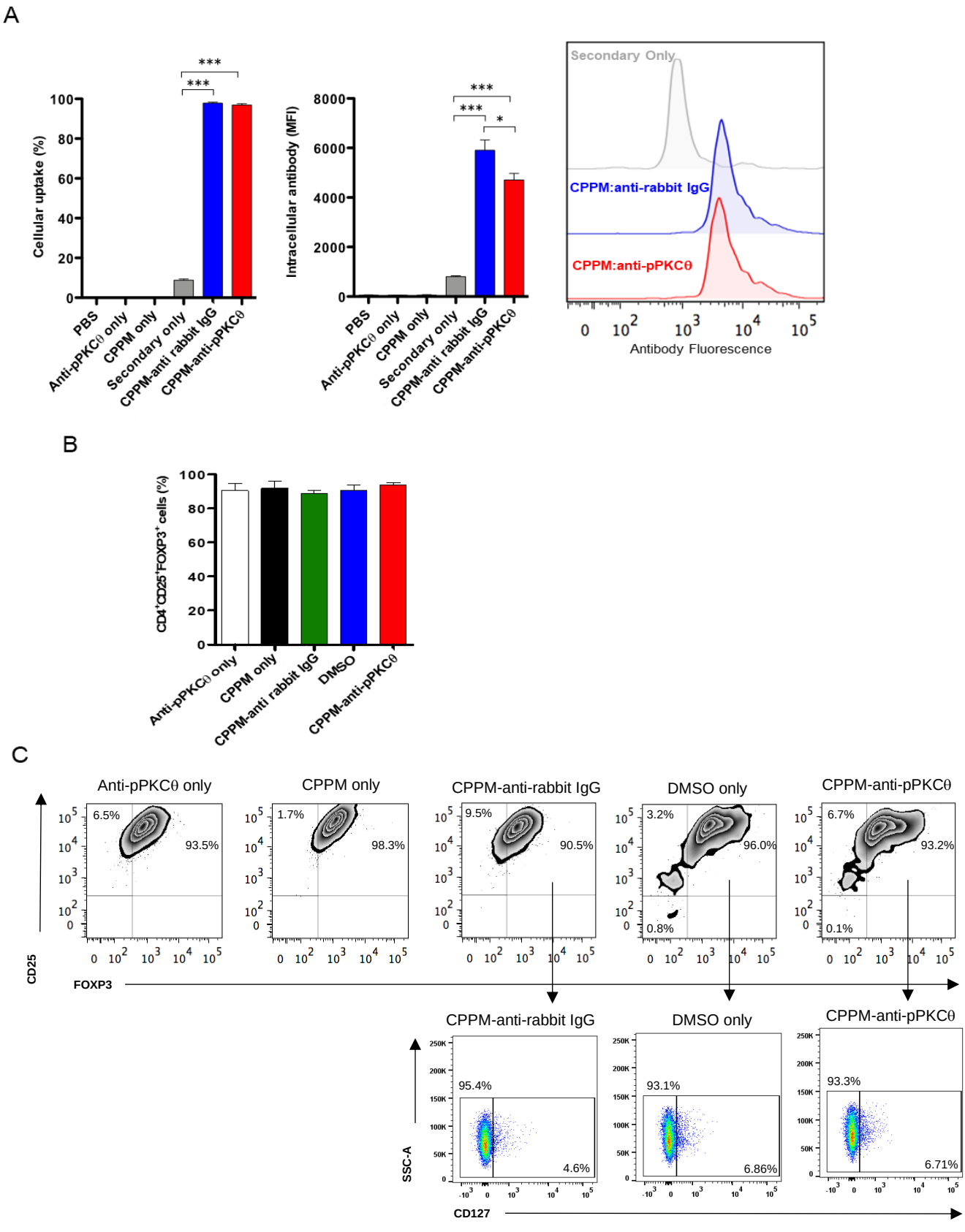
A
Cellular uptake (%)
PBS
Anti-pPKCθ only
CPPM only
Secondary only
CPPM-anti rabbit IgG
CPPM-anti-pPKCθ
Intracellular antibody (MFI)
Secondary Only
CPPM:anti-rabbit IgG
CPPM:anti-pPKCθ
Antibody Fluorescence
B
CD4+CD25+FOXP3+ cells (%)
Anti-pPKCθ only
CPPM only
CPPM-anti rabbit IgG
DMSO
CPPM-anti-pPKCθ
C
Anti-pPKCθ only
CPPM only
CPPM-anti-rabbit IgG
DMSO only
CPPM-anti-pPKCθ
6.5%
93.5%
1.7%
98.3%
9.5%
90.5%
3.2%
96.0%
0.8%
6.7%
93.2%
0.1%
CD25
FOXP3
95.4%
4.6%
93.1%
6.86%
93.3%
6.71%
SSC-A
CD127

Figure S1. Assessment of intracellular antibody delivery and determination of experimental controls for *ex vivo*-generated iTregs. To verify that only antibody complexed to synthetic cell-penetrating peptide mimics are delivered across the cell membrane, CD4 T cells were isolated and pre-treated for four hours with phosphate buffered saline (PBS), anti-pPKCθ only, CPPMs only, secondary antibody only, CPPM complexed to anti-rabbit IgG, or CPPM complexed to anti-pPKCθ, prior to in vitro differentiation into iTregs. At the end of the differentiation period, cells were permeabilized and stained with an anti-rabbit secondary antibody conjugated to Qdot 625. Flow cytometry was used to (**A**) determine percent of cells taking up CPPM-complexed antibody (left panel) and the extent to which CPPM-complexed antibody was delivered on a per cell basis (middle panel), as indicated by median fluorescent intensity of the bound Qdot-labeled secondary antibody. A representative histogram is shown in the far-right panel. In separate experiments, CD4 T cells were isolated and pre-treated for four hours with anti-pPKCθ only, CPPM only, CPPM complexed to anti-rabbit IgG, dimethyl sulfoxide only (DMSO), or CPPM complexed to anti-pPKCθ, prior to in vitro differentiation into iTregs. (**B**) The percent of iTreg cells successfully differentiated after the various pre-treatments was determined by flow cytometry following intracellular staining with anti-CD25 and anti-FOXP3. Representative histograms of CD25 and FOXP3 expression are shown in panels that correspond to the various pretreatment conditions; representative histograms showing CD127+ cells within the CD25+FOXP3+ populations are shown below individual panels. Only the DMSO-treated cells showed a similar expression pattern of CD25 and FOXP3, and, thus was used as the control for CPPM-anti-pPKCθ experiments throughout this study. Data represent mean ± SEM of three independent experiments. Unpaired, two-tailed Student's t test was used for analysis; *$p < 0.05$, ***$p < 0.001$.

Figure S2

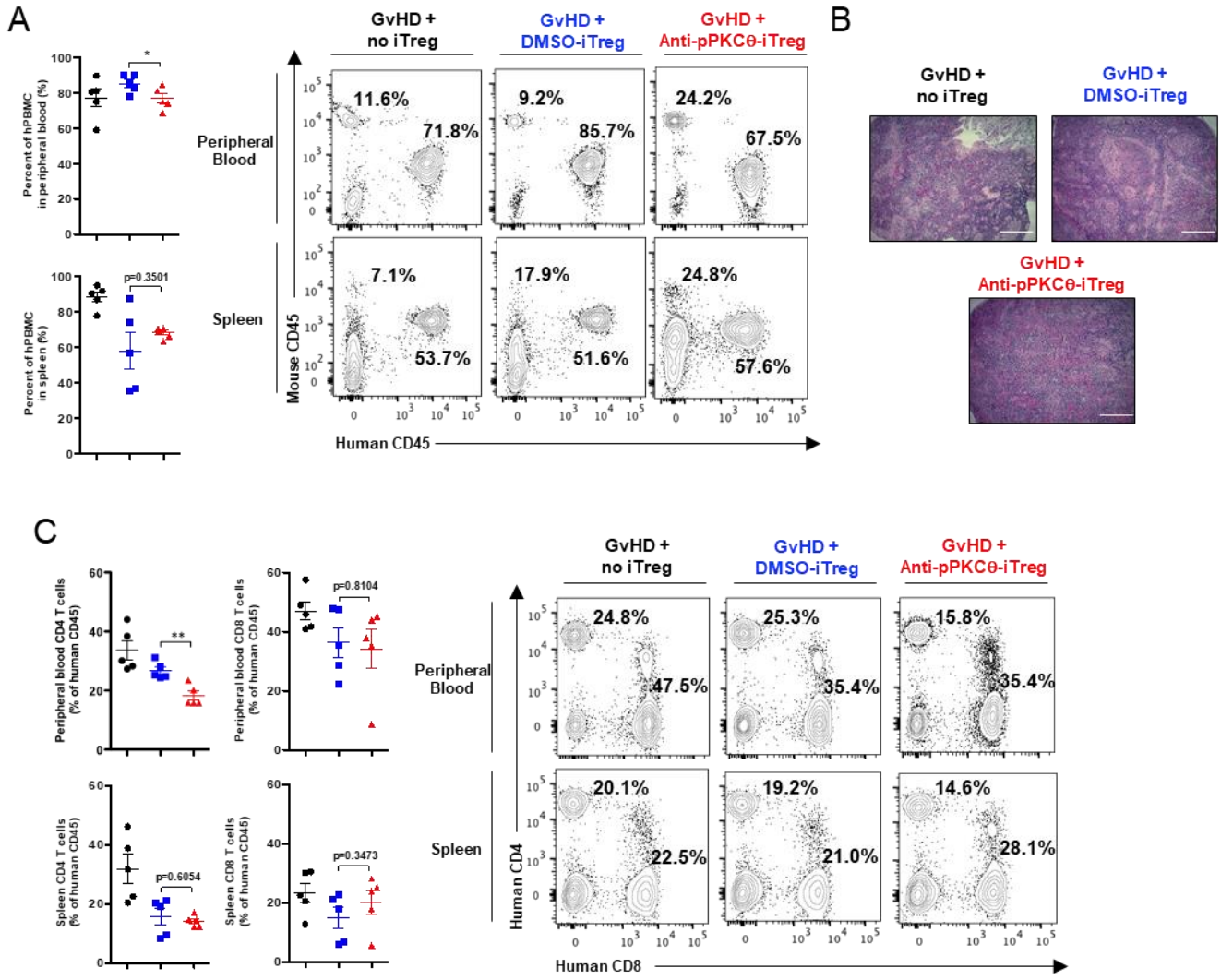
A
GvHD + no iTreg
GvHD + DMSO-iTreg
GvHD + Anti-pPKCθ-iTreg
Percent of hPBMC in peripheral blood (%)
Percent of hPBMC in spleen (%)
p=0.3501
Peripheral Blood
Spleen
Mouse CD45
Human CD45
11.6%
71.8%
9.2%
85.7%
24.2%
67.5%
7.1%
53.7%
17.9%
51.6%
24.8%
57.6%
B
GvHD + no iTreg
GvHD + DMSO-iTreg
GvHD + Anti-pPKCθ-iTreg
C
Peripheral blood CD4 T cells (% of human CD45)
Peripheral blood CD8 T cells (% of human CD45)
Spleen CD4 T cells (% of human CD45)
Spleen CD8 T cells (% of human CD45)
p=0.8104
p=0.6054
p=0.3473
Peripheral Blood
Spleen
Human CD4
Human CD8
24.8%
47.5%
25.3%
35.4%
15.8%
35.4%
20.1%
22.5%
19.2%
21.0%
14.6%
28.1%

Supplemental Figure 2. Assessment of hPBMC distribution in peripheral blood and spleens on day +17 from a humanized mouse model of GvHD. GvHD was induced in mice and cohorts were left untreated (GvHD+no iTregs) or treated with iTregs generated in the presence of DMSO (GvHD+DMSO iTregs) or after CPPM-anti-pPKCθ delivery (GvHD+anti-pPKCθ-iTregs). (**A**) Aggregated data showing the percentages of hPBMCs in peripheral blood and spleen, together with representative flow cytometry dot plots. (**B**) Representative micrographs of spleens harvested 17 days after GvHD-induction and stained with hematoxylin and eosin. (**C**) Aggregated data showing percentages of human CD4 and CD8 T cells recovered from peripheral blood and spleen, together with representative flow cytometry dot plots. 5 mice were used per group. Pooled data represent the mean ± SEM of three independent experiments. Unpaired, two-tailed Student's t test was used for analysis; *$p < 0.05$, **$p < 0.01$.

Figure S3

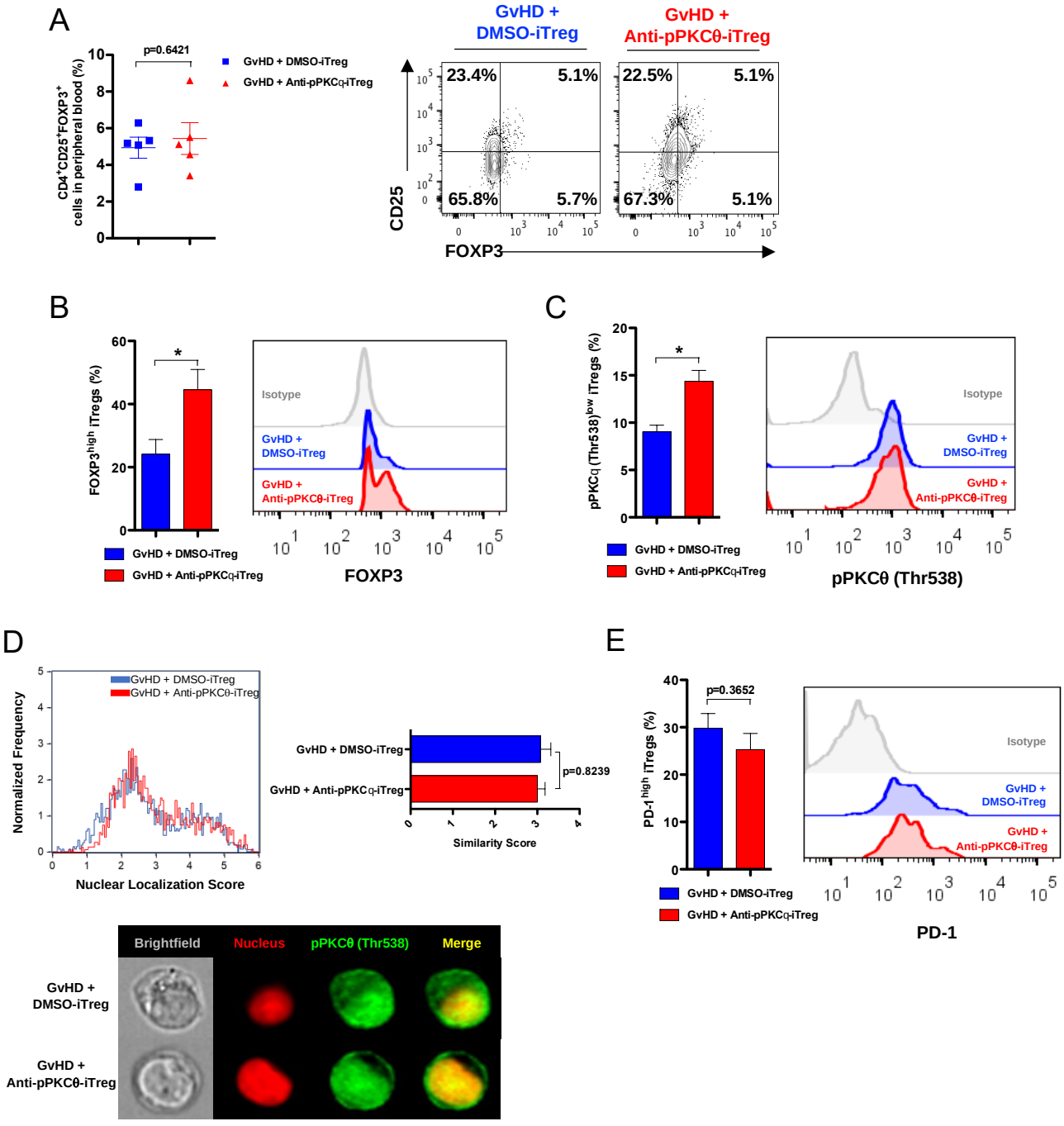
A
p=0.6421
GvHD + DMSO-iTreg
GvHD + Anti-pPKCθ-iTreg
CD4+CD25+FOXP3+ cells in peripheral blood (%)
GvHD + DMSO-iTreg
GvHD + Anti-pPKCθ-iTreg
23.4%
5.1%
65.8%
5.7%
22.5%
5.1%
67.3%
5.1%
CD25
FOXP3
B
FOXP3high iTregs (%)
GvHD + DMSO-iTreg
GvHD + Anti-pPKCθ-iTreg
Isotype
GvHD + DMSO-iTreg
GvHD + Anti-pPKCθ-iTreg
FOXP3
C
pPKCθ (Thr538)low iTregs (%)
GvHD + DMSO-iTreg
GvHD + Anti-pPKCθ-iTreg
Isotype
GvHD + DMSO-iTreg
GvHD + Anti-pPKCθ-iTreg
pPKCθ (Thr538)
D
GvHD + DMSO-iTreg
GvHD + Anti-pPKCθ-iTreg
Normalized Frequency
Nuclear Localization Score
GvHD + DMSO-iTreg
GvHD + Anti-pPKCθ-iTreg
p=0.8239
Similarity Score
Brightfield
Nucleus
pPKCθ (Thr538)
Merge
GvHD + DMSO-iTreg
GvHD + Anti-pPKCθ-iTreg
E
p=0.3652
PD-1high iTregs (%)
GvHD + DMSO-iTreg
GvHD + Anti-pPKCθ-iTreg
Isotype
GvHD + DMSO-iTreg
GvHD + Anti-pPKCθ-iTreg
PD-1

Figure S3. Immunophenotyping of iTregs recovered from peripheral blood on day +17 from a humanized mouse model of GvHD. GvHD was induced in mice and cohorts were treated with iTregs generated in the presence of DMSO (GvHD+DMSO-iTregs) or after CPPM-anti-pPKCθ delivery (GvHD+anti-pPKCθ-iTregs). (**A**) Aggregated data showing percent of CD4+CD25+FOXP3+ iTregs recovered from peripheral blood, together with representative dot plots showing CD25 and FOXP3 expression, in DMSO-iTregs and anti-pPKCθ-iTregs recovered from the peripheral blood of diseased mice 17 days after GvHD-induction. (**B**) Aggregated data and representative histogram of FOXP3high-iTregs in the peripheral blood of DMSO- or anti-pPKCθ-iTreg-treated mice 17 days after GvHD-induction. (**C**) Aggregated data and representative histogram of $pPKC\theta^{low}$-iTregs in the peripheral blood of DMSO- or anti-pPKCθ-iTreg-treated mice 17 days after GvHD-induction. (**D**) Nuclear localization score histograms, aggregated data and representative images of nuclear pPKCθ-positive CD4+CD25+FOXP3+ iTregs in the peripheral blood of DMSO- or anti-pPKCθ-iTreg-treated mice 17 days after GvHD-induction. (**E**) Aggregated data and representative histogram of $PD1^{high}$-iTregs in the peripheral blood of DMSO- or anti-pPKCθ-iTreg-treated mice 17 days after GvHD-induction. 3-5 mice were used per group. Pooled data represent the mean ± SEM of three independent experiments. Unpaired, two-tailed Student's t test was used for analysis; $*p < 0.05$.

Figure S4

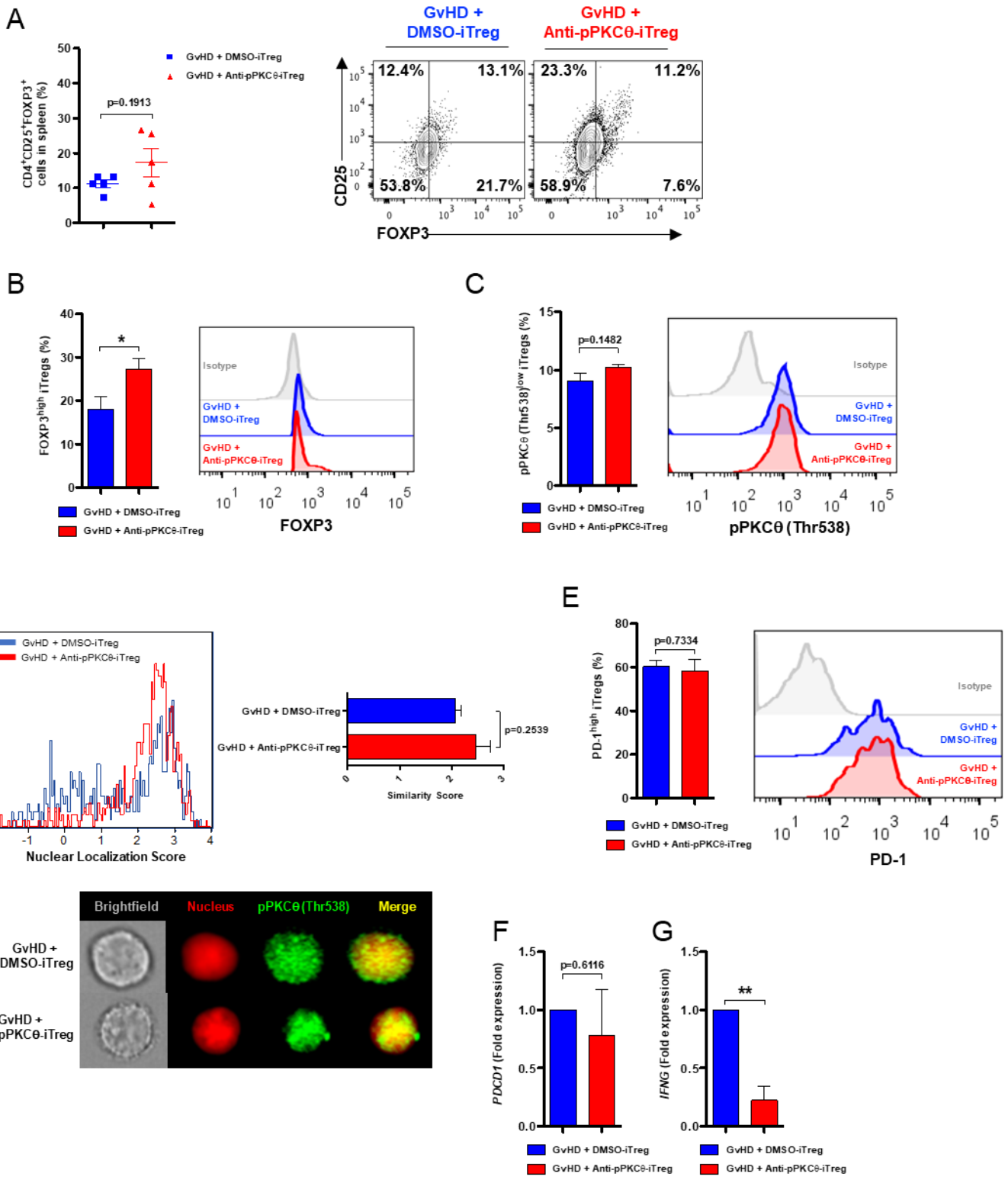
A
GvHD + DMSO-iTreg
GvHD + Anti-pPKCθ-iTreg
p=0.1913
CD4+CD25+FOXP3+ cells in spleen (%)
12.4%
13.1%
53.8%
21.7%
23.3%
11.2%
58.9%
7.6%
CD25
FOXP3
B
FOXP3high iTregs (%)
*
Isotype
FOXP3
C
pPKCθ (Thr538)low iTregs (%)
p=0.1482
pPKCθ (Thr538)
D
Normalized Frequency
Nuclear Localization Score
p=0.2539
Similarity Score
Brightfield
Nucleus
pPKCθ(Thr538)
Merge
E
PD-1high iTregs (%)
p=0.7334
PD-1
F
PDCD1 (Fold expression)
p=0.6116
G
IFNG (Fold expression)
**

Figure S4. Immunophenotyping of iTregs recovered from spleens on day +17 from a humanized mouse model of GvHD. GvHD was induced in mice and cohorts were treated with iTregs generated in the presence of DMSO (GvHD+DMSO-iTregs) or after CPPM-anti-pPKCθ delivery (GvHD+anti-pPKCθ-iTregs). (**A**) Aggregated data showing percent of CD4+CD25+FOXP3+ iTregs recovered from spleens, together with representative dot plots showing CD25 and FOXP3 expression in DMSO-iTregs and anti-pPKCθ-iTregs recovered from the spleens of diseased mice 17 days after GvHD-induction. (**B**) Aggregated data and representative histogram of FOXP3high-iTregs recovered from spleens of DMSO- or anti-pPKCθ-iTreg-treated mice 17 days after GvHD-induction. (**C**) Aggregated data and representative histogram of $pPKC\theta^{low}$-iTregs recovered from spleens of DMSO- or anti-pPKCθ-iTreg-treated mice 17 days after GvHD-induction. (**D**) Nuclear localization score histograms, aggregated data and representative images of nuclear pPKCθ-positive CD4+CD25+FOXP3+ iTregs recovered from spleens of DMSO- or anti-pPKCθ-iTreg-treated mice 17 days after GvHD-induction. (**E**) Aggregated data and representative histogram of $PD\text{-}1^{high}$-iTregs recovered from spleens of DMSO- or anti-pPKCθ-iTreg-treated mice 17 days after GvHD-induction. (**F**) *PDCD1*, and (**G**) *IFNG* gene expression in CD4+CD25+ (iTreg) cells recovered from the spleens of DMSO- or anti-pPKCθ-iTreg-treated mice 17 days after GvHD-induction. 3-5 mice were used per group. Pooled data represent the mean ± SEM of three independent experiments. Unpaired, two-tailed Student's t test was used for analysis; $*p < 0.05$, $**p < 0.01$.

Table S1

List of qPCR primers used in this study

Gene	Forward Primer (5'-3')	Reverse Primer (5'-3')
ACTB (Housekeeping)	GTTGTCGACGACGAGCG	GCACAGAGCCTCGCCTT
FOXP3	TGACCAAGGCTTCATCTGTG	GAGGAACTCTGGGAATGTGC
IFNG	CTCTTGGCTGTTACTGCCAGG	CTCCACACTCTTTTGGATGCT
PDCD1	CCCTGGTGGTTGGTGTCGT	GCCTGGCTCCTATTGTCCCTC
PRKCQ	CTATCAATAGCCGAGAAACCATG	CTCATCCAACGGAGACTCCC

Molecular Therapy
Original Article

Protein Kinase C Theta Modulates PCMT1 through hnRNPL to Regulate FOXP3 Stability in Regulatory T Cells

E. Ilker Ozay,[1,4] Sudarvili Shanthalingam,[2] Joe A. Torres,[1] Barbara A. Osborne,[1,2] Gregory N. Tew,[1,2,3] and Lisa M. Minter[1,2]

[1]Graduate Program in Molecular and Cellular Biology, University of Massachusetts Amherst, Amherst, MA 01003, USA; [2]Department of Veterinary and Animal Sciences, University of Massachusetts Amherst, Amherst, MA 01003, USA; [3]Department of Polymer Science and Engineering, University of Massachusetts Amherst, Amherst, MA 01003, USA

T cell receptor signaling, together with cytokine-induced signals, can differentially regulate RNA processing to influence T helper versus regulatory T cell fate. Protein kinase C family members have been shown to function in alternative splicing and RNA processing in various cell types. T cell-specific protein kinase C theta, a molecular regulator of T cell receptor downstream signaling, has been shown to phosphorylate splicing factors and affect post-transcriptional control of T cell gene expression. In this study, we explored how using a synthetic cell-penetrating peptide mimic for intracellular anti-protein kinase C theta delivery fine-tunes differentiation of induced regulatory T cells through its differential effects on RNA processing. We identified protein kinase C theta signaling as a critical modulator of two key RNA regulatory factors, heterogeneous nuclear ribonucleoprotein L (hnRNPL) and protein-L-isoaspartate *O*-methyltransferase-1 (PCMT1), and loss of protein kinase C theta function initiated a "switch" in post-transcriptional organization in induced regulatory T cells. More interestingly, we discovered that protein-L-isoaspartate *O*-methyltransferase-1 acts as an instability factor in induced regulatory T cells, by methylating the forkhead box P3 (FOXP3) promoter. Targeting protein-L-isoaspartate *O*-methyltransferase-1 using a cell-penetrating antibody revealed an efficient means of modulating RNA processing to confer a stable regulatory T cell phenotype.

INTRODUCTION

Immunological signals emanating from the T cell receptor (TCR) culminate in translation of mRNA in immune cells. Depending on the input, alterations in this process can be mediated by RNA binding protein (RBP) assemblies to coordinate downstream biological outcomes, such as T cell activation, tolerance, and plasticity. Modifications in RBP-mediated post-transcriptional regulation can influence cellular reactivity during inflammatory responses and autoimmunity.[1] RBPs include two main classes of proteins: heterogeneous nuclear ribonucleoproteins (hnRNPs) that bind to splicing silencers, and serine-arginine-rich (SR) proteins that bind to splicing enhancers.[2–4] Initially discovered as spliceosome components regulating alternative splicing, these proteins are involved in numerous other cellular processes such as transcription, chromatin dynamics, mRNA stability, mRNA nuclear export, and translation.[5,6] These multifunctional RBPs remain bound to mRNA, facilitating nucleation of other regulatory proteins that aid in mRNA export to the cytoplasm and subsequent translation.[4,7,8] By necessity, these proteins are tightly regulated, including by phosphorylation in response to extracellular stimuli, which can alter their activity and subcellular localization.[9–12]

TCR-mediated signaling pathways effect multiple changes in cell morphology and function through alternative splicing and by orchestrating interactions between positively and negatively regulating RBPs and 3′ untranslated regions (UTRs).[1–3,6] Many immunological effectors, including cytokines and chemokines, harbor 3′ UTR regulatory elements that enable fine-tuning of immunological responses based on cellular requirements.[13–15] Alternative splicing and RNA processing can be regulated in a tissue- and cell-specific fashion, downstream of environmental cues.[16–18] However, our full understanding of the molecular mechanisms that convey differences in post-transcriptional regulation remain incomplete.

For example, alternative splicing of the leukocyte surface protein protein tyrosine phosphatase receptor type C (encoded by *PTPRC*) and commonly referred to as CD45 represents one well-characterized example of how external stimuli result in changes in expression of alternatively spliced proteins.[19–21] Protein kinase C (PKC) and Ras signaling induce exon skipping within *PTPRC*, generating alternate

Received 8 January 2020; accepted 10 June 2020;
https://doi.org/10.1016/j.ymthe.2020.06.012.

[4]Present address: SQZ Biotechnologies, 200 Arsenal Yards Boulevard, Watertown, MA 02472, USA.

Correspondence: Lisa M. Minter, Department of Veterinary and Animal Sciences, University of Massachusetts Amherst, 661 North Pleasant Street, 427K ISB, Amherst, MA 01003, USA.
E-mail: lminter@vasci.umass.edu

forms of CD45 that concomitantly exhibit reduced phosphatase activity.[19,22,23] Different CD45 isoforms are generated by multi-protein complexes of RBPs, including hnRNPL.[24] Studies using immune cells have focused on hnRNPL as a critical nuclear RBP, with four RNA recognition motifs and capable of mediating basal splicing, mRNA stability, and nuclear export.[25–28] hnRNPL binds to CA-repeat motifs and CA-rich elements, thereby repressing exon skipping.[26,29] T cell activation can induce post-translational modifications of hnRNPL to increase its silencing activity.[30,31] Because hnRNPL activity is higher in resting cells, these cells express primarily the longer CD45 isoforms, CD45RA and or CD45RB. In activated and memory T cells, in which hnRNPL activity is low, increased levels of the shortest isoform, CD45RO, predominate.[21] CD45 isoform expression in regulatory T cells (Tregs) has also been associated with *FOXP3* stability and Treg suppressive capacity, as well as with Treg homing *in vivo*.[32] Furthermore, differential splicing and mRNA processing regulated by TCR and hnRNPL are key drivers of T helper versus Treg fate choice. hnRNPL knockdown suppressed Treg induction, suggesting that hnRNPL, as an mRNA regulatory protein, is critical to maintaining the integrity of Treg differentiation programs.[33]

Tregs function to control immune responses and maintain self-tolerance within the immune system.[34,35] Demethylation of the Treg-specific demethylated region (TSDR), located within the intronic sequence of the *FOXP3* promoter, is a prerequisite for stable *FOXP3* expression and Treg suppressive function.[36–38] Our previous studies demonstrated that we could modulate T cell fate by delivering a cell-penetrating antibody directed against phosphorylated PKCθ (pPKCθ), and intracellular anti-pPKCθ delivery into human CD4 T cells prior to *in vitro* iTreg differentiation generated highly stable induced Tregs (iTregs) with a unique phenotype.[39] Inhibiting PKCθ function by constraining its intracellular movement in iTregs resulted in superior suppressive capacity and correlated with unusual transcriptional changes, both *in vitro* and *in vivo*. This led us to investigate how these transcriptional changes were regulated by PKCθ during iTreg differentiation. An interesting, potential link between PKCθ and transcriptional diversity has been explored in T cells.[40–42] PKCθ directly phosphorylates the splicing factor SC35 within its RNA recognition motif and SR domain.[40,43] PKCθ and SC35 colocalize with RNA polymerase II, as well as with active histone marks, to enhance transcriptional elongation.[40] Moreover, SC35 binds to exonic splicing enhancers and coordinates alternative splicing, RNA stability, mRNA export, and translation.[44–47] Intriguingly, a FOXP3 stabilizing protein, TIP60, was shown to promote SC35 degradation via acetylation at lysine residue 52, in close proximity to PKCθ phosphorylation sites, suggesting that PKCθ may act to regulate splicing factors in the context of Treg suppressive function.[48,49] Given that PKCθ phosphorylates SC35 and controls epigenetic and transcriptional regulation in T cells, we hypothesized that PKCθ may regulate alternative splicing and, furthermore, RNA processing during iTreg differentiation.

In this study, we show that intracellular anti-pPKCθ delivery into CD4 T cells prior to iTreg differentiation effectively "switches" alternative splicing and RNA processing programs to favor stable over plastic iTreg phenotypes. PKCθ critically modulates two key RNA regulatory factors, hnRNPL and protein-L-isoaspartate *O*-methyltransferase-1 (PCMT1), thereby reprogramming mRNA splicing, stability, nuclear export, and translational control. More interestingly, we demonstrate that PCMT1 acts as a Treg instability factor by methylating the *FOXP3* promoter. Targeting PCMT1 using a cell-penetrating antibody revealed an efficient means for modulating RNA processing to confer stable Treg function.

RESULTS

Ex Vivo Anti-pPKCθ Delivery into iTregs Modulates Splicing Regulatory Proteins and RNA Processing

PKCθ has been described as a negative regulator of Treg differentiation. It has also been linked to the splicing machinery in CD4 T cells, through its demonstrated phosphorylation of the splicing regulator SC35.[40] Therefore, we sought to determine whether PKCθ may affect iTreg differentiation by modulating regulatory and splicing proteins. We previously showed that we could modulate pPKCθ activity, *ex vivo*, using synthetic protein transduction domain mimics to efficiently carry a functional antibody across the membrane of human CD4 T cells.[50] In this study, we utilized this same approach to probe the function of PKCθ during *ex vivo* iTreg differentiation. We cultured human CD4 T cells with or without cell-penetrating peptide mimics (CPPMs) complexed to anti-pPKCθ in the presence of iTreg polarizing or with DMSO only, to generate anti-pPKCθ-iTregs or DMSO-iTregs, respectively.[39] For comparison, we also cultured CD4 T cells with or without CPPM-anti-pPKCθ for the same length of time, but in the absence of iTreg polarizing conditions, to generate anti-pPKCθ-conventional T cells (Tconvs) and DMSO-Tconvs, respectively. After 5 days of differentiation, we assessed the cytosolic and nuclear distribution of phosphorylated (p)SC35 (Figure 1A). We observed that pSC35 expression was abrogated in iTregs differentiated in the presence of anti-pPKCθ. This was not entirely unexpected, as SC35 has been reported to be a substrate of PKCθ,[40] and loss of pSC35 confirms that anti-pPKCθ delivery attenuates PKCθ activity.

Since the SC35 splicing regulator was affected by anti-pPKCθ delivery to iTregs, we questioned whether there were differences in alternative splicing or 3′ UTR processing in key iTreg molecules. Properly generating 3′ UTRs is critical for mRNA stability, since 3′ UTRs include recognition motifs for RBPs that may stabilize or destabilize mRNA through their influences on mRNA degradation and silencing. In addition, shorter 3′ UTR lengths have been associated with stable mRNA production and increased protein translation in a signal-dependent manner.[51] Immune cells recruit specific RBPs to sites of translation to form riboclusters. Arrangement of RBPs on the 3′ UTR elements (AU-rich and CA-rich elements) in the riboclusters determine whether mRNA will be translated or directed to nonsense-mediated decay. CD45 splicing has been extensively studied in T cells and shown to be regulated by hnRNPL. Therefore, we first examined CD45 splicing in iTregs, as a proof-of-concept target. We noted that anti-pPKCθ delivery increased RB and RO forms both in iTregs and Tconvs, compared to untreated cells (Figures 1B and

Please cite this article in press as: Ozay et al., Protein Kinase C Theta Modulates PCMT1 through hnRNPL to Regulate FOXP3 Stability in Regulatory T Cells, Molecular Therapy (2020), https://doi.org/10.1016/j.ymthe.2020.06.012

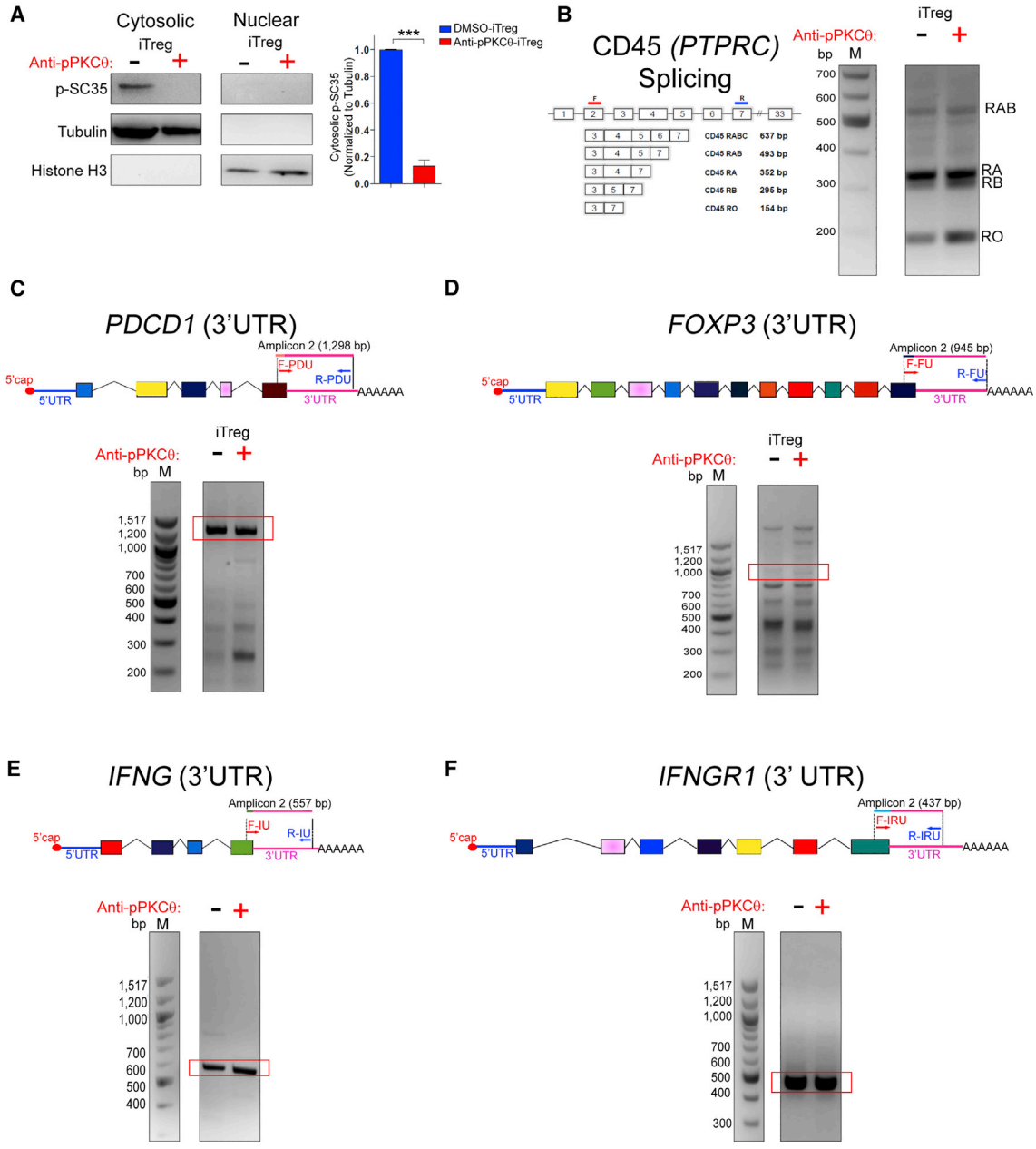

Figure 1. *Ex Vivo* Anti-pPKCθ Delivery into iTregs Modulates Splicing Regulatory Proteins and RNA Processing

(A) Cytoplasmic and nuclear distribution of pSC35 in anti-pPKCθ-iTregs was analyzed by immunoblotting. Normalized densities for cytoplasmic pSC35 were quantified relative to tubulin expression. (B) Alternative splicing of CD45 (*PTPRC*) was analyzed in iTregs using RT-PCR. Primers were designed to assess 3′ UTR processing using RT-PCR and covered sequences from the last exon to the polyadenylation site. (C–F) Results and cartoon representations are shown for (C) *PDCD1*, (D) *FOXP3*, (E) *IFNG*, and (F) *IFNGR1*. Red frames indicate expected amplicon sizes for mature mRNA with its 3′ UTR. Data represent the mean ± SEM of two or three independent experiments. An unpaired, two-tailed Student's t test was used for analysis. ***$p < 0.001$.

S1A). In a companion study, we showed that anti-pPKCθ-treated iTregs displayed unique characteristics, including higher FOXP3, PD1, and interferon (IFN)γ expression.[39] Given the fact that FOXP3 and PD1 reportedly undergo alternative splicing,[52–54] we asked whether anti-pPKCθ delivery affected mRNA processing of these and other key iTreg genes. We analyzed the splicing patterns and 3′ UTR lengths of *PDCD1*, *FOXP3*, *IFNG*, and *IFNGR1*. Conventional mRNAs for those genes consist of exons 1-2-3-4-5 (*PDCD1*), exons 2-3-4-5 (*FOXP3*), 4 exons (*IFNG*), and 7 exons (*IFNGR1*). We observed similar splicing patterns for all four genes in iTregs

Please cite this article in press as: Ozay et al., Protein Kinase C Theta Modulates PCMT1 through hnRNPL to Regulate FOXP3 Stability in Regulatory T Cells, Molecular Therapy (2020), https://doi.org/10.1016/j.ymthe.2020.06.012

with or without anti-pPKCθ treatment (Figures S1B–S1E). Anti-pPKCθ delivery into Tconvs produced similar spliced forms, except for *FOXP3* mRNA, which showed truncated sequences following anti-pPKCθ treatment (Figure S1C). Interestingly, anti-pPKCθ delivery affected 3′ UTR processing in a gene-specific manner. When we evaluated these four genes in iTregs and Tconvs, we detected *PDCD1* mRNA variants with markedly shorter 3′ UTR lengths following anti-pPKCθ treatment compared to DMSO-iTregs (Figures 1C and S1F), while *FOXP3*, *IFNG*, and *IFNGR1* 3′ UTR lengths did not change after antibody treatment (Figures 1D–1F and S1G–S1I). Expression of a shorter 3′ UTR sequence in *PDCD1* is consistent with increased expression of surface PD1 observed on iTregs differentiated following anti-pPKCθ delivery.[39] Collectively, these results suggest that PKCθ modulates splicing regulators and RNA processing in a cell- and gene-specific context.

Ex Vivo Treatment of iTregs Conveys Durable Tissue-, Cell-, and Gene-Specific Modulation of RNA Processing *In Vivo*

We noted increased CD45RB and CD45RO expression in iTregs differentiated following *ex vivo* anti-pPKCθ delivery, in the absence of robust differences in alternative splicing of *PDCD1*, *FOXP3*, *IFNG*, or *IFNGR1*. However, *in vivo*, iTregs can behave differently due to their differential trafficking and exposure to cytokines. Furthermore, reports suggest that these influences and others may prime Tregs for additional alternative splicing events in response to external signals. We explored this possibility by analyzing the expression of CD45 (*PTPRC*), *PDCD1*, *FOXP3*, *IFNG*, and *IFNGR1* in iTregs isolated from the bone marrow (BM) and spleen of mice, used in a humanized model of graft-versus-host disease (GvHD).[39] In this pre-clinical model, lethal GvHD results from acute BM infiltration of destructive immune cells, approximately 3 weeks after human peripheral blood mononuclear cells are transferred into lightly irradiated nonobese diabetic (NOD).Cg-*Prkdc*^{scid} *Il2rg*^{tm1Wjl}/SzJ (NSG) mice. In our companion study, we determined that administering anti-pPKCθ-iTregs at the time of disease induction was highly efficacious in preventing GvHD. We detected high numbers of anti-pPKCθ-iTregs in the BM at the peak day of the disease (day 17), and these iTregs exhibited a unique and stable gene expression pattern.[39] To determine whether alternate RNA processing leads to more stable mRNA variants in these iTregs, we adoptively transferred anti-pPKCθ-iTregs or DMSO-iTregs into humanized mice on the day of GvHD induction and analyzed RNA processing in iTregs on day 17, at the peak of disease. We used magnetic beads to purify cells collected from BM and spleen based on CD4, CD25, and CD127 expression. In contrast with *in vitro* results, anti-pPKCθ-iTregs isolated from BM showed increased expression of the CD45RA/RB isoforms, compared to DMSO-iTregs, while iTregs isolated from spleens had comparable expression of CD45 isoforms, regardless of treatment during differentiation (Figure 2A). When we analyzed naive T cells, we found that they expressed similar patterns of CD45 splice variants in both tissues, regardless of iTreg treatment (Figure S2A). These data suggested that *ex vivo* anti-pPKCθ delivery into iTregs alters CD45 splicing and is iTreg-specific. Moreover, increased CD45RA/RB expression by anti-pPKCθ-iTregs is consistent with reports showing that this population of iTregs preferentially migrates to the BM.[32]

When we further assessed iTregs recovered from the BM and spleens of diseased mice, we found that, in anti-pPKCθ-iTregs, both *PDCD1* and *FOXP3* displayed differences in mRNA expression. Whereas *PDCD1* transcripts were nearly undetectable in BM-infiltrating DMSO-iTregs, anti-pPKCθ-iTregs isolated from BM and spleen showed robust expression of *PDCD1* as well as extensive editing in the 3′ UTR length, suggesting that transcripts generated in these cells may be more stable compared to DMSO-iTregs (Figure 2B). Quite surprisingly, the expression level, as well as the expression pattern, of *FOXP3* splice variants in anti-pPKCθ-iTregs recovered from the BM also differed significantly from those of DMSO-iTregs. iTregs isolated from spleens of diseased mice showed minimal variability in *FOXP3* isoform expression, regardless of how the iTregs were generated (Figure 2C). While we were unable to amplify *FOXP3* 3′ UTR of the expected size in BM-infiltrating iTregs, we did detect shorter 3′ UTR variants only in BM-resident anti-pPKCθ-iTregs, again suggesting that unique 3′ UTR editing also occurs in these cells (Figure 2C). Naive T cells recovered from the BM and spleen of diseased mice showed comparable expression patterns of *PDCD1* and *FOXP3* splice variants and 3′ UTR editing, with the exception of naive T cells isolated from spleens of DMSO-iTreg-treated mice, which showed multiple short isoforms of *FOXP3* (Figures S2B and S2C).

Consistent with the alterations in *PDCD1* and *FOXP3* that we observed to be unique to BM-infiltrating anti-pPKCθ-treated iTregs, we also noted distinct and exclusive mRNA splicing and 3′ UTR editing of *IFNG* and *IFNGR1* in these cells as well (Figures 2D and 2E). We could amplify *IFNG* and *IFNGR1* splice variants and 3′ UTR transcripts of the expected amplicon sizes in anti-pPKCθ-iTregs isolated from BM, but not from BM-infiltrating DMSO-iTregs (Figures 2D and 2E). We also noted some tissue-specific differences in the isoform expression and 3′ UTR length in these genes, amplified from naive T cells recovered from BM and spleens of mice (Figures S2B–S2E). Additionally, although we detected *IFNG* mRNA splice variants in naive T cells from BM (Figure S2D), they were lacking *IFNGR1* mRNA, due to differential 3′ UTR editing (Figure S2E). This raises the intriguing prospect that iTregs may exert a cell-extrinsic effect on naive T cells that makes them refractory to the effects of IFNγ signaling, although further experimentation is needed to test this possibility. Altogether, these data suggest that alternative splicing and 3′ UTR shortening of key iTreg genes were selectively modulated in anti-pPKCθ-iTregs, during *in vivo* immune responses, and these occurred in a tissue-, cell-, and gene-specific fashion.

In iTregs, PCMT1 Is Regulated through Post-translational and Post-transcriptional Processes

The protein repair enzyme, PCMT1, repairs damaged proteins by methylating the carboxyl group of L-isoaspartate or D-aspartyl residues.[55] PCMT1 can also regulate critical cellular processes such as RNA maturation, stability, export, histone homeostasis, and post-translational control.[56–59] PCMT1 shares similarities with two other

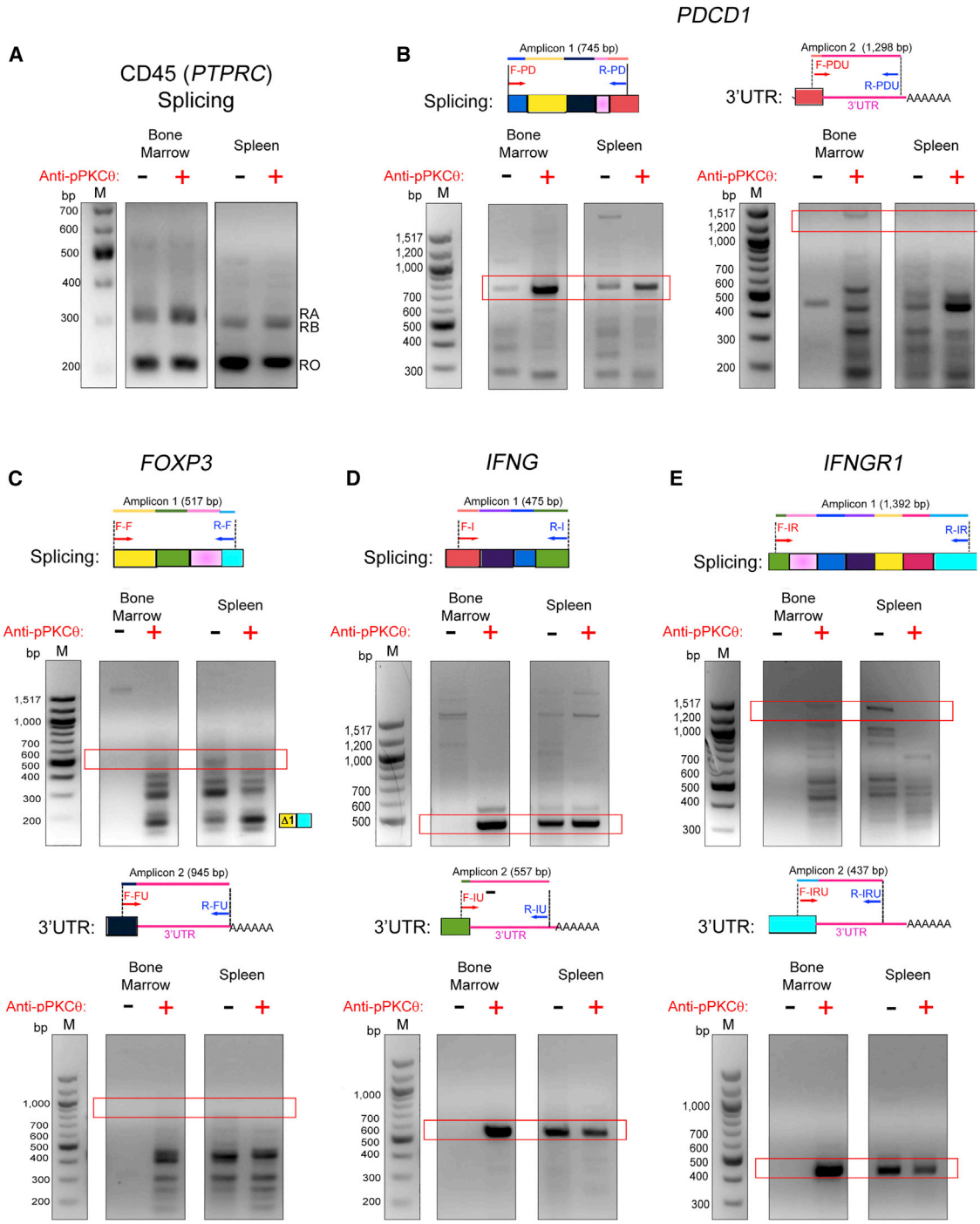

Figure 2. *Ex Vivo* Treatment of iTregs Conveys Durable Tissue-, Cell-, and Gene-Specific Modulation of RNA Processing *In Vivo*

hPBMCs were transferred on day 0 together with anti-pPKCθ-iTregs (or DMSO-iTregs) at a ratio of 3:1. On day 17, tissues were harvested and iTregs were isolated based on $CD4^+$, $CD25^+$, $CD127^-$ expression, using magnetic beads. Total RNA was extracted from *ex vivo*-treated iTregs recovered from BM and spleen on day 17. (A–E) RT-PCR was used to evaluate alternatively spliced (A) CD45 (*PTPRC*), and alternative splicing and 3′ UTR processing of (B) *PDCD1*, (C) *FOXP3*, (D) *IFNG*, and (E) *IFNGR1*. Red frames indicate the expected amplicon size, and the cartoon representation for expected amplicon size is shown for each gene. Data are representative of three independent experiments from five mice per condition.

Please cite this article in press as: Ozay et al., Protein Kinase C Theta Modulates PCMT1 through hnRNPL to Regulate FOXP3 Stability in Regulatory T Cells, Molecular Therapy (2020), https://doi.org/10.1016/j.ymthe.2020.06.012

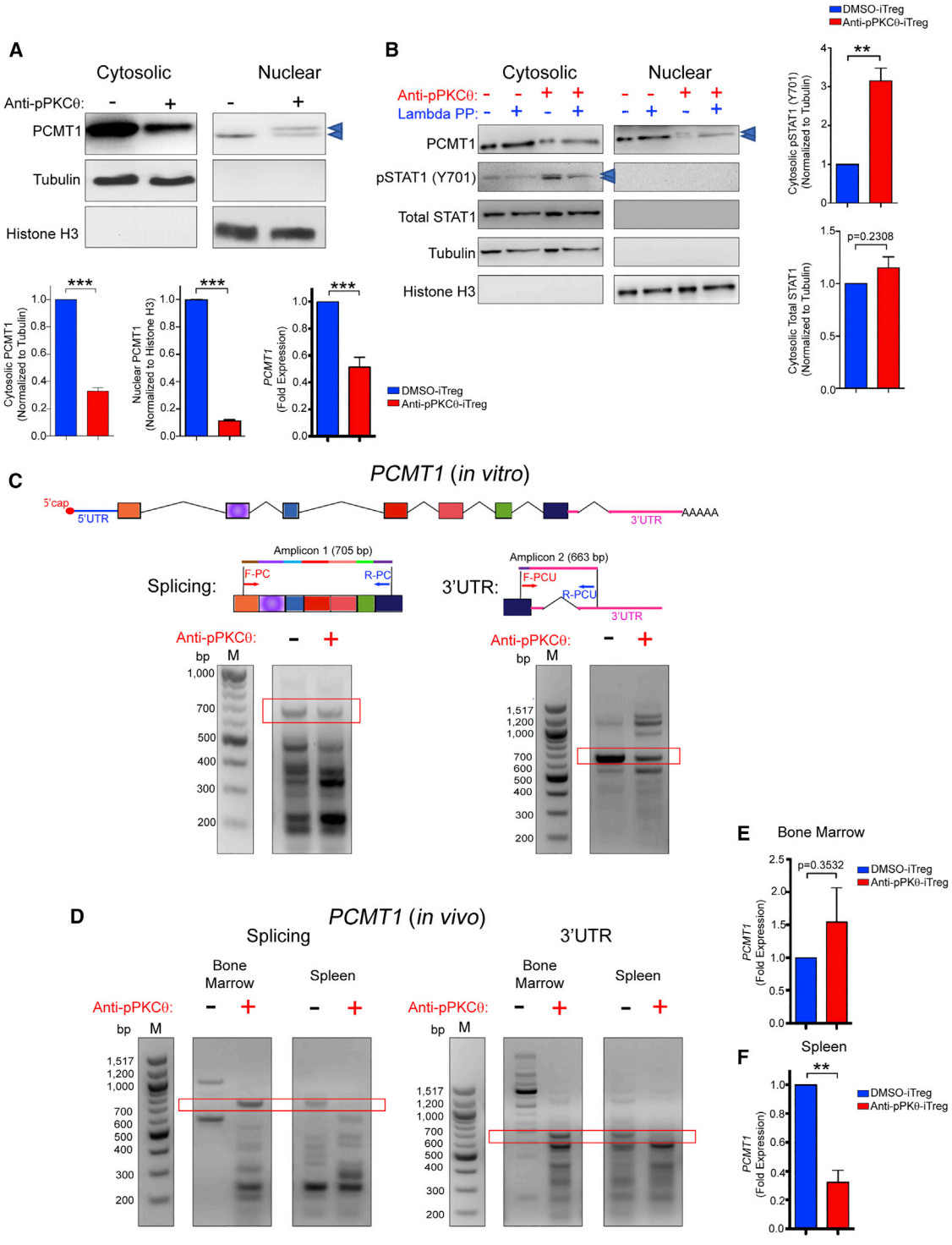

Figure 3. In iTregs, PCMT1 Is Regulated through Post-translational and Post-transcriptional Processes

(A) PCMT1 protein in cytosolic and nuclear extracts was detected using immunoblotting, and band intensity was quantified relative to tubulin and histone H3 expression, respectively, using ImageJ software. (B) λ-Phosphatase treatment was used to confirm PCMT1 phosphorylation. pSTAT1 was used as a phosphorylation control. Total

(legend continued on next page)

Please cite this article in press as: Ozay et al., Protein Kinase C Theta Modulates PCMT1 through hnRNPL to Regulate FOXP3 Stability in Regulatory T Cells, Molecular Therapy (2020), https://doi.org/10.1016/j.ymthe.2020.06.012

methyltransferases shown to methylate proteins and RNA: *S*-adenosylmethionine-dependent protein arginine methyltransferase (PRMT) and PRIP-interacting protein with methyltransferase domain (PIMT), respectively. Therefore, we investigated PCMT1 regulation in the context of iTreg differentiation with and without anti-pPKCθ delivery.

PCMT1 was expressed at high levels in the cytosol but we could also detect low levels in the nucleus of DMSO-iTregs (Figure 3A). Following anti-pPKCθ delivery, cytosolic and nuclear PCMT1 levels were significantly diminished, as was gene expression (Figure 3A). We also noted decreased cytosolic PCMT1 expression and altered splice variants in anti-pPKCθ-Tconvs (Figures S3A–S3C). Interestingly, we detected two separate PCMT1 bands in the nuclear lysates only of anti-pPKCθ-iTregs, raising the possibility that nuclear PCMT1 in these cells is a phosphorylated species (Figure 3A). We generated additional cytosolic and nuclear samples and treated half of each sample with λ-phosphatase, to determine whether the upper band represented phosphorylated PCMT1. We detected significantly higher pSTAT1 (Y701) levels in anti-pPKCθ-iTregs (Figure 3B), consistent with reports of elevated pSTAT1 in highly suppressive iTregs. Therefore, we also included pSTAT1 (Y701) as an internal control. As expected, pSTAT1 was not detected following phosphatase treatment (Figure 3B). Similarly, the upper band of nuclear PCMT1 was undetectable in nuclear lysates following phosphatase treatment (Figures 3A and 3B). These results suggest that one means by which pPKCθ may negatively regulate iTreg differentiation is by suppressing PCMT1 phosphorylation, which may further impact its nuclear function.

Having detected differences in RNA splice variants in anti-pPKCθ-iTregs, *in vitro* and *in vivo* (Figures 1 and 2, respectively), we next asked whether anti-pPKCθ delivery affected RNA processing of *PCMT1* in iTregs, as well. Conventional *PCMT1* mRNA has seven exons with a 3′ UTR that contains approximately 700 bp. In anti-pPKCθ-iTregs, we observed evidence of exon skipping in *PCMT1* transcripts, detecting shorter mRNA variants together with longer-than-expected 3′ UTRs (Figure 3C). We were also interested in whether anti-pPKCθ treatment conveyed durable differences in iTregs recovered from the BM and spleens of mice in our humanized model of GvHD. Strikingly, we detected markedly different splice variants of *PCMT1*, as well as shorter 3′ UTR lengths, in anti-pPKCθ-iTregs isolated from BM, while iTregs in the spleen displayed similar patterns of *PCMT1* processing, regardless of prior treatment (Figure 3D). We did not detect significantly diminished *PCMT1* in anti-pPKCθ-iTregs recovered from the BM; however, *PCMT1* expression was significantly downregulated in anti-pPKCθ iTregs found in the spleen (Figure 3E). Naive T cells showed comparable levels of *PCMT1* in the BM, but significantly reduced transcripts in the spleen, of mice treated with anti-pPKCθ-iTregs, compared to mice that received DMSO-iTregs (Figure S3D). Interestingly, the *PCMT1* splicing pattern in naive T cells was reversed compared to *in vivo*-recovered iTregs (Figure S3E). Altogether, these data demonstrate that in iTregs, PKCθ plays an important role in regulating the protein methyltransferase, PCMT1, both post-translationally and post-transcriptionally.

Ex Vivo Anti-PCMT1 Delivery Enhances iTreg Differentiation

We sought to further investigate how modulating PCMT1 affected mRNA-RBP interactions in iTregs. To do this, we delivered anti-PCMT1 into human CD4 T cells and then differentiated the cells, *ex vivo*, toward an iTreg phenotype (anti-PCMT1-iTregs). We then compared the phenotype of anti-PCMT1-iTregs to anti-PKCθ-iTregs. Interestingly, we observed a significant increase in the percentage of $CD4^+CD25^+FOXP3^+$ iTregs generated following anti-PCMT1 delivery, and which was comparable to the percentage of $CD4^+CD25^+FOXP3^+$ iTregs treated with anti-pPKCθ (Figure 4A). In addition, relative to DMSO-iTregs, FOXP3 expression was higher in anti-pPKCθ- and in anti-PCMT1-treated iTregs, with each treatment producing a greater percentage of iTregs that were $FOXP3^{hi}$, compared to DMSO-iTregs (Figure 4B). We previously found that anti-PKCθ-iTregs expressed significantly more IFNγ than did DMSO-iTregs, a characteristic consistent with a unique population of highly suppressive Tregs.[39,60,61] Therefore, we also assessed IFNγ expression in anti-PCMT1 iTregs. Delivering either anti-pPKCθ or anti-PCMT1 into CD4 T cells increased the percentage of $IFN\gamma^{hi}$-expressing iTregs and suggests that PKCθ and PCMT1 operate within the same pathway to regulate iTreg IFNγ production (Figure 4C).

PCMT1 has been implicated in multiple RNA processing functions, including regulating mRNA nuclear export to facilitate protein translation. We speculated that this is likely further mediated by its regulation of, or interaction with, RBPs. Among these, hnRNPL has been shown to be a key regulator of iTreg post-transcriptional regulation. To explore the possible link between PCMT1 and hnRNPL, we first asked whether anti-pPKCθ treatment affected hnRNPL expression. In anti-pPKCθ-iTregs, hnRNPL cytosolic expression was increased, while nuclear hnRNPL levels were diminished (Figure 4D). However, in anti-PKCθ-Tconvs, we observed decreased cytosolic and increased nuclear hnRNPL (Figures S5A and S5B). These results suggested to us that hnRNPL cellular localization not only contributes to iTreg differentiation, but that its cytosolic versus nuclear accumulation is regulated in a PKCθ-dependent manner.

Our *in vitro* data suggested that PKCθ and PCMT1 may act within the same signaling pathway to regulate FOXP3 and IFNγ expression. Therefore, we asked whether either of these pathways converge at the level of hnRNPL association. To determine whether PKCθ or

STAT1 and pSTAT1 (Y701) were quantified using ImageJ software. (C) *PCMT1* splicing and 3′ UTR lengths were analyzed using RT-PCR in *ex vivo*-treated iTregs. (D) *PCMT1* splicing and 3′ UTR length were analyzed using RT-PCR and *PCMT1* gene expression was quantified using qPCR in iTregs isolated from (E) BM and (F) spleen of iTreg-treated mice on day 17. Red frames indicate the expected amplicon sizes. Data represent the mean ± SEM of two or three independent experiments. For *in vivo* experiments, four mice per group were used. An unpaired, two-tailed Student's t test was used for analysis. $^{**}p < 0.01$, $^{***}p < 0.001$.

Please cite this article in press as: Ozay et al., Protein Kinase C Theta Modulates PCMT1 through hnRNPL to Regulate FOXP3 Stability in Regulatory T Cells, Molecular Therapy (2020), https://doi.org/10.1016/j.ymthe.2020.06.012

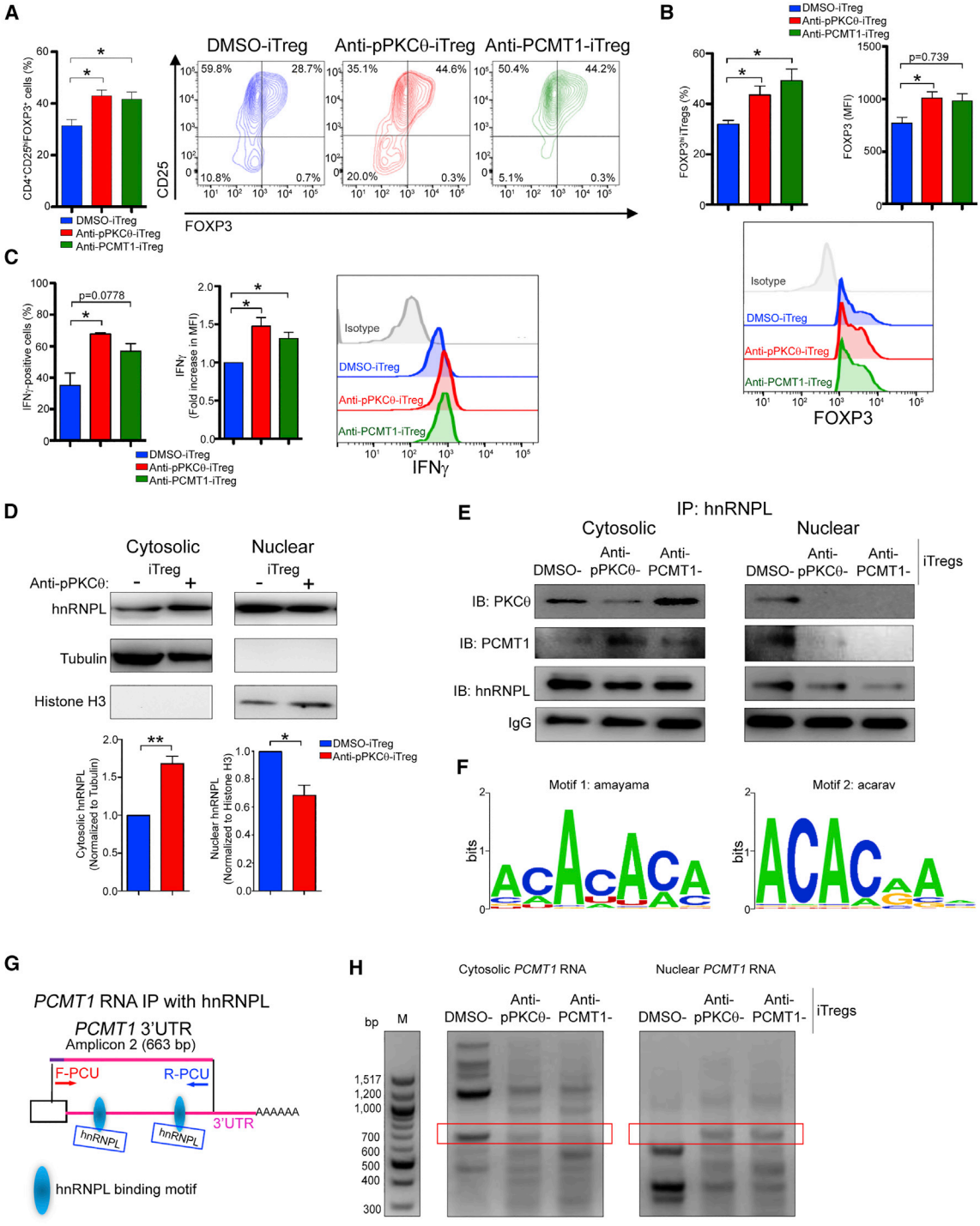

Figure 4. *Ex Vivo* Anti-PCMT1 Delivery Enhances iTreg Differentiation

(A) Percentages of $CD4^+CD25^+FOXP3^+$ T cells with representative scatterplots following *ex vivo* treatment with cell-penetrating anti-pPKCθ or anti-PCMT1 delivery. (B) Percentage of $FOXP3^{high}$ iTregs and FOXP3 median fluorescent intensities (MFIs) together with their representative histograms of iTregs treated as in (A). (C) Percentage of $IFN\gamma^+$ iTregs and fold increase in IFNγ MFI, together with representative histograms, of iTregs treated as in (A). (D) Cytoplasmic and nuclear distributions of hnRNPL in anti-pPKCθ-iTregs were analyzed by immunoblotting. Normalized densities for cytoplasmic and nuclear hnRNPL were quantified relative to tubulin and histone H3 expression,

(legend continued on next page)

PCMT1 physically interacts with hnRNPL, we immunoprecipitated cytosolic and nuclear hnRNPL and examined the degree of PKCθ- and PCMT1-hnRNPL interaction in iTregs treated either with anti-pPKCθ or with anti-PCMT1. We observed that, in DMSO-iTregs, hnRNPL and PKCθ interactions appear equivalent in the cytosol and the nucleus, while hnRNPL-PCMT1 interactions are reduced, but detectable in the cytosol, and are more robust in the nucleus (Figure 4E). Nuclear association of PKCθ or of PCMT1 with hnRNPL was significantly diminished in iTregs following either anti-pPKCθ or anti-PCMT1 treatment. Cytosolic hnRNPL-PKCθ association was significantly reduced in anti-pPKCθ-treated iTregs but increased in anti-PCMT-iTregs. We found the opposite trend for hnRNPL-PCMT1 interactions: cytosolic hnRNPL-PCMT1 binding increased in anti-pPKCθ-iTregs but was lower in anti-PCMT1-iTregs (Figure 4E). These data are consistent with a model whereby PKCθ and PCMT1 may interact with each other and compete for binding to hnRNPL, which may act to shuttle both proteins into the nucleus. Constraining either pPKCθ or PCMT1 via intracellular antibody delivery may allow increased cytosolic association of the other protein with hnRNPL (Figure 4E, upper two panels, left side). The fact that both PKCθ and PCMT1 are undetectable in nuclear extracts in anti-pPKCθ- and anti-PCMT1-iTregs supports the notion that these two proteins interact in the cytosol, and delivering an antibody to one protein effectively constrains nuclear translocation of both (Figure 4E, upper two panels, right side). We noted that hnRNPL is also diminished in nuclear extracts from anti-pPKCθ- and anti-PCMT1-iTregs, further suggesting that constraining pPKCθ or PCMT1 may also impede hnRNPL nuclear shuttling, when bound to either of these proteins in the cytosol (Figure 4E, third panel, right side). Altogether, these results confirmed that both PKCθ and PCMT1 interact with hnRNPL, and that the cellular compartment in which these interactions take place can be manipulated via anti-pPKCθ or anti-PCMT1 delivery into iTregs.

A major function of RBPs, such as hnRNPL, is to aid in mRNA export prior to translation. Given the reduced nuclear interactions of hnRNPL with PKCθ and PCMT1 following antibody delivery, we asked whether this also negatively affected the ability of hnRNPL to bind *PCMT1* mRNA. Using several bioinformatics tools, including the Catalog of Inferred Sequence Binding Preferences of RNA binding proteins (CISBP-RNA) database, we identified two CA-rich RNA binding motifs recognized by hnRNPL (Figure 4F). CA-rich elements within 3′ UTR sequences serve as central hubs for further RNA processing events, influencing RNA stability and nuclear export.[62] In general, incorrectly spliced mRNAs, such as those with retained introns or aberrant exon skipping, can undergo either nuclear RNA decay or nonsense-mediated RNA decay in the cytoplasm. Only correctly spliced, stable mRNAs are properly exported and translated.[63] To investigate whether hnRNPL-PCMT1 or hnRNPL-PKCθ association is important for correctly spliced, stable mRNA export in iTregs, we isolated cytoplasmic and nuclear RNA from iTregs followed by RNA immunoprecipitation. We designed 3′ UTR-specific primers to amplify putative hnRNPL binding sites, including two putative hnRNPL binding sites within the 3′ UTR of *PCMT1* (Figure 4G). We subsequently identified hnRNPL binding sites located within the 3′ UTR of all of the key iTreg genes studied herein, namely *FOXP3*, *IFNG*, *IFNGR1,* and *PDCD1* (Figure S4). Strikingly, we found robust hnRNPL-*PCMT1* mRNA association in the cytosol of DMSO-iTregs. These interactions were markedly reduced in iTregs treated either with anti-pPKCθ or with anti-PCMT1 and were accompanied by a concomitant increase in nuclear hnRNPL-*PCMT1* association (Figure 4H). We detected hnRNPL-*PDCD1* interactions, mainly in the nucleus, of DMSO-iTregs, while anti-PCMT1-treated iTregs showed slightly more hnRNPL-*PDCD1* association in the cytosol (Figure S5C). Cytosolic hnRNPL-*FOXP3* interactions remained intact in anti-pPKCθ-iTregs but were lost in anti-PCMT1-iTregs (Figure S5D). Nuclear export of stable *IFNG* and *IFNGR1* mRNA was not appreciably affected by anti-pPKCθ or anti-PCMT1 delivery (Figures S5E and S5F). These results indicate that stable mRNA export of *PCMT1* is tightly regulated by hnRNPL through its association with PCMT1 and PKCθ. More importantly, both PKCθ and PCMT1 can regulate selective mRNA export of key iTreg genes in a gene-specific manner.

PCMT1 Acts to Destabilize the iTreg Phenotype through Its Effects on *FOXP3* Methylation

In many aspects, delivering anti-PCMT1 into iTregs phenocopied the results we obtained when we generated anti-pPKCθ-iTregs. This included producing equivalent populations of FOXP3^{hi} and IFNγ^{hi} iTregs. Therefore, we asked whether PCMT1 directly regulates *FOXP3* gene expression. Using chromatin immunoprecipitation (ChIP), followed by qPCR, we determined that PCMT1 binds directly to *FOXP3* in iTregs. Moreover, anti-pPKCθ and anti-PCMT1 treatment dramatically reduced PCMT1-*FOXP3* interactions in iTregs (Figure 5A). These data suggest that fully functional PKCθ and PCMT1 are critical for PCMT1-*FOXP3* association. *FOXP3* expression is tightly regulated by several transcription factors that bind the TSDR, following its demethylation. To date, a highly demethylated TSDR is the most reliable marker for stable *FOXP3* expression. In most iTregs, the TSDR is methylated, leading to destabilized *FOXP3* expression.[64,65] This instability is thought to result from reduced STAT5 binding within the TSDR.[66,67] We identified 15 CpG islands within the human *FOXP3* TSDR sequence, including two that flanked the proximal STAT5 binding site, and two that overlapped with the distal STAT5 binding site (Figure 5B). As a logical extension to our discovery that PCMT1, a methlytransferase, directly binds to *FOXP3*, we evaluated the level of TSDR methylation in DMSO-iTregs and

respectively. (E) Cytosolic and nuclear association of hnRNPL with PKCθ and PCMT1 in iTregs was determined using co-immunoprecipitation. (F) Predicted hnRNPL RNA binding motifs using the Catalog of Inferred Sequence Binding Preferences of RNA binding proteins (CISBP-RNA) database in humans. (G) Schematic of hnRNPL binding to the *PCMT1* 3′ UTR and (H) hnRNPL association with cytosolic and nuclear *PCMT1* mRNA in anti-pPKCθ-iTregs and anti-PCMT1-iTregs. Red frames indicate the expected amplicon size. Data represent the mean ± SEM of two or three independent experiments. An unpaired, two-tailed Student's t test was used for analysis. *$p < 0.05$, **$p < 0.01$.

Please cite this article in press as: Ozay et al., Protein Kinase C Theta Modulates PCMT1 through hnRNPL to Regulate FOXP3 Stability in Regulatory T Cells, Molecular Therapy (2020), https://doi.org/10.1016/j.ymthe.2020.06.012

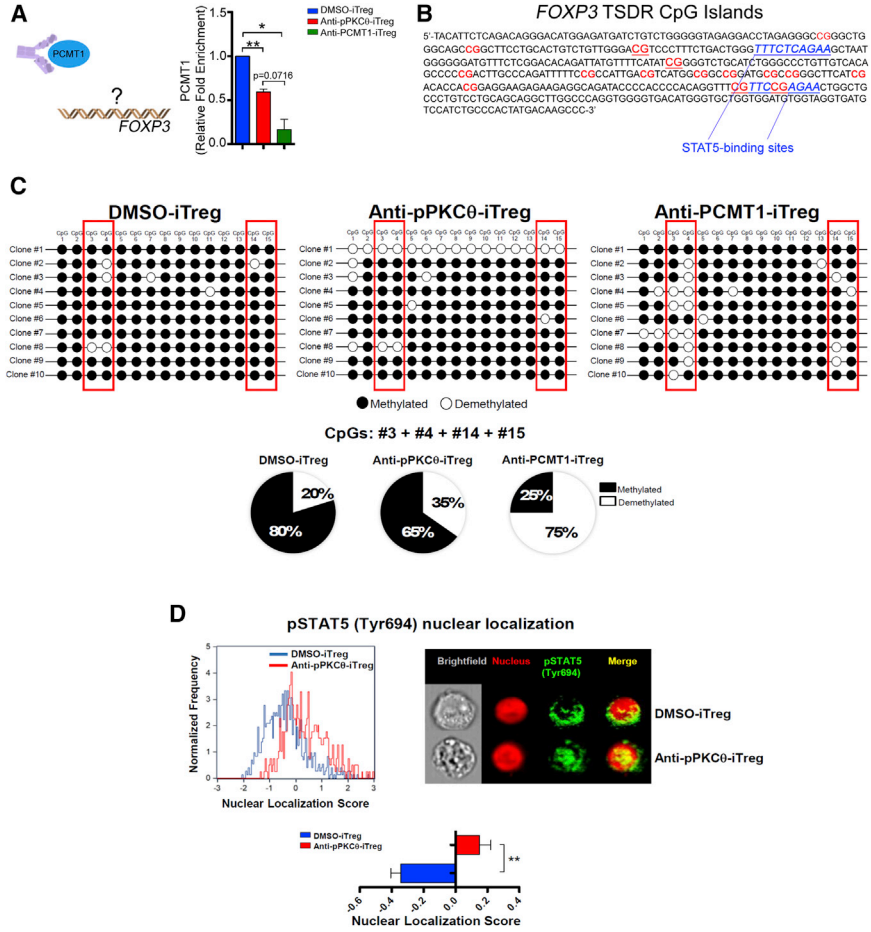

Figure 5. PCMT1 Acts to Destabilize the iTreg Phenotype through Its Effects on *FOXP3* Methylation

(A) Chromatin immunoprecipitation quantifying PCMT1 occupancy on the *FOXP3* promoter in iTregs. (B) CpG islands (indicated in bold type) and STAT5-binding sites (underlined in blue) in the human *FOXP3* TSDR. (C) Bisulfite sequencing of 10 different clones per iTreg treatment showing *FOXP3* TSDR CpG islands. Percentages of CpGs demethylated at sites #3, #4, #14, and #15 were quantified and are shown as pie charts. (D) Nuclear localization of pSTAT5 (Tyr694) was quantified by imaging flow cytometry using Amnis ImageStream analysis. Representative cell frequency histograms, along with representative images at ×60 magnification, show anti-pPKCθ-iTregs with nuclear pSTAT5. The Amnis IDEAS wizard, with nuclear masking applied, was used to quantify nuclear localization of pSTAT5, based on similarity score. Data represent mean ± SEM of two or three independent experiments. An unpaired, two-tailed Student's t test was used for analysis. *$p < 0.05$, **$p < 0.01$.

compared it with that of anti-pPKCθ- and anti-PCMT1-treated iTregs, using bisulfite sequencing of 10 individual clones isolated from each of the three iTreg treatment conditions, as indicated (Figure 5C). When we assessed the methylation of the four specific CpGs flanking the STAT5 binding site, we observed that DMSO-iTregs showed the lowest percentage (20%) of demethylation of these CpGs in the clones analyzed. Interestingly, in anti-pPKCθ-iTregs, approximately 35% of these CpG sites within the TSDR were demethylated. Following anti-PCMT1 treatment, however, we found that of the clones tested, 75% of CpG sites that either flanked or overlapped with STAT5 binding sites were demethylated (Figure 5C), strongly suggesting that inhibiting PCMT1 may enhance the stability of *FOXP3* expression by reducing methylation of key CpG sites within the TSDR. We further speculated that increased demethylation of CpG islands surrounding the STAT5 binding sites would increase nuclear retention of pSTAT5. To examine this possibility, we used imaging flow cytometry to evaluate levels of nuclear pSTAT5 in DMSO- and anti-pPKCθ-iTregs *in vitro*. Consistent with our prediction, anti-pPKCθ-iTregs exhibited significantly greater amounts of nuclear pSTAT5, compared to iTregs differentiated in the presence of DMSO (Figure 5D).

Overall, we provide strong evidence that PKCθ negatively regulates iTreg induction through its modulation of two key components of RNA processing, PCMT1 and hnRNPL, via multiple cellular mechanisms. Furthermore, our data suggest that this inhibitory pathway can be interrupted in iTregs through the intracellular delivery either of anti-pPKCθ or anti-PCMT1, to modulate these mechanisms in favor of enhancing iTreg suppressive functions. Finally, we identified, for the first time, that the protein repair methyltransferase, PCMT1, acts as a key iTreg instability factor through its control of *FOXP3* TSDR methylation.

DISCUSSION

A great deal has been learned about transcriptional regulation of immune cell responses. A growing area of interest focuses on alternative splicing and RNA processing in regulating T cell differentiation and function following antigenic stimulation, as distinct protein isoforms for many T cell genes have been identified.[19,22,68–70] These processes operate together with RBPs, transcription factors, and epigenetic modifiers.[6,69] Although numerous immune-related genes undergo alternative splicing and RNA processing, differential isoform expression and RNA processing in Treg differentiation remain largely unexplored.

Our studies provide an extensive analysis of altered RNA processing in the context of iTreg differentiation and function, and we utilized several approaches to investigate PKCθ modulation of splicing regulators, RNA splicing, stability, and nuclear export. We specifically targeted pPKCθ, using a cell-penetrating antibody, to probe post-transcriptional RNA processing in iTregs. We discovered that PKCθ influenced RNA processing of several iTreg genes, including CD45

Please cite this article in press as: Ozay et al., Protein Kinase C Theta Modulates PCMT1 through hnRNPL to Regulate FOXP3 Stability in Regulatory T Cells, Molecular Therapy (2020), https://doi.org/10.1016/j.ymthe.2020.06.012

(*PTPRC*), *FOXP3*, *PDCD1*, *IFNG*, and *IFNGR1*, in cell-specific and tissue-specific contexts. Furthermore, splicing regulator analysis revealed that two RNA regulatory proteins, hnRNPL and PCMT1, were controlled by PKCθ at multiple levels. We found that PKCθ regulated both the subcellular localization of hnRNPL and its binding to mRNA. Additionally, we showed that PKCθ regulated PCMT1 alternative splicing, stabilized *PCMT1* mRNA through its association with hnRNPL, and enhanced its nuclear export prior to its translation into stable protein. However, anti-pPKCθ delivery into iTregs altered the *PCMT1* splicing pattern and destabilized and prevented the nuclear export of *PCMT1* mRNA, due to loss of *PCMT1*-hnRNPL binding. Utilizing our cell-penetrating peptide-intracellular antibody delivery strategy to target PCMT1, we identified a practical approach to promote iTreg differentiation and function. We determined that PCMT1 directly binds to the *FOXP3* promoter and, more interestingly, inhibiting PCMT1 increased *FOXP3* TSDR demethylation, thereby enhancing FOXP3 stability and iTreg maintenance. In conjunction with our recent discovery that intracellular anti-pPKCθ delivery generates a unique, highly suppressive population of FOXP3^{hi}PD1^{hi}IFNγ^{hi} iTregs,[39] this study supports the notion that PKCθ negatively regulates iTreg differentiation and stability by modulating key RNA processing regulators.

We observed elevated pSTAT1 (Y701) levels in anti-pPKCθ-iTregs, compared to DMSO-iTregs. Reduced pAKT, coupled with upregulated pSTAT1, has previously been associated with enhanced IFNγ production by CD4^{+}CD25^{+}FOXP3^{+} Tregs in mice. Moreover, AKT and STAT1 were found to function within the same pathway, with both induced by IFNγ, and served to control skin graft rejection *in vivo*.[60,61] IFNγ produced by these Tregs also induced indoleamine 2,3-dioxygenase (IDO) production by antigen-presenting cells, to further suppress immune cell activity.[71] Anti-pPKCθ-iTregs exhibited higher IFNγ expression and greater suppressive capacity, both *in vitro* and *in vivo*, suggesting that this pathway may critically contribute to the suppressive function of iTregs through autonomous IFNγ signaling. Anti-pPKCθ-iTregs also express high levels of PD1, which may also be related to this pathway. A downstream phosphatase of PD1 signaling, SHP-2, was shown to interact with cytosolic STAT1, reducing its recruitment to the IFNγ receptor (IFNγR), and dampening Th1 function.[72] Further studies investigating how PD1 and IFNγ signaling pathways might intersect downstream of PKCθ modulation in iTregs are needed to fully elucidate cellular mechanisms that regulate suppressive function and Th1-Treg plasticity.

Members of the PKC family can influence mRNA splicing in various cell types and have been shown to phosphorylate SC35, which functions in co-transcriptional regulation of alternative splicing.[19,40,70] As previously indicated, we found that PKCθ regulated cytoplasmic versus nuclear distribution of splicing regulators. Among these, we focused on hnRNPL, as it was uniquely altered in iTregs following PKCθ inhibition. Unlike other splicing regulators we investigated, only hnRNPL was sequestered in the cytosol after anti-pPKCθ delivery. This correlated with increased exon skipping of CD45 (*PTPRC*), as well as greater expression of CD45RO, which is consistent with reduced levels of nuclear hnRNPL in anti-pPKCθ-iTregs, compared to DMSO-iTregs. Alternatively, we saw no differences in the splicing patterns of *FOXP3*, *PDCD1*, *IFNG*, and *IFNGR1* in iTregs, regardless of treatment, suggesting that these genes may not be alternatively spliced during *in vitro* differentiation. We did observe shorter 3′ UTR lengths in *PDCD1*, indicating that anti-pPKCθ-iTregs implement gene-specific 3′ UTR processing, which may further stabilize PD1 expression *in vitro*. Similar mechanisms may account for the *in vivo* RNA dynamics we observed, in the context of immune response and Treg differentiation. Anti-pPKCθ-iTregs, which exhibited elevated PD1 expression and superior suppressive function, were long-lasting and accumulated in high numbers in the BM and spleen of mice following adoptive iTreg transfer in a humanized mouse model of GvHD.[39] Studies have reported that Tregs can lose FOXP3 expression and take on a proinflammatory phenotype in several disease environments.[73] However, we determined that only anti-pPKCθ-iTregs maintained their *FOXP3* expression in the BM, since we were unable to amplify stable mRNA in DMSO-iTregs. Of note, we detected tissue-specific changes in the alternative splicing patterns of *FOXP3*, *PDCD1*, *IFNG*, and *IFNGR1* in anti-pPKCθ-iTregs. Moreover, only in anti-pPKCθ-iTregs recovered from the BM could we detect stable mRNA production. A host of immune cells are available to act differentially on iTregs *in vivo* through direct and indirect mechanisms. Thus, one potential explanation for the differences in alternative splicing patterns we observed in anti-pPKCθ-iTregs *in vitro* and *in vivo* may be attributed to the interactions of iTregs with other cell types. Additional studies are needed to identify these *in vivo* modulators.

Most strikingly, our data reveal an as-yet-undescribed contribution of the protein methyltransferase PCMT1 to *FOXP3* methylation, and which we demonstrate is regulated by PKCθ signaling. We showed that PCMT1 expression was downregulated following anti-pPKCθ delivery. Additionally, in anti-pPKCθ-iTregs, we observed phosphorylated PCMT1 in the nucleus, suggesting that post-translational control of PCMT1 is modulated downstream of PKCθ signaling. In the brain, PCMT1 reportedly regulates the phosphatidylinositol 3-kinase (PI3K)/AKT/mammalian target of rapamycin (mTOR) signaling pathway, as increased AKT/GSK3β signaling is seen in the hippocampus of *Pcmt1* knockout mice.[74,75] Additionally, GSK3β phosphorylation at serine 9, which inhibits GSK3β function, was low in *Pcmt1*$^{+/+}$ mice, indicating an abundance of activated GSK3β, and this suggests that *Pcmt1* and GSK3β may function in a positive feedback loop.[76] Considering that PKCθ and GSK3β work in opposition, it is interesting to speculate that GSK3β may phosphorylate PCMT1 to regulate its function when PKCθ activity is inhibited in iTregs. Furthermore, the AKT/GSK3β pathway is a critical signaling axis in iTreg differentiation, since inhibiting mTOR promotes Treg induction.[77] Collectively, these studies suggest that inhibiting PCMT1 could promote Treg induction, in agreement with the data we present in this report; however, additional studies are needed to identify the upstream kinases responsible for phosphorylating PCMT1.

Our results also indicate that PKCθ can regulate *PCMT1* post-transcriptionally. Anti-pPKCθ-iTregs displayed distinct *PCMT1* splicing patterns and less stable mRNA *in vitro*. Furthermore, and consistent with our *in vitro* data, we observed a tissue- and cell-specific switch in *PCMT1* RNA processing *in vivo* as well. Based on these robust post-translational and post-transcriptional modifications to PCMT1, downstream of PKCθ signaling, we delivered anti-PCMT1 to iTregs to further investigate PCMT1 functions in iTreg differentiation. As we predicted, anti-PCMT1 delivery also generated a higher percentage of iTregs, which showed high FOXP3 and IFNγ expression *in vitro*. Moreover, we found that PCMT1 also interacted with hnRNPL. Both anti-pPKCθ and anti-PCMT1 delivery reduced the interaction of these respective proteins with hnRNPL in the nucleus and resulted in an inverse association of these hnRNPL-interacting proteins in the cytosol: hnRNPL-PKCθ binding was diminished in the cytosol, while hnRNPL-PCMT1 interactions increased following anti-pPKCθ delivery. Conversely, in anti-PCMT1-treated iTregs, cytosolic hnRNPL-PKCθ binding increased, while hnRNPL-PCMT1 interactions were attenuated. Previous reports suggested that PCMT1 is part of an RNA nuclear export complex and can associate with multiple RBPs.[58] Considering PCMT1-hnRNPL interactions in the context of RNA export, we found that PKCθ regulates hnRNPL-RNA interactions in iTregs. Interestingly, inhibiting PKCθ or PCMT1 abrogated stable *PCMT1* mRNA export to the cytoplasm, likely due to loss of hnRNPL-*PCMT1* binding, and suggests that PCMT1 may also regulate its own mRNA export. Finally, we observed that PKCθ and PCMT1 selectively regulated mRNA export and hnRNPL interactions with *FOXP3*, *PDCD1*, *IFNG*, and *IFNGR1* mRNA. It remains to be determined whether anti-pPKCθ and anti-PCMT1 delivery differentially influence translational control of these mRNAs in the cytosol of iTregs.

Our parallel findings in anti-pPKCθ- and anti-PCMT1-iTregs also revealed the possibility that more stable iTregs resulted from epigenetic modification of *FOXP3*, together with unique expression of IFNγ. Currently, the most reliable marker for determining Treg stability is the methylation status of the *FOXP3* TSDR.[78] Other reports indicate that IFNγ-expressing Tregs exhibited a more stable Treg phenotype, and this was associated with a more highly demethylated TSDR.[79] Intriguingly, we observed direct binding of PCMT1 to *FOXP3* in iTregs, and this binding could be prevented by intracellular delivery either of anti-pPKCθ or anti-PCMT1. PCMT1 contains a domain with global methyltransferase activity, and we further analyzed the methylation status of the *FOXP3* TSDR in anti-PCMT1-treated iTregs. Strikingly, we observed significantly lower TSDR methylation in anti-PCMT1-treated iTregs, and, more importantly, demethylated CpGs overlapped with the STAT5 binding site, consistent with a requirement for STAT5 binding for the maintenance of *FOXP3* gene expression. A deeper analysis of the TSDR methylation pattern in anti-PCMT1-treated iTregs revealed that the fourth CpG island showed consistently high demethylation. We followed up this observation by running the PROMO algorithm to identify putative transcription factor binding sites surrounding this CpG. We were intrigued to find that the GATA-1 transcription factor binding site spans this demethylated CpG, in close proximity to XBP1, TFIID, and RXR-α binding sites.[80,81] GATA-1 is considered a "Treg phenotype-locking" transcription factor able to enhance transcriptional activity of *FOXP3*.[82,83] Hence, our results reinforce the idea that targeting PCMT may be a beneficial strategy for maximizing iTreg stability and suppressive function.

Collectively, our data reveal that the T cell-specific kinase PKCθ and the protein methyltransferase PCMT1 are intimately involved in controlling iTreg differentiation, stability, and function *in vitro* and *in vivo*. Furthermore, using synthetic CPPMs we could deliver functional antibodies across the cell membrane of human CD4 T cells, which allowed us to define and manipulate *in vitro* the cellular mechanisms that regulate iTreg differentiation. This approach shows great promise as a tool for probing intracellular signaling pathways, as well as for manipulating human immune cells *ex vivo*, in the context of advancing cell-based therapies.

MATERIALS AND METHODS

Animals

All animal studies were approved by, and conducted under the oversight of, the Institutional Animal Care and Use Committee of the University of Massachusetts Amherst. Seven-week old female NSG mice were purchased from The Jackson Laboratory (Bar Harbor, ME, USA). Mice were rested for 1 week prior to use, housed under pathogen-free conditions in micro-isolator cages, and received acidified water (pH 3.0) supplemented with antibiotics (trimethoprim + sulfamethoxazole) throughout the duration of the experimental procedures.

Antibodies and Reagents

Immunoblotting antibodies used in this study were as follows: anti-mouse pSC35 (clone SC35; Santa Cruz Biotechnology, Dallas, TX, USA), anti-mouse hnRNPL (clone 4D11; Novus Biologicals, Littleton, CO, USA), anti-rabbit PCMT1 (polyclonal; LifeSpan Biosciences, Seattle, WA), anti-mouse pSTAT1 (Y701; clone KIKSI0803; Thermo Fisher Scientific, Waltham, MA, USA), anti-mouse STAT1 (clone 10C4B40; BioLegend, San Diego, CA, USA), anti-rabbit pAKT (S473; polyclonal), anti-rabbit AKT (polyclonal), anti-mouse histone H3 (clone 96C10; all from Cell Signaling Technology, Danvers, MA, USA), and anti-mouse α-tubulin (clone B-5-1-2; Sigma, St. Louis, MO, USA). Flow cytometry antibodies used in this study were anti-CD4 (Brilliant Violet 711 [BV711]; clone RPA-T4), anti-CD25 (phycoerythrin [PE]-Cy7; clone BC96), anti-CD127 (Alexa Fluor 700 [AF700]; clone A019D5), anti-FOXP3 (Alexa Fluor 488 [AF488]; clone 150D; all from BioLegend), anti-IFNγ (allophycocyanin [APC]; clone B27; BD Biosciences, Franklin Lakes, NJ, USA), anti-rabbit PCMT1 (unconjugated, polyclonal; LifeSpan Biosciences), and $F(ab')_2$-goat anti-rabbit IgG (H+L) secondary antibody (Qdot 625; polyclonal; Life Technologies, Carlsbad, CA, USA). Live/dead staining was performed utilizing a Zombie Aqua fixable viability kit (BioLegend).

Human iTreg Differentiation following Intracellular Anti-pPKCθ or Anti-PCMT1 Delivery

1 μM synthetic CPPM and 25 nM anti-pPKCθ (Thr538, clone F4H4L1; Life Technologies) or 1 μM $P_{13}D_5$ and 25 nM anti-PCMT1 (polyclonal; LifeSpan Biosciences) were complexed in PBS (phosphate-buffered saline, pH 7.2) at a specific ratio (CPPM/antibody of 40:1). The CPPM/antibody complex was incubated for 30 min at room temperature (RT). Meanwhile, CD4 T cells were isolated from human peripheral blood mononuclear cells (PBMCs) (purchased from STEMCELL Technologies, Vancouver, BC, Canada) using the MojoSort human T cell isolation kit (BioLegend). Isolated human CD4 T cells were then treated with the CPPM/antibody complex for 4 h at 37°C (some cells were treated with DMSO as vehicle control). Cells were harvested and washed with PBS. Cells were thoroughly washed twice with 20 U/mL heparin in PBS for 5 min on ice to remove residual complexes bound to the exterior of the cell membrane. For iTreg differentiation, a CellXVivo human Treg differentiation kit (R&D Systems, Minneapolis, MN, USA) was used and iTreg differentiation medium was prepared using X-VIVO 15 chemically defined, serum-free hematopoietic cell medium according to the manufacturer's instructions. Treated cell pellets were resuspended in iTreg differentiation media (concentration) and seeded into wells of a 12-well tissue culture plate precoated with 5 μg/mL anti-CD3ε plus 2.5 μg/mL anti-CD28 and stimulated for 5 days at 37°C.

Immunoblotting

iTregs were harvested on day 5 of differentiation. Nuclear and cytosolic extracts were prepared by using an NE-PER nuclear and cytosolic extraction kit (Thermo Scientific). 1× sodium dodecyl sulfate (SDS) Laemmli buffer was added into the samples for running on 8% SDS-PAGE for immunoblotting. The blots were probed for RBPs for further analysis. Anti-α-tubulin was probed as a cytosolic lysate loading control, and anti-histone H3 was probed as a nuclear lysate loading control.

In Vivo RNA Analysis of iTregs in a Humanized GvHD Model

Total CD4 T cells were isolated from human PBMCs (hPBMCs) collected from a healthy donor, treated with a CPPM/anti-pPKCθ complex, and then differentiated for 5 days into iTregs, as previously described. On day 4, total hPBMCs from the same donor were thawed and rested overnight in fresh RPMI 1640 complete media (10% fetal bovine serum, 100 U/mL penicillin-streptomycin, 1 mM sodium pyruvate, 2 mM L-glutamine) at 37°C in a 5% CO_2 incubator. On day 5, NSG mice were conditioned with 2 Gy of total body irradiation using a ^{137}Cs source and then rested for 4–6 h. 10×10^6 total hPBMCs were mixed with 3.3×10^6 iTregs and adoptively transferred into irradiated NSG mice via the tail vein. Body weight and disease symptoms were observed daily. On day 17, some animals were sacrificed for tissue analysis. BM cells, recovered from the tibias and femurs, and splenocytes were isolated by manipulation through a 40-μm filter. Red blood cells were lysed in ACK lysis buffer, and the remaining white blood cells were enumerated using trypan blue exclusion. Afterward, cells were incubated with human CD4 T lymphocyte enrichment cocktail (BD Biosciences) followed by incubation with BD IMag streptavidin particles plus (BD Biosciences) to deplete non-CD4 T cell fractions. CD4 T cells were sequentially incubated with biotinylated anti-CD127 antibody followed by incubation with BD IMag streptavidin particles plus. The $CD127^-$ fraction was collected and further incubated with biotinylated anti-CD25 antibody followed by incubation with BD IMag streptavidin particles plus to obtain the $CD25^+$ iTreg fraction. The naive $CD127^+CD25^-$ T cell fraction was also recovered. Total RNA was isolated as described below.

qPCR

Total RNA was isolated using the Quick-RNA isolation kit (Zymo Research, Irvine, CA, USA) according to the manufacturer's protocol. 1 μg of total RNA was reverse transcribed to cDNA using 2′-deoxynucleoside 5′-triphosphates (dNTPs) (New England Biolabs, Ipswich, MA, USA), Moloney murine leukemia virus (M-MuLV) reverse transcription buffer (New England Biolabs), oligo(dT) (Promega, Madison, WI, USA), RNase inhibitor (Promega), and M-MuLV reverse transcription (New England Biolabs) on a Mastercycler gradient thermal cycler (Eppendorf, Hamburg, Germany). Primers used for *PCMT* amplification were forward primer (5′-GCTGAAGAAGCCCCTTATGA-3′) and reverse primer (5′- TCTTCCTCCGGGCTTTAACT-3′). qPCR was performed in duplicate with 2× SYBR Green qPCR master mix (BioTool, Ely, UK) using the Mx3000P system (Agilent Technologies, Santa Clara, CA, USA). qPCR conditions were as follows: 95°C for 1 min, 95°C for 25 s, 62°C for 25 s (40 cycles), 95°C for 1 min, 62°C for 1 min, and 95°C for 30 s. Relative gene expression was determined using the ΔΔCt method. The results are presented as the fold expression of the gene of interest normalized to the housekeeping gene β-actin (*ACTB*) for cells and relative to the Tconv + DMSO sample for *in vitro* experiments and naive + DMSO for *in vivo* experiments.

RT-PCR for Splicing and 3′ UTR Analyses

Total RNA was isolated using the Quick-RNA isolation kit (Zymo Research) according to the manufacturer's protocol. 0.5 μg of total RNA was reverse transcribed to cDNA using random hexamers (Integrated DNA Technologies, Coralville, IA, USA) with M-MuLV reverse transcriptase (New England Biolabs) on a Mastercycler gradient thermal cycler (Eppendorf). Splicing primers (Table S1) and 3′ UTR primers (Table S2) were specifically designed for the genes analyzed in this study. PCR (35 cycles) was performed using Phusion high-fidelity DNA polymerase (New England Biolabs) followed by resolution on 2% agarose gel. PCR conditions were as follows: initial denaturation at 98°C for 30 s, annealing at 98°C for 5 s, 52°C for 20 s, and 72°C for 1 min, and final extension at 72°C for 5 min. Amplicons were imaged using the G:BOX gel documentation system (Syngene, Frederick, MD, USA).

λ-Phosphatase Treatment

Cells were lysed in radioimmunoprecipitation assay (RIPA) buffer (150 mM NaCl, 1% IGEPAL CA-630, 0.1% SDS, 50 mM Tris [pH 8.0], 0.5% sodium deoxycholate). Lysates were treated with 100 U of λ protein phosphatase (New England Biolabs) in the presence of 1 mM $MnCl_2$ for 1 h at 30°C. 1× SDS Laemmli buffer was added

into the samples and they were boiled for 5 min at 95°C. The samples were run on 8% SDS-PAGE for immunoblotting.

hnRNPL Immunoprecipitation

iTregs were harvested after 5 days of differentiation and lysed in immunoprecipitation lysis buffer (50 mM HEPES [pH 7.8], 250 mM NaCl, 1% Nonidet P-40 [NP-40], protease + phosphatase inhibitors). DynaBeads (protein G) were coupled with 3 μg of anti-hnRNPL (4D11; Novus Biologicals, Littleton, CO, USA) in the presence of 1% BSA in PBS and incubated for 2 h at 4°C with rotation. After the incubation, the antibody-coupled DynaBeads were washed six times with 1 mL of immunoprecipitation wash buffer (Tris-HCl [pH 8.0], 200 mM NaCl, 0.1% NP-40). Later, cell lysates were incubated with antibody-coupled DynaBeads for 1 h at 4°C using a rotator. Subsequently, beads were washed six times with 0.5 mL of immunoprecipitation wash buffer. 1× SDS Laemmli buffer was added into the samples, and lysates were run on an 8% SDS-PAGE, followed by immunoblotting with anti-hnRNPL, anti-PKCθ, and anti-PCMT1.

RNA Immunoprecipitation

After harvesting on day 5 of differentiation, cells were lysed in RNA immunoprecipitation lysis buffer (50 mM HEPES [pH 7.8], 250 mM NaCl, 1% NP-40, 1× protease + phosphatase inhibitors, 100 U/mL RNase inhibitor). DynaBeads (protein G) were coupled with 3 μg of anti-hnRNPL (4D11; Novus Biologicals) or anti-IgG (control antibody) in the presence of 1% BSA in PBS and incubated for 2 h at 4°C with rotation. After the incubation, the antibody-coupled DynaBeads were washed six times with 1 mL of immunoprecipitation wash buffer (Tris-HCl [pH 8.0], 200 mM NaCl, 0.1% NP-40). Cell lysates were incubated with antibody-coupled DynaBeads for 1 h at 4°C using a rotator. Subsequently, beads were washed six times with 0.5 mL of immunoprecipitation wash buffer + 100 U/mL RNase inhibitor. RNA was purified via a Quick-RNA isolation kit (Zymo Research) according to the manufacturer's protocol to further use on RT-PCR experiments.

ChIP-qPCR

Cells were crosslinked with 1% formaldehyde, lysed in SDS lysis buffer (1% SDS, 10 mM EDTA, and 50 mM Tris [pH 8.1]), and sonicated with a Bioruptor sonicator (Diagenode, Denville, NJ, USA). Cell lysates were incubated with 2 mg of anti-PCMT1 (LifeSpan Biosciences, polyclonal) or normal rabbit immunoglobulin G (IgG) (Santa Cruz Biotechnology) coupled to DynaBeads at 4°C for 2 h. Protein-DNA complexes were recovered with DynaBeads, washed, eluted with elution buffer (1% SDS, 0.1 M $NaHCO_3$), and reverse crosslinked overnight at 65°C. DNA was purified by proteinase K digestion and extracted with phenol-chloroform extraction. Aqueous phase was transferred into a fresh tube and the DNA was precipitated with 3 M sodium acetate containing 2 mL of glycogen and 4 vol of ethanol by keeping overnight at −20°C. Genes were amplified using qPCR primers designed as follows: human *FOXP3*, forward (5′-TGACCAAGGCTTCATCTGTG-3′), reverse (5′-GAGGAACTCT GGGAATGTGC-3′); and human *IFNG*, forward (5′-CTCTTGGC TGTTACTGCCAGG-3′), reverse (5′-CTCCACACTCTTTTGGAT GCT-3′). qPCR was performed in duplicate with 2× SYBR Green qPCR master mix (BioTool) using the Mx3000P system (Agilent Technologies). qPCR conditions were as follows: 95°C for 1 min, 95°C for 25 s, 62°C for 25 s (40 cycles), 95°C for 1 min, 62°C for 1 min, and 95°C for 30 s. Relative gene expression was determined using the ΔΔCt method. The results are presented as the fold expression of the gene of interest normalized to the housekeeping gene *ACTB* for cells and relative to the Tconv + DMSO sample.

Bioinformatics for RBP Motifs

Splice variants, intron-exon sequences, and 3′ UTR sequences were analyzed and obtained from Ensembl. RBP motifs for hnRNPL were analyzed utilizing the CISBP-RNA database.[84] 3′ UTR sequences were analyzed for hnRNPL-binding sites using RBPmap.[85]

Bisulfite Sequencing

Sodium bisulfite modification of genomic DNA was carried out using the EZ DNA Methylation-Direct kit (Zymo Research) according to the manufacturer's protocol. Bisulfite-treated DNA was PCR amplified using the following methylation-specific primers and ZymoTaq DNA polymerase (Zymo Research): forward primer, 5′-TGTTT GGGGGTAGAGGATTT-3′, reverse primer, 5′-TATCACCCCACC TAAACCAA-3′. PCR conditions were as follows: initial denaturation at 95°C for 10 min, 40 cycles of denaturation at 95°C for 30 s + annealing at 55°C for 40 s + extension at 72°C for 1 min, and final extension at 72°C for 7 min. Amplified DNA products were gel purified using a GeneJET gel extraction kit (Thermo Scientific) and cloned into pMiniT 2.0 cloning vector using the NEB PCR cloning kit (New England Biolabs). Competent cells were transformed with the vector. Ten individual positive bacterial colonies were selected, from which recombinant plasmid DNA was purified and sequenced with Sanger sequencing (Genewiz, South Plainfield, NJ, USA).

Statistical Analysis

The results shown are the mean ± SEM. All *in vitro* experimental replicates were repeated at least three times. All *in vivo* experimental replicates were repeated in three separate experiments. An unpaired, two-tailed Student's t test using Prism 5 (GraphPad, San Diego, CA, USA) was used for statistical comparison of two groups, with Welch's correction applied when variances were significantly different. Survival benefit was determined using Kaplan-Meier analysis with an applied log rank test. p values of ≤ 0.05 were considered significantly different.

SUPPLEMENTAL INFORMATION

Supplemental Information can be found online at https://doi.org/10.1016/j.ymthe.2020.06.012.

AUTHOR CONTRIBUTIONS

Conceptualization: E.I.O. and L.M.M.; Methodology: E.I.O., S.S., and L.M.M.; Investigations: E.I.O., S.S., and J.A.T.; Writing – Original Draft: E.I.O. and L.M.M.; Writing – Review & Editing: E.I.O., B.A.O., and L.M.M.; Project Administration: G.N.T. and L.M.M.;

Funding Acquisition: B.A.O. and L.M.M.; Supervision: B.A.O., G.N.T., and L.M.M.

CONFLICTS OF INTEREST

The authors declare no competing interests.

ACKNOWLEDGMENTS

The authors thank A.S. Burnside, Director of the Flow Cytometry Core Facility, Institute for Applied Life Sciences, University of Massachusetts Amherst, Amherst, MA, for guidance, C. Marcho for providing critical help with bisulfite sequencing analysis, and R.A. Goldsby for critical assessment of the manuscript. This research was supported in part by the National Institutes of Health (NIH 5P01CA16600 to B.A.O.) and the Department of Defense (W81XWH1910540 to L.M.M.).

REFERENCES

1. Kafasla, P., Skliris, A., and Kontoyiannis, D.L. (2014). Post-transcriptional coordination of immunological responses by RNA-binding proteins. Nat. Immunol. *15*, 492–502.
2. Black, D.L. (2003). Mechanisms of alternative pre-messenger RNA splicing. Annu. Rev. Biochem. *72*, 291–336.
3. Matlin, A.J., Clark, F., and Smith, C.W.J. (2005). Understanding alternative splicing: towards a cellular code. Nat. Rev. Mol. Cell Biol. *6*, 386–398.
4. Kornblihtt, A.R., Schor, I.E., Alló, M., Dujardin, G., Petrillo, E., and Muñoz, M.J. (2013). Alternative splicing: a pivotal step between eukaryotic transcription and translation. Nat. Rev. Mol. Cell Biol. *14*, 153–165.
5. Melton, A.A., Jackson, J., Wang, J., and Lynch, K.W. (2007). Combinatorial control of signal-induced exon repression by hnRNP L and PSF. Mol. Cell. Biol. *27*, 6972–6984.
6. Ip, J.Y., Tong, A., Pan, Q., Topp, J.D., Blencowe, B.J., and Lynch, K.W. (2007). Global analysis of alternative splicing during T-cell activation. RNA *13*, 563–572.
7. Keene, J.D. (2007). RNA regulons: coordination of post-transcriptional events. Nat. Rev. Genet. *8*, 533–543.
8. Han, S.P., Tang, Y.H., and Smith, R. (2010). Functional diversity of the hnRNPs: past, present and perspectives. Biochem. J. *430*, 379–392.
9. Allemand, E., Guil, S., Myers, M., Moscat, J., Cáceres, J.F., and Krainer, A.R. (2005). Regulation of heterogenous nuclear ribonucleoprotein A1 transport by phosphorylation in cells stressed by osmotic shock. Proc. Natl. Acad. Sci. USA *102*, 3605–3610.
10. Blaustein, M., Pelisch, F., Tanos, T., Muñoz, M.J., Wengier, D., Quadrana, L., Sanford, J.R., Muschietti, J.P., Kornblihtt, A.R., Cáceres, J.F., et al. (2005). Concerted regulation of nuclear and cytoplasmic activities of SR proteins by AKT. Nat. Struct. Mol. Biol. *12*, 1037–1044.
11. Patel, N.A., Kaneko, S., Apostolatos, H.S., Bae, S.S., Watson, J.E., Davidowitz, K., Chappell, D.S., Birnbaum, M.J., Cheng, J.Q., and Cooper, D.R. (2005). Molecular and genetic studies imply Akt-mediated signaling promotes protein kinase CβII alternative splicing via phosphorylation of serine/arginine-rich splicing factor SRp40. J. Biol. Chem. *280*, 14302–14309.
12. van der Houven van Oordt, W., Diaz-Meco, M.T., Lozano, J., Krainer, A.R., Moscat, J., and Cáceres, J.F. (2000). The MKK(3/6)-p38-signaling cascade alters the subcellular distribution of hnRNP A1 and modulates alternative splicing regulation. J. Cell Biol. *149*, 307–316.
13. Ganguly, K., Giddaluru, J., August, A., and Khan, N. (2016). Post-transcriptional regulation of immunological responses through riboclustering. Front. Immunol. *7*, 161.
14. Meininger, I., Griesbach, R.A., Hu, D., Gehring, T., Seeholzer, T., Bertossi, A., Kranich, J., Oeckinghaus, A., Eitelhuber, A.C., Greczmiel, U., et al. (2016). Alternative splicing of MALT1 controls signalling and activation of $CD4^+$ T cells. Nat. Commun. *7*, 11292.
15. Uehata, T., Iwasaki, H., Vandenbon, A., Matsushita, K., Hernandez-Cuellar, E., Kuniyoshi, K., Satoh, T., Mino, T., Suzuki, Y., Standley, D.M., et al. (2013). Malt1-induced cleavage of regnase-1 in $CD4^+$ helper T cells regulates immune activation. Cell *153*, 1036–1049.
16. Grabowski, P.J. (1998). Splicing regulation in neurons: tinkering with cell-specific control. Cell *92*, 709–712.
17. Screaton, G.R., Xu, X.N., Olsen, A.L., Cowper, A.E., Tan, R., McMichael, A.J., and Bell, J.I. (1997). LARD: a new lymphoid-specific death domain containing receptor regulated by alternative pre-mRNA splicing. Proc. Natl. Acad. Sci. USA *94*, 4615–4619.
18. Wang, J., Shen, L., Najafi, H., Kolberg, J., Matschinsky, F.M., Urdea, M., and German, M. (1997). Regulation of insulin preRNA splicing by glucose. Proc. Natl. Acad. Sci. USA *94*, 4360–4365.
19. Lynch, K.W., and Weiss, A. (2000). A model system for activation-induced alternative splicing of CD45 pre-mRNA in T cells implicates protein kinase C and Ras. Mol. Cell. Biol. *20*, 70–80.
20. Heyd, F., and Lynch, K.W. (2010). Phosphorylation-dependent regulation of PSF by GSK3 controls CD45 alternative splicing. Mol. Cell *40*, 126–137.
21. Oberdoerffer, S., Moita, L.F., Neems, D., Freitas, R.P., Hacohen, N., and Rao, A. (2008). Regulation of CD45 alternative splicing by heterogeneous ribonucleoprotein, hnRNPLL. Science *321*, 686–691.
22. Lynch, K.W. (2004). Consequences of regulated pre-mRNA splicing in the immune system. Nat. Rev. Immunol. *4*, 931–940.
23. Rothrock, C., Cannon, B., Hahm, B., and Lynch, K.W. (2003). A conserved signal-responsive sequence mediates activation-induced alternative splicing of CD45. Mol. Cell *12*, 1317–1324.
24. Preussner, M., Schreiner, S., Hung, L.H., Porstner, M., Jäck, H.M., Benes, V., Rätsch, G., and Bindereif, A. (2012). HnRNP L and L-like cooperate in multiple-exon regulation of CD45 alternative splicing. Nucleic Acids Res. *40*, 5666–5678.
25. Hui, J., Stangl, K., Lane, W.S., and Bindereif, A. (2003). HnRNP L stimulates splicing of the eNOS gene by binding to variable-length CA repeats. Nat. Struct. Biol. *10*, 33–37.
26. Hui, J., Reither, G., and Bindereif, A. (2003). Novel functional role of CA repeats and hnRNP L in RNA stability. RNA *9*, 931–936.
27. Rossbach, O., Hung, L.-H., Schreiner, S., Grishina, I., Heiner, M., Hui, J., and Bindereif, A. (2009). Auto- and cross-regulation of the hnRNP L proteins by alternative splicing. Mol. Cell. Biol. *29*, 1442–1451.
28. Gaudreau, M.-C., Grapton, D., Helness, A., Vadnais, C., Fraszczak, J., Shooshtarizadeh, P., Wilhelm, B., Robert, F., Heyd, F., and Möröy, T. (2016). Heterogeneous nuclear ribonucleoprotein L is required for the survival and functional integrity of murine hematopoietic stem cells. Sci. Rep. *6*, 27379.
29. Rothrock, C.R., House, A.E., and Lynch, K.W. (2005). HnRNP L represses exon splicing via a regulated exonic splicing silencer. EMBO J. *24*, 2792–2802.
30. Gaudreau, M.-C., Heyd, F., Bastien, R., Wilhelm, B., and Möröy, T. (2012). Alternative splicing controlled by heterogeneous nuclear ribonucleoprotein L regulates development, proliferation, and migration of thymic pre-T cells. J. Immunol. *188*, 5377–5388.
31. Vu, N.T., Park, M.A., Shultz, J.C., Goehe, R.W., Hoeferlin, L.A., Shultz, M.D., Smith, S.A., Lynch, K.W., and Chalfant, C.E. (2013). hnRNP U enhances caspase-9 splicing and is modulated by AKT-dependent phosphorylation of hnRNP L. J. Biol. Chem. *288*, 8575–8584.
32. Booth, N.J., McQuaid, A.J., Sobande, T., Kissane, S., Agius, E., Jackson, S.E., Salmon, M., Falciani, F., Yong, K., Rustin, M.H., et al. (2010). Different proliferative potential and migratory characteristics of human $CD4^+$ regulatory T cells that express either CD45RA or CD45RO. J. Immunol. *184*, 4317–4326.
33. Hawse, W.F., Boggess, W.C., and Morel, P.A. (2017). TCR signal strength regulates Akt substrate specificity to induce alternate murine Th and T regulatory cell differentiation programs. J. Immunol. *199*, 589–597.
34. Vignali, D.A.A., Collison, L.W., and Workman, C.J. (2008). How regulatory T cells work. Nat. Rev. Immunol. *8*, 523–532.
35. Rudensky, A.Y. (2011). Regulatory T cells and Foxp3. Immunol. Rev. *241*, 260–268.

36. Gavin, M.A., Torgerson, T.R., Houston, E., DeRoos, P., Ho, W.Y., Stray-Pedersen, A., Ocheltree, E.L., Greenberg, P.D., Ochs, H.D., and Rudensky, A.Y. (2006). Single-cell analysis of normal and FOXP3-mutant human T cells: FOXP3 expression without regulatory T cell development. Proc. Natl. Acad. Sci. USA *103*, 6659–6664.

37. Polansky, J.K., Kretschmer, K., Freyer, J., Floess, S., Garbe, A., Baron, U., Olek, S., Hamann, A., von Boehmer, H., and Huehn, J. (2008). DNA methylation controls *Foxp3* gene expression. Eur. J. Immunol. *38*, 1654–1663.

38. Lal, G., and Bromberg, J.S. (2009). Epigenetic mechanisms of regulation of Foxp3 expression. Blood *114*, 3727–3735.

39. Ozay, E.I., Shanthalingam, S., Sherman, H.L., Torres, J.A., Osborne, B.A., Tew, G.N., et al. (2020). Cell-Penetrating Anti-Protein Kinase C Theta Antibodies Act Intracellularly to Generate Stable, Highly Suppressive Regulatory T Cells. Mol. Ther. Published online May 23, 2020. https://doi.org/10.1016/j.ymthe.2020.05.020.

40. McCuaig, R.D., Dunn, J., Li, J., Masch, A., Knaute, T., Schutkowski, M., Zerweck, J., and Rao, S. (2015). PKC-theta is a novel SC35 splicing factor regulator in response to T cell activation. Front. Immunol. *6*, 562.

41. Tabellini, G., Bortul, R., Santi, S., Riccio, M., Baldini, G., Cappellini, A., Billi, A.M., Berezney, R., Ruggeri, A., Cocco, L., and Martelli, A.M. (2003). Diacylglycerol kinase-θ is localized in the speckle domains of the nucleus. Exp. Cell Res. *287*, 143–154.

42. Boronenkov, I.V., Loijens, J.C., Umeda, M., and Anderson, R.A. (1998). Phosphoinositide signaling pathways in nuclei are associated with nuclear speckles containing pre-mRNA processing factors. Mol. Biol. Cell *9*, 3547–3560.

43. Qian, W., Liang, H., Shi, J., Jin, N., Grundke-Iqbal, I., Iqbal, K., Gong, C.X., and Liu, F. (2011). Regulation of the alternative splicing of tau exon 10 by SC35 and Dyrk1A. Nucleic Acids Res. *39*, 6161–6171.

44. Lin, S., Coutinho-Mansfield, G., Wang, D., Pandit, S., and Fu, X.-D. (2008). The splicing factor SC35 has an active role in transcriptional elongation. Nat. Struct. Mol. Biol. *15*, 819–826.

45. Zhong, X.-Y., Wang, P., Han, J., Rosenfeld, M.G., and Fu, X.-D. (2009). SR proteins in vertical integration of gene expression from transcription to RNA processing to translation. Mol. Cell *35*, 1–10.

46. Kavanagh, S.J., Schulz, T.C., Davey, P., Claudianos, C., Russell, C., and Rathjen, P.D. (2005). A family of RS domain proteins with novel subcellular localization and trafficking. Nucleic Acids Res. *33*, 1309–1322.

47. Graveley, B.R., and Maniatis, T. (1998). Arginine/serine-rich domains of SR proteins can function as activators of pre-mRNA splicing. Mol. Cell *1*, 765–771.

48. Edmond, V., Moysan, E., Khochbin, S., Matthias, P., Brambilla, C., Brambilla, E., Gazzeri, S., and Eymin, B. (2011). Acetylation and phosphorylation of SRSF2 control cell fate decision in response to cisplatin. EMBO J. *30*, 510–523.

49. Bin Dhuban, K., d'Hennezel, E., Nagai, Y., Xiao, Y., Shao, S., Istomine, R., Alvarez, F., Ben-Shoshan, M., Ochs, H., Mazer, B., et al. (2017). Suppression by human FOXP3^{+} regulatory T cells requires FOXP3-TIP60 interactions. Sci. Immunol. *2*, eaai9297.

50. Ozay, E.I., Gonzalez-Perez, G., Torres, J.A., Vijayaraghavan, J., Lawlor, R., Sherman, H.L., et al. (2016). Intracellular Delivery of Anti-PKCΘ (Thr538) via Protein Transduction Domain Mimics for Immunomodulation. Mol. Ther. *24*, 2118–2130.

51. Gruber, A.R., Martin, G., Keller, W., and Zavolan, M. (2014). Means to an end: mechanisms of alternative polyadenylation of messenger RNA precursors. Wiley Interdiscip. Rev. RNA *5*, 183–196.

52. Nielsen, C., Ohm-Laursen, L., Barington, T., Husby, S., and Lillevang, S.T. (2005). Alternative splice variants of the human PD-1 gene. Cell. Immunol. *235*, 109–116.

53. Ryder, L.R., Woetmann, A., Madsen, H.O., Ødum, N., Ryder, L.P., Bliddal, H., Danneskiold-Samsøe, B., Ribel-Madsen, S., and Bartels, E.M. (2010). Expression of full-length and splice forms of FoxP3 in rheumatoid arthritis. Scand. J. Rheumatol. *39*, 279–286.

54. Smith, E.L., Finney, H.M., Nesbitt, A.M., Ramsdell, F., and Robinson, M.K. (2006). Splice variants of human FOXP3 are functional inhibitors of human CD4^{+} T-cell activation. Immunology *119*, 203–211.

55. Misra, P., Qi, C., Yu, S., Shah, S.H., Cao, W.-Q., Rao, M.S., Thimmapaya, B., Zhu, Y., and Reddy, J.K. (2002). Interaction of PIMT with transcriptional coactivators CBP, p300, and PBP differential role in transcriptional regulation. J. Biol. Chem. *277*, 20011–20019.

56. Enünlü, I., Pápai, G., Cserpán, I., Udvardy, A., Jeang, K.T., and Boros, I. (2003). Different isoforms of PRIP-interacting protein with methyltransferase domain/trimethylguanosine synthase localizes to the cytoplasm and nucleus. Biochem. Biophys. Res. Commun. *309*, 44–51.

57. Yang, H., Lowenson, J.D., Clarke, S., and Zubarev, R.A. (2013). Brain proteomics supports the role of glutamate metabolism and suggests other metabolic alterations in protein L-isoaspartyl methyltransferase (PIMT)-knockout mice. J. Proteome Res. *12*, 4566–4576.

58. Dufu, K., Livingstone, M.J., Seebacher, J., Gygi, S.P., Wilson, S.A., and Reed, R. (2010). ATP is required for interactions between UAP56 and two conserved mRNA export proteins, Aly and CIP29, to assemble the TREX complex. Genes Dev. *24*, 2043–2053.

59. MacKay, K.B., Lowenson, J.D., and Clarke, S.G. (2012). Wortmannin reduces insulin signaling and death in seizure-prone *Pcmt1*$^{-/-}$ mice. PLoS ONE *7*, e46719.

60. Koenecke, C., Lee, C.-W., Thamm, K., Föhse, L., Schafferus, M., Mittrücker, H.-W., Floess, S., Huehn, J., Ganser, A., Förster, R., and Prinz, I. (2012). IFN-γ production by allogeneic Foxp3^{+} regulatory T cells is essential for preventing experimental graft-versus-host disease. J. Immunol. *189*, 2890–2896.

61. Sawitzki, B., Kingsley, C.I., Oliveira, V., Karim, M., Herber, M., and Wood, K.J. (2005). IFN-gamma production by alloantigen-reactive regulatory T cells is important for their regulatory function in vivo. J. Exp. Med. *201*, 1925–1935.

62. Iadevaia, V., and Gerber, A.P. (2015). Combinatorial control of mRNA fates by RNA-binding proteins and non-coding RNAs. Biomolecules *5*, 2207–2222.

63. Bergeron, D., Pal, G., Beaulieu, Y.B., Chabot, B., and Bachand, F. (2015). Regulated intron retention and nuclear pre-mRNA decay contribute to *PABPN1* autoregulation. Mol. Cell. Biol. *35*, 2503–2517.

64. Toker, A., and Huehn, J. (2011). To be or not to be a Treg cell: lineage decisions controlled by epigenetic mechanisms. Sci. Signal. *4*, pe4.

65. Li, X., Liang, Y., LeBlanc, M., Benner, C., and Zheng, Y. (2014). Function of a Foxp3 *cis*-element in protecting regulatory T cell identity. Cell *158*, 734–748.

66. Huehn, J., Polansky, J.K., and Hamann, A. (2009). Epigenetic control of FOXP3 expression: the key to a stable regulatory T-cell lineage? Nat. Rev. Immunol. *9*, 83–89.

67. Ogawa, C., Tone, Y., Tsuda, M., Peter, C., Waldmann, H., and Tone, M. (2014). TGF-β-mediated *Foxp3* gene expression is cooperatively regulated by Stat5, Creb, and AP-1 through CNS2. J. Immunol. *192*, 475–483.

68. Martinez, N.M., and Lynch, K.W. (2013). Control of alternative splicing in immune responses: many regulators, many predictions, much still to learn. Immunol. Rev. *253*, 216–236.

69. Martinez, N.M., Pan, Q., Cole, B.S., Yarosh, C.A., Babcock, G.A., Heyd, F., Zhu, W., Ajith, S., Blencowe, B.J., and Lynch, K.W. (2012). Alternative splicing networks regulated by signaling in human T cells. RNA *18*, 1029–1040.

70. Revil, T., Toutant, J., Shkreta, L., Garneau, D., Cloutier, P., and Chabot, B. (2007). Protein kinase C-dependent control of *Bcl-x* alternative splicing. Mol. Cell. Biol. *27*, 8431–8441.

71. Wei, B., Baker, S., Wieckiewicz, J., and Wood, K.J. (2010). IFN-γ triggered STAT1-PKB/AKT signalling pathway influences the function of alloantigen reactive regulatory T cells. Am. J. Transplant. *10*, 69–80.

72. Wu, X., Guo, W., Wu, L., Gu, Y., Gu, L., Xu, S., Wu, X., Shen, Y., Ke, Y., Tan, R., et al. (2012). Selective sequestration of STAT1 in the cytoplasm via phosphorylated SHP-2 ameliorates murine experimental colitis. J. Immunol. *189*, 3497–3507.

73. Overacre, A.E., and Vignali, D.A.A. (2016). T_{reg} stability: to be or not to be. Curr. Opin. Immunol. *39*, 39–43.

74. Dung, T.T.M., Yi, Y.-S., Heo, J., Yang, W.S., Kim, J.H., Kim, H.G., Park, J.G., Yoo, B.C., Cho, J.Y., and Hong, S. (2016). Critical role of protein L-isoaspartyl methyltransferase in basic fibroblast growth factor-mediated neuronal cell differentiation. BMB Rep. *49*, 437–442.

75. Farrar, C., and Clarke, S. (2002). Altered levels of *S*-adenosylmethionine and S-adenosylhomocysteine in the brains of L-isoaspartyl (D-aspartyl) *O*-methyltransferase-deficient mice. J. Biol. Chem. *277*, 27856–27863.

76. Farrar, C., Houser, C.R., and Clarke, S. (2005). Activation of the PI3K/Akt signal transduction pathway and increased levels of insulin receptor in protein repair-deficient mice. Aging Cell *4*, 1–12.

77. Singh, Y., Garden, O.A., Lang, F., and Cobb, B.S. (2015). MicroRNA-15b/16 enhances the induction of regulatory T cells by regulating the expression of Rictor and mTOR. J. Immunol. *195*, 5667–5677.

78. Schmidt, A., Eriksson, M., Shang, M.M., Weyd, H., and Tegnér, J. (2016). Comparative analysis of protocols to induce human $CD4^{+}Foxp3^{+}$ regulatory T cells by combinations of IL-2, TGF-beta, retinoic acid, rapamycin and butyrate. PLoS ONE *11*, e0148474.

79. Daniel, V., Wang, H., Sadeghi, M., and Opelz, G. (2014). Interferon-gamma producing regulatory T cells as a diagnostic and therapeutic tool in organ transplantation. Int. Rev. Immunol. *33*, 195–211.

80. Messeguer, X., Escudero, R., Farré, D., Núñez, O., Martínez, J., and Albà, M.M. (2002). PROMO: detection of known transcription regulatory elements using species-tailored searches. Bioinformatics *18*, 333–334.

81. Farré, D., Roset, R., Huerta, M., Adsuara, J.E., Roselló, L., Albà, M.M., and Messeguer, X. (2003). Identification of patterns in biological sequences at the ALGGEN server: PROMO and MALGEN. Nucleic Acids Res. *31*, 3651–3653.

82. Fu, W., Ergun, A., Lu, T., Hill, J.A., Haxhinasto, S., Fassett, M.S., Gazit, R., Adoro, S., Glimcher, L., Chan, S., et al. (2012). A multiply redundant genetic switch "locks in" the transcriptional signature of regulatory T cells. Nat. Immunol. *13*, 972–980.

83. Akimova, T., Zhang, T., Negorev, D., Singhal, S., Stadanlick, J., Rao, A., Annunziata, M., Levine, M.H., Beier, U.H., Diamond, J.M., et al. (2017). Human lung tumor $FOXP3^{+}$ Tregs upregulate four "Treg-locking" transcription factors. JCI Insight *2*, 1–20.

84. Ray, D., Kazan, H., Cook, K.B., Weirauch, M.T., Najafabadi, H.S., Li, X., Gueroussov, S., Albu, M., Zheng, H., Yang, A., et al. (2013). A compendium of RNA-binding motifs for decoding gene regulation. Nature *499*, 172–177.

85. Paz, I., Kosti, I., Ares, M., Jr., Cline, M., and Mandel-Gutfreund, Y. (2014). RBPmap: a web server for mapping binding sites of RNA-binding proteins. Nucleic Acids Res. *42*, W361–W367.

Protein Kinase C theta modulates PCMT1 through hnRNPL to increase FOXP3 stability in regulatory T cells

Authors: E. Ilker Ozay[1#], Sudarvili Shanthalingam[2], Joe A. Torres[1], Barbara A. Osborne[1,2], Gregory N. Tew[1,2,3], Lisa M. Minter[1,2*]

Affiliations:

[1]Molecular and Cellular Biology Graduate Program, University of Massachusetts Amherst, Amherst, MA, 01003.

[2]Department of Veterinary and Animal Sciences, University of Massachusetts Amherst, Amherst, MA, 01003.

[3]Department of Polymer Science and Engineering, University of Massachusetts Amherst, Amherst, MA, 01003.

#Current address: SQZ Biotechnologies, 200 Arsenal Yards Boulevard, Watertown, MA, 02472

*Corresponding author: lminter@vasci.umass.edu

Figure S1

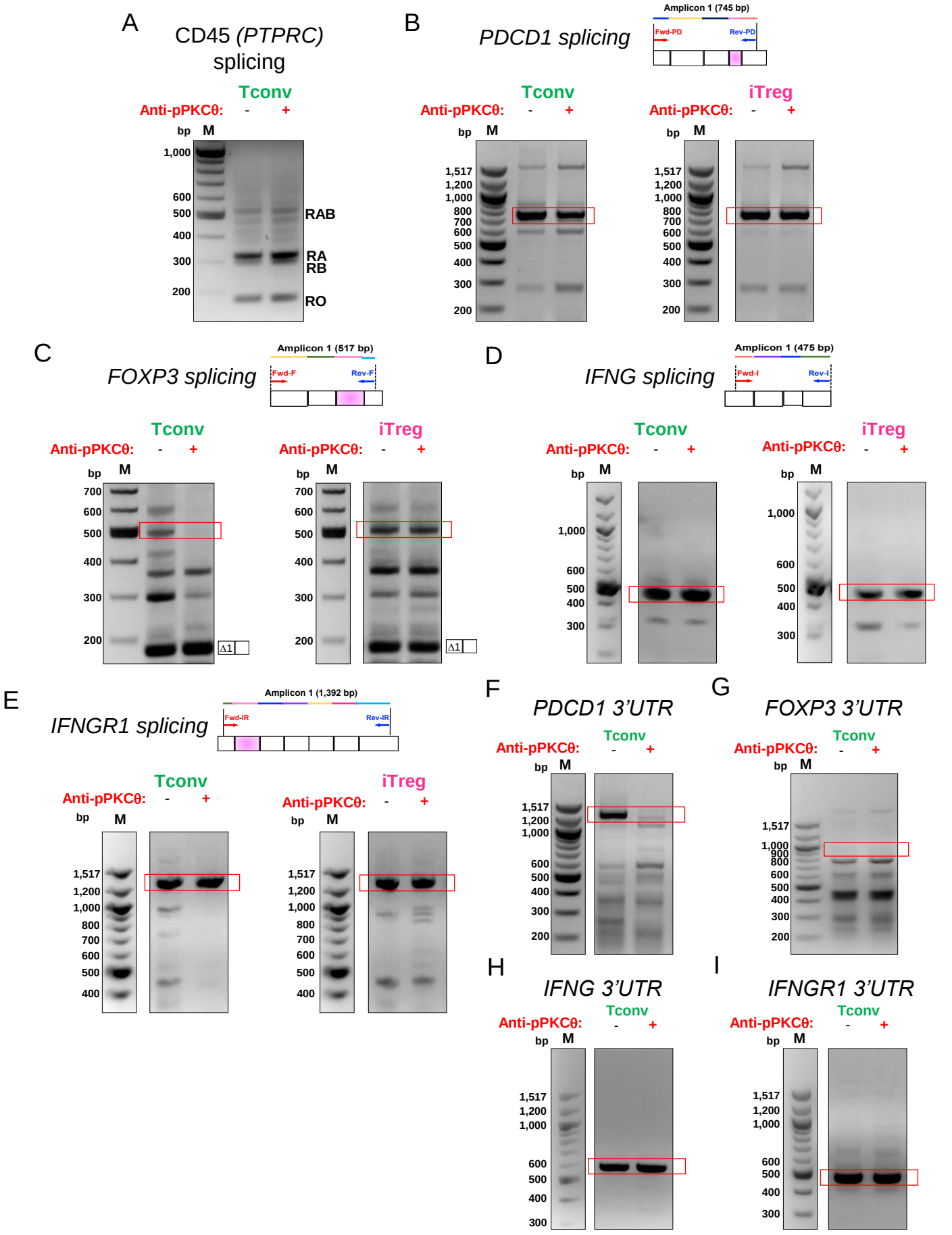
A
CD45 (PTPRC) splicing
Tconv
Anti-pPKCθ: - +
bp M
1,000
600
500
400
300
200
RAB
RA
RB
RO
B
PDCD1 splicing
Amplicon 1 (745 bp)
Fwd-PD
Rev-PD
Tconv
Anti-pPKCθ: - +
iTreg
Anti-pPKCθ: - +
1,517
1,200
1,000
800
700
600
500
400
300
200
C
FOXP3 splicing
Amplicon 1 (517 bp)
Fwd-F
Rev-F
Tconv
Anti-pPKCθ: - +
iTreg
Anti-pPKCθ: - +
Δ1
D
IFNG splicing
Amplicon 1 (475 bp)
Fwd-I
Rev-I
Tconv
Anti-pPKCθ: - +
iTreg
Anti-pPKCθ: - +
E
IFNGR1 splicing
Amplicon 1 (1,392 bp)
Fwd-IR
Rev-IR
Tconv
Anti-pPKCθ: - +
iTreg
Anti-pPKCθ: - +
F
PDCD1 3'UTR
Tconv
Anti-pPKCθ: - +
G
FOXP3 3'UTR
Tconv
Anti-pPKCθ: - +
H
IFNG 3'UTR
Tconv
Anti-pPKCθ: - +
I
IFNGR1 3'UTR
Tconv
Anti-pPKCθ: - +

Figure S1. Effects of anti-pPKCθ delivery on alternative splicing in non-differentiated T cells (Tconvs) *in vitro*. (A) Alternative splicing analysis of CD45 (*PTPRC*) in Tconvs using RT-PCR. Schematic representations and splicing analysis of **(B)** *PDCD1*, **(C)** *FOXP3*, **(D)** *IFNG*, and **(E)** *IFNGR1* in Tconvs following anti-pPKCθ delivery. Analysis of **(F)** *PDCD1*, **(G)** *FOXP3*, **(H)** *IFNG*, and **(I)** *IFNGR1* 3'UTR in Tconv using RT-PCR. Red frames indicate the expected amplicon sizes. Data shown are representative results of two or three independent experiments.

Figure S2

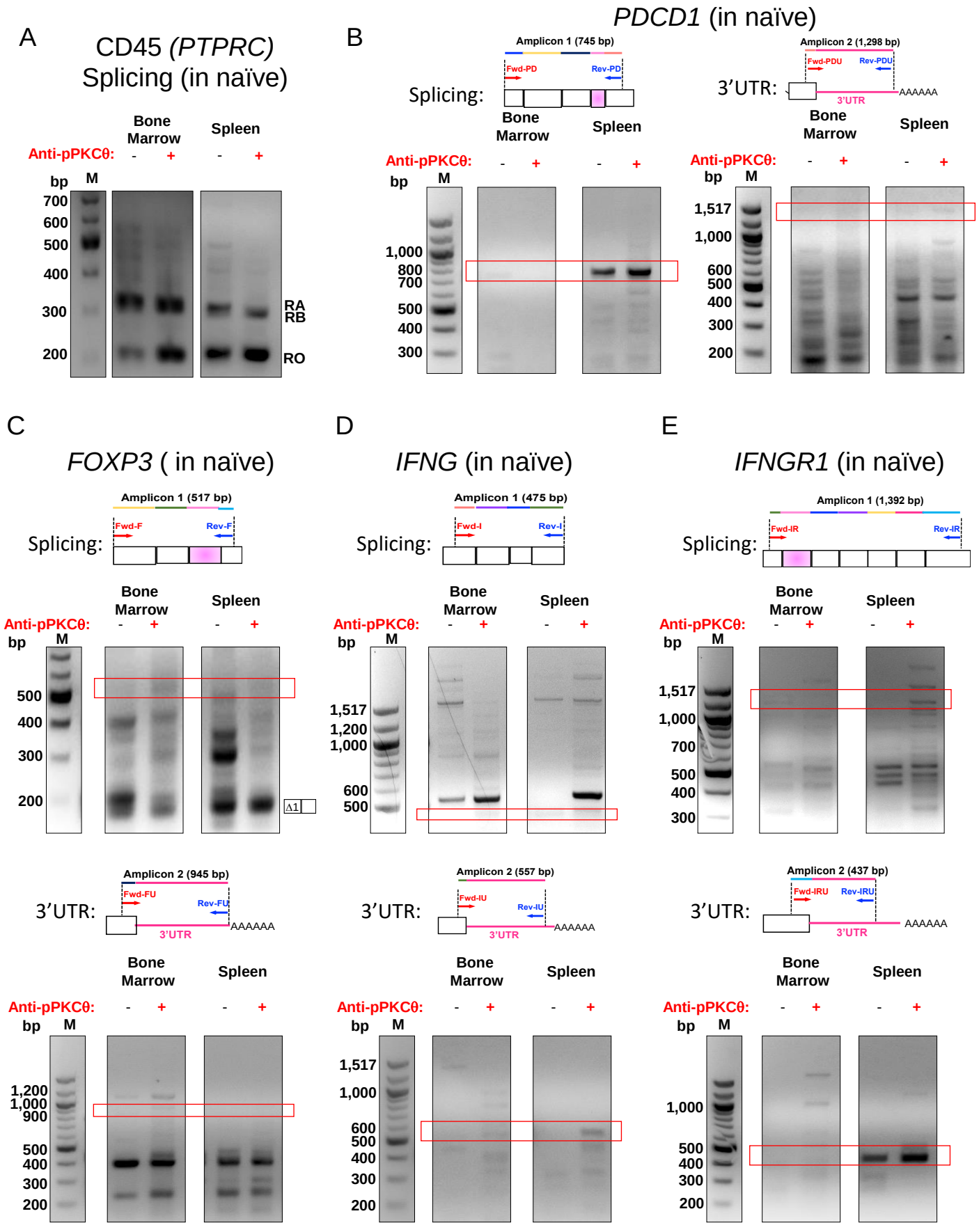
A
CD45 (PTPRC) Splicing (in naïve)
Bone Marrow
Spleen
Anti-pPKCθ: - + - +
bp M
700
600
500
400
300
200
RA
RB
RO
B
PDCD1 (in naïve)
Splicing:
Amplicon 1 (745 bp)
Fwd-PD
Rev-PD
Bone Marrow
Spleen
Anti-pPKCθ: - + - +
bp M
1,000
800
700
500
400
300
3'UTR:
Amplicon 2 (1,298 bp)
Fwd-PDU
Rev-PDU
3'UTR
AAAAAA
Bone Marrow
Spleen
Anti-pPKCθ: - + - +
bp M
1,517
1,000
600
500
400
300
200
C
FOXP3 (in naïve)
Splicing:
Amplicon 1 (517 bp)
Fwd-F
Rev-F
Bone Marrow
Spleen
Anti-pPKCθ: - + - +
bp M
500
400
300
200
Δ1
3'UTR:
Amplicon 2 (945 bp)
Fwd-FU
Rev-FU
3'UTR
AAAAAA
Bone Marrow
Spleen
Anti-pPKCθ: - + - +
bp M
1,200
1,000
900
500
400
300
200
D
IFNG (in naïve)
Splicing:
Amplicon 1 (475 bp)
Fwd-I
Rev-I
Bone Marrow
Spleen
Anti-pPKCθ: - + - +
bp M
1,517
1,200
1,000
600
500
3'UTR:
Amplicon 2 (557 bp)
Fwd-IU
Rev-IU
3'UTR
AAAAAA
Bone Marrow
Spleen
Anti-pPKCθ: - + - +
bp M
1,517
1,000
600
500
400
300
200
E
IFNGR1 (in naïve)
Splicing:
Amplicon 1 (1,392 bp)
Fwd-IR
Rev-IR
Bone Marrow
Spleen
Anti-pPKCθ: - + - +
bp M
1,517
1,000
700
500
400
300
3'UTR:
Amplicon 2 (437 bp)
Fwd-IRU
Rev-IRU
3'UTR
AAAAAA
Bone Marrow
Spleen
Anti-pPKCθ: - + - +
bp M
1,000
500
400
300
200

Figure S2. Effects of anti-pPKCθ delivery on RNA processing in naïve T cells *in vivo*. hPBMCs were transferred on Day 0 together with anti-pPKCθ (or DMSO-) iTregs at a 3:1 ratio. On day +17, bone marrow and spleens were harvested, and naïve T cells were separated using magnetic beads based on CD4+CD25-CD127+ expression, using magnetic beads. Total RNA was extracted. RT-PCR was performed to evaluate alternative splicing and 3'UTR processing. **(A)** CD45 (*PTPRC*) alternative splicing in naïve T cells recovered from bone marrow and spleen. Splice variants and 3'UTR lengths in naïve T cells from bone marrow and spleen were analyzed using primers specific for **(B)** *PDCD1* **(C)** *FOXP3,* **(D)** *IFNG,* and **(E)** *IFNGR1*. Red frames indicate the expected amplicon sizes. Data shown are representative results of two independent experiments, 5 mice per condition.

Figure S3

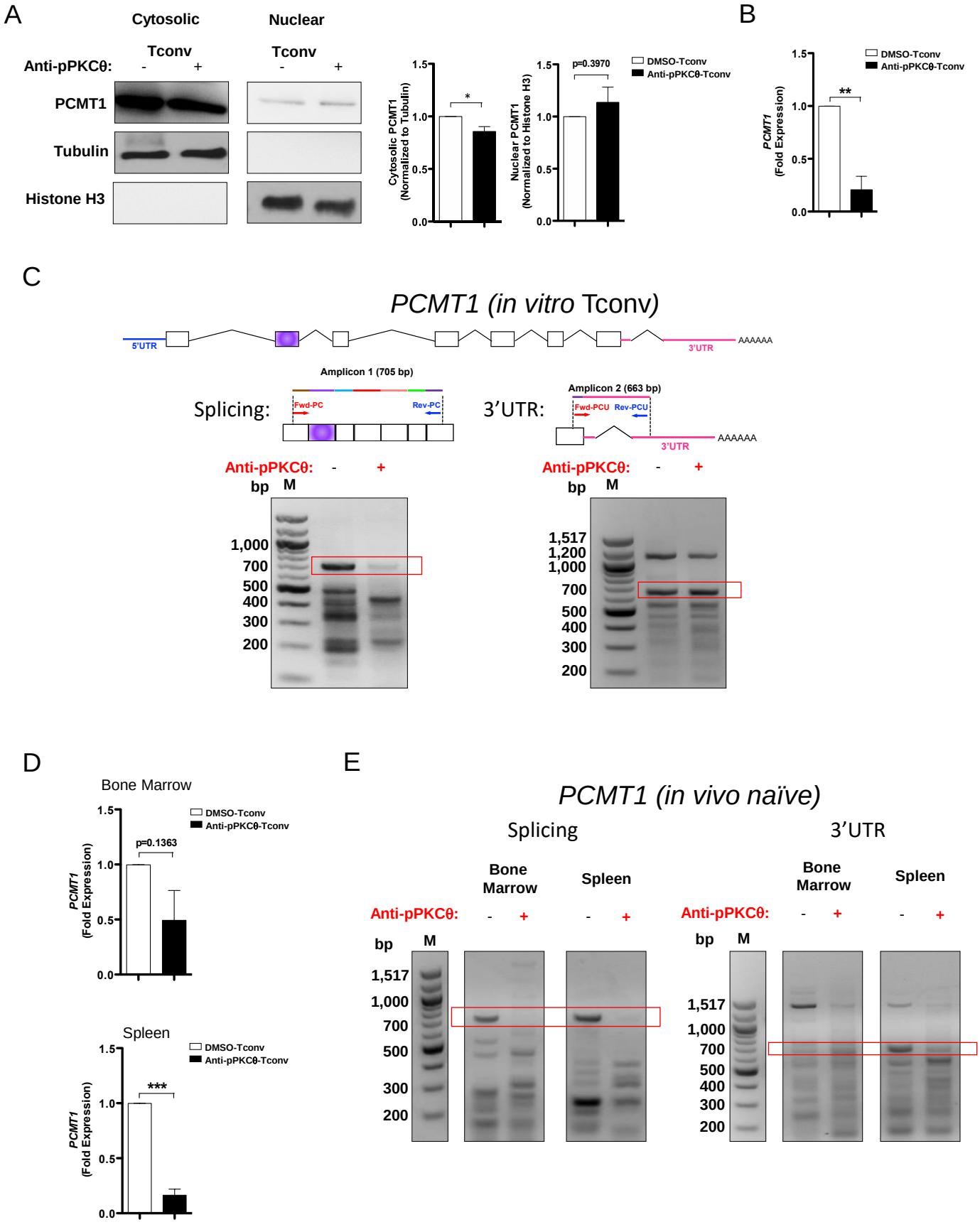
A
Cytosolic
Nuclear
Tconv
Tconv
Anti-pPKCθ: - + - +
PCMT1
Tubulin
Histone H3
Cytosolic PCMT1 (Normalized to Tubulin)
Nuclear PCMT1 (Normalized to Histone H3)
*
p=0.3970
DMSO-Tconv
Anti-pPKCθ-Tconv
B
PCMT1 (Fold Expression)
**
C
PCMT1 (in vitro Tconv)
5'UTR
3'UTR
AAAAAA
Amplicon 1 (705 bp)
Splicing:
Fwd-PC
Rev-PC
Amplicon 2 (663 bp)
3'UTR:
Fwd-PCU
Rev-PCU
Anti-pPKCθ: - +
bp M
1,000
700
500
400
300
200
1,517
1,200
1,000
D
Bone Marrow
p=0.1363
Spleen
***
E
PCMT1 (in vivo naïve)
Splicing
3'UTR
Bone Marrow
Spleen

Figure S3. *PCMT1* splicing and 3'UTR analyses in Tconvs *in vitro* and *in vivo.* (A) PCMT1 protein expression in cytosolic or nuclear extracts were determined by immunoblotting. Band intensities were quantified relative to tubulin or histone H3, respectively, using ImageJ software. **(B)** *PCMT1* gene expression in Tconvs was quantified by qPCR. **(C)** *PCMT1* splicing and 3'UTR length were analyzed *in vitro*. **(D)** *PCMT1* gene expression in naïve T cells recovered from bone marrow and spleens on day +17 from GVHD mice was quantified by qPCR. **(E)** Analysis of *PCMT1* splicing and 3'UTR length in naïve T cells recovered from bone marrow and spleens on day +17 from GVHD mice was analyzed using RT-PCR. Red frames indicate the expected amplicon sizes. Data represent mean ± SEM of two or three independent experiments. For *in vivo* experiments, 4 mice per group were used. Unpaired, two-tailed Student's t test was used for analysis; *$p < 0.05$; **$p < 0.01$; ***$p < 0.001$.

Figure S4

FOXP3 3'UTR (945 bp)

GCTGGAGTTCCGCAAGAAACGGAGCCAGAGGCCCAGCAGGTGTTCCAACCCTACACCTGGCCCCTGACCTCAAGATCAAGGAAAGGAGGAT
GGACGAACAGGGGCCAAACTGGTGGGAGGCAGAGGTGGTGGGGGCAGGGATGATAGGCCCTGGATGTGCCCACAGGGACCAAGAAGTGAG
GTTTCCACTGTCTTGCCTGCCAGGGCCCCTGTTCCCCCGCTGGCAGCCACCCCCTCCCCCATCATATCCTTTGCCCCAAGGCTGCTCAGAGGG
GCCCCGGTCCTGGCCCCAGCCCCCACCTCCGCCCCAGACACACCCCCCAGTCGAGCCCTGCAGCCAAACAGAGCCTTCACAACCAGCCACA
CAGAGCCTGCCTCAGCTGCTCGCACAGATTACTTCAGGGCTGGAAAAGTCACACAG**ACACACA**AAATGTCACAATCCTGTCCCTCACTCAA
CACAAACCCCAAAACACAGAGAGCCTGCCTCAGTACACTCAAACAACCTCAAAGCTGCATCATCACACAATC**ACACACA**AGCACAGCCCTG
ACAACCCACACACCCCAAGGCACGCACCCACAGCCAGCCTCAGGGCCCACAGGGGCACTGTCAACACAGGGGTGTGCCCAGAGGCCTACAC
AGAAGCAGCGTCAGTACCCTCAGGATCTGAGGTCCCAACACGTGCTCGCTC**ACACACA**CGGCCTGTTAGAATTCACCTGTGTATCTCACGC
ATATGCACACGCACAGCCCCCCAGTGGGTCTCTTGAGTCCCGTGCAG**ACACACA**CAGCC**ACACACA**CTGCCTTGCCAAAAATACCCCGT
GTCTCCCCTGCCACTCACCTCACTCCCATTCCCTGAGCCCTGATCCATGCCTCAGCTTAGACTGCAGAGGAACTACTCATTTATTTGGGATCCA
AGGCCCCCAA**CCCACAGTACCGTCCCCAATAAA**

IFNG 3'UTR (557 bp)

GGAGTCAGATGCTGTTTCGAGGTCGAAGAGCATCCCAGTAATGGTTGTCCTGCCTGCAATATTTGAATTTTAAATCTAAATCTATTTATTAATATT
TAACATTATTTATATGGGGAATATATTTTTAGACTCATCAATCAAATAAGTATTTATAATAGCAACTTTTGTGTAATGAAAATGAATATCTATTAATA
TATGTATTATTTATAATTCCTATATCCTGTGACTGTCTCACTTAATCCTTTGTTTTCTGACTAATTAGGCAAGGCTATGTGATTACAAGGCTTTATC
TCAGGGGCCAACTAGGCAGCCAACCTAAGCAAGATCCCATGGGTTGTGTGTTTATTTCACTTGATGATACAATGAACACTTATAAGTGAAGTGA
TACTATCCAGTTACTGCCGGTTTGAAAATATGCCTGCAATCTGAGCCAGTGCTTTAATGGCATG**TCAGACA**GAACTTGAATGTGTCAGGTGA
CCCTGATGAAAACATAGCATCTCAGGAGATTTCATGCCTGGTGCTTCCAAATATTGTTG**ACAACTGTGACTGTACCCAAA**

IFNGR1 3'UTR (437 bp)

ATCTACTTGTGGATGATAGCGGTAAAGAGTCCTTGATTGGTTATAGACCAACAGAAGATTCCAAAGAATTTTCATGAGATCAGCTAAGTTGCAC
CAACTTTGAAGTCTGATTTTCCTGGACAGTTTTCTGCTTTAATTTCATGAAAAGATTATGATCTCAGAAATTGTATCTTAGTTGGTATCAACCAAAT
GGAGTGACTTAGTGTACATGAAAGCGTAAAGAGGATGTGTGGCATTTTCACTTTTGGCTTGTAAAGT**ACAGACT**TTTTTTTTTTTTT**AAACA**
AAAAAAGCATTGTAACTTATGAACCTTTACATCCAGATAGGTTACCAGTAACGGAACAGTATCCAGTACTCCTGGTTCCTAGGTGAGCAGGTGA
TGCCCCAGGGACCTTTGTAGCCACTTCACTTTTTTTCTT**TTCTCTGCCTTGGTATAGCAT**

PCMT1 3'UTR (663 bp)

AAGCAGTGGTCCAGGTGGAAGTGATTTTATCTTCTGCTCTTTCTTCTT**CCACACATGCA**AGGGATGAATTGTAAAAGCAACATCAGCTTGA
CCAGTATAAAATTACAGTGGATTGCTCATCTCAGTCCTCAAAGCTTTTTGAAAACCAACACCATCACAGCTTGTTTTGGACTTTGTTACACTGTTA
TTTTCAGCATGAAAATGTGTGTTTTTTTTAGGGTTTCTGATTCTTCAAAGAGGCACAGAGCCAAATTGGTAGAGGAAGGATGCAAAGTATAAATTT
GTGTAATATTACTTTAACATGCCCATATTTTACTTGGAAATATTAAAAGAAAGGGTTCTGTAAAATGGAAAACTTAGTTTGTGAATTGATTTTGAG
GAGTGGTTTTTCTTTTCTTGGACACTTAATTCTGTTCTGATATTA*ATTTA*TCAGATTGCTTTTGTGCATTGGATA**ACACCAC**CATTCACAAGTTA
AGATTCTTGGTATTTGGATATCTGTTAGATGCTACTAAGAAAATAGAGATGAGCTTTCTTTTTAAAGCTTTTGATGTGGTGTCATAGAATAGCATG
TTGTAGATACAATCAGCTGCTTTGTTACCTTAAAACTAGGCATTTGTAAATATTAAACCATAAGATGGCAGGTGAT**GTCCTGTAAACACTCAGC**

PDCD1 3'UTR (1298 bp)

TTTCCAGTGGCGAGAGAAGACCCCGGAGCCCCCCGTGCCCTGTGTCCCTGAGCAGACGGAGTATGCCACCATTGTCTTTCCTAGCGGAATGG
GCACCTCATCCCCCGCCCGCAGGGGCTCAGCTGACGGCCCTCGGAGTGCCCAGCCACTGAGGCCTGAGGATGGACACTGCTCTTGGCCCCT
CTGA**CCGGCTTCCTTGGCCACCAGTGTTCTGCAGACCCTCCACCATGAGCCCGGGTCAGCGCATTTCCTCAGGAGAAGCAGGCAGGGTGCAG**
GCCATTGCAGGCCGTCCAGGGGCTGAGCTGCCTGGGGGCGACCGGGGCTCCAGCCTGCACCTGCACCAGGCACAGCCCCACC**ACAGGA**
CTCATGTCTCAATGCCCACAGTGAGCCCAGGCAGCAGGTGTCACCGTCCCCTACAGGGAGGGCCAGATGCAGTCACTGCTTCAGGTCCTGCC
AGCACAGAGCTGCCTGCGTCCAGCTCCCTGAATCTCTGCTGCTGCTGCTGCTGCTGCTGCTGCCTGCGGCCCGGGGCTGAAGGCGCCG
TGGCCCTGCCTGACGCCCCGGAGCCTCCTGCCTGAACTTGGGGGCTGGTTGGAGATGGCCTTGGAGCAGCCAAGGTGCCCCTGGCAGTGGC
ATCCCGAAACGCCCTGGACGCAGGGCCCAAGACTGGGCACAGGAGTGGGAGGTACATGGGGCTGGGGACTCCCCAGGAGTTATCTGCTCCC
TGCAGGCCTAGAGAAGTTTCAGGGAAGGTCAGAAGAGCTCCTGGCTGTGGTGGGCAGGGCAGGAAACCCCTCCACCTTTACACATGCCCAGG
CAGCACCTCAGGCCCTTTGTGGGGCAGGGAAGCTGAGGCAGTAAGCGGGCAGGCAGAGCTGGAGGCCTTTCAGGCCCAGCCAGCACTCTGG
CCTCCTGCCGCCGCATTCCACCCCAGCCCCTCACACCACTCGGGAGAGGGACATCCTACGGTCCCAAGGTCAGGAGGGCAGGGCTGGGGTT
GACTCAGGCCCCTCCCAGCTGTGGCCACCTGGGTGTTGGGAGGGCAGAAGTGCAGGCACCTAGGGCCCCCCATGTGCCCACCCTGGGAGCT
CTCCTTGGAACCCATTCCTGAAATTATTTAAAGGGGTTGGCCGGGCTCCCACCAGGGCCTGGGTGGGAAGGTACAGGCGTTCCCCCGGGGCC
TAGTACCCCCGCCGTGGCCTATCCACTCCTC**ACATCCACACACT**GCACCCCCACTCCTGGGGCAGGGCCACCAGCATCCAGGCGGCCA
GCAGG**CACCTGAGTGGCTGGGACAA**

Figure S4. hnRNPL binding sites within 3'UTR sequences of iTreg-associated genes. 3'UTR sequences (red sequences) were determined using Ensembl. These sequences were copied and run on RBPmap to define hnRNPL binding sites (bold in blue). Forward and reverse primers were designed to amplify these regions using RT-PCR (Primers were designed to bind black, bold sequences).

Figure S5

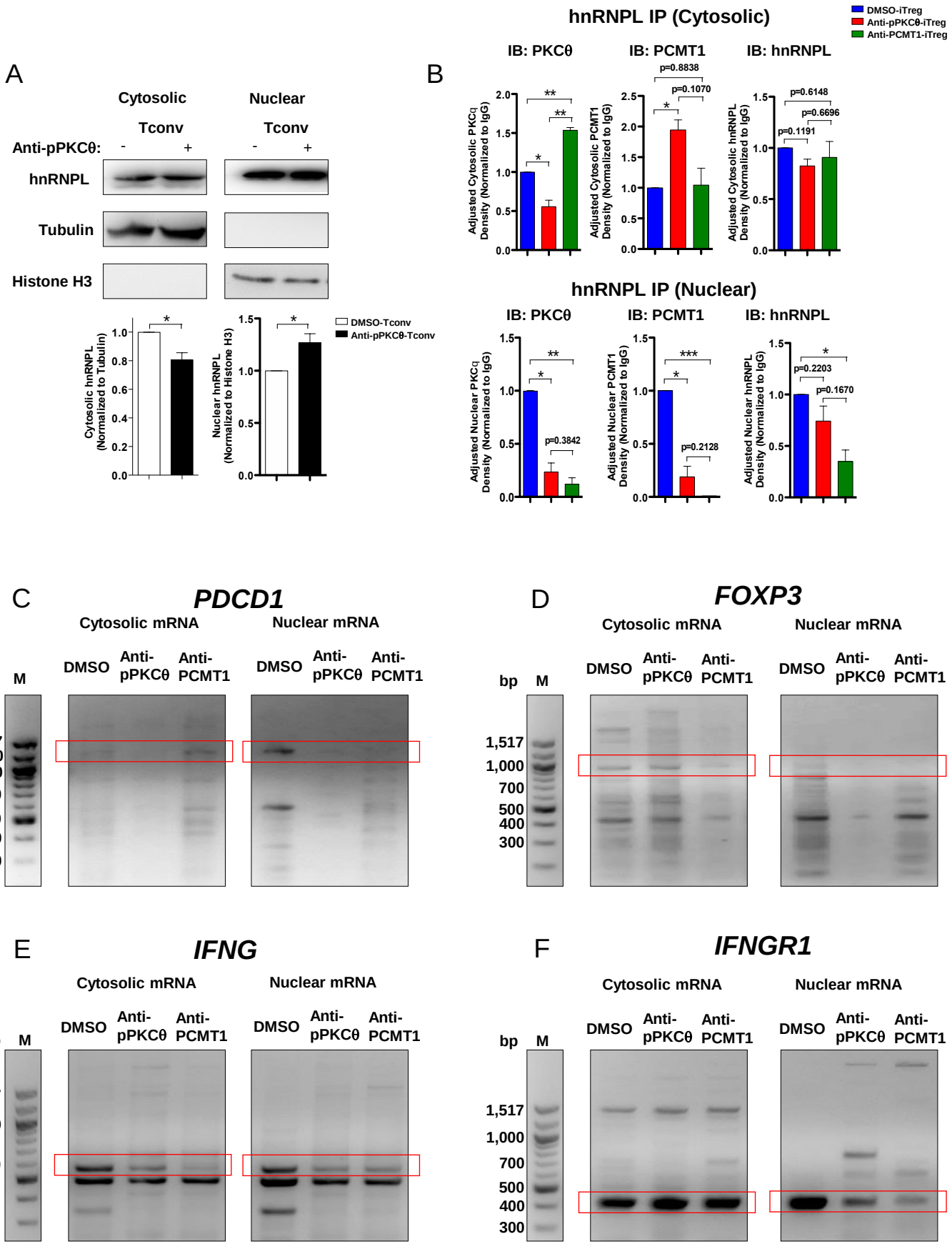
A
Cytosolic
Nuclear
Tconv
Tconv
Anti-pPKCθ: - + - +
hnRNPL
Tubulin
Histone H3
Cytosolic hnRNPL (Normalized to Tubulin)
Nuclear hnRNPL (Normalized to Histone H3)
DMSO-Tconv
Anti-pPKCθ-Tconv
B
hnRNPL IP (Cytosolic)
DMSO-iTreg
Anti-pPKCθ-iTreg
Anti-PCMT1-iTreg
IB: PKCθ
IB: PCMT1
IB: hnRNPL
Adjusted Cytosolic PKCq Density (Normalized to IgG)
Adjusted Cytosolic PCMT1 Density (Normalized to IgG)
Adjusted Cytosolic hnRNPL Density (Normalized to IgG)
p=0.8838
p=0.1070
p=0.6148
p=0.6696
p=0.1191
hnRNPL IP (Nuclear)
IB: PKCθ
IB: PCMT1
IB: hnRNPL
Adjusted Nuclear PKCq Density (Normalized to IgG)
Adjusted Nuclear PCMT1 Density (Normalized to IgG)
Adjusted Nuclear hnRNPL Density (Normalized to IgG)
p=0.3842
p=0.2128
p=0.2203
p=0.1670
C
PDCD1
Cytosolic mRNA
Nuclear mRNA
bp M
DMSO
Anti-pPKCθ
Anti-PCMT1
1,517
1,200
1,000
700
500
400
300
D
FOXP3
Cytosolic mRNA
Nuclear mRNA
bp M
DMSO
Anti-pPKCθ
Anti-PCMT1
1,517
1,000
700
500
400
300
E
IFNG
Cytosolic mRNA
Nuclear mRNA
bp M
DMSO
Anti-pPKCθ
Anti-PCMT1
1,517
1,000
700
600
500
400
300
F
IFNGR1
Cytosolic mRNA
Nuclear mRNA
bp M
DMSO
Anti-pPKCθ
Anti-PCMT1
1,517
1,000
700
500
400
300

Figure S5. Cytoplasmic and nuclear *PCMT1* mRNA association with hnRNPL in anti-pPKCθ- or anti-PCMT1-iTregs. (A) hnRNPL expression in cytosolic and nuclear lysates from Tconvs was determined by immunoblotting. Band intensities were quantified relative to tubulin or histone H3, respectively, using ImageJ software. **(B)** Band intensities of PKCθ and PCMT1, bound to immunoprecipitated cytosolic or nuclear hnRNPL in iTregs, was quantified using ImageJ software. hnRNPL association with cytosolic or nuclear **(C)** *PDCD1,* **(D)** *FOXP3,* **(E)** *IFNG,* and **(F)** *IFNGR1* mRNAs. Red frames indicate the expected amplicon sizes. Data represent mean ± SEM of two independent experiments. Unpaired, two-tailed Student's t test was used for analysis; *$p < 0.05$; **$p < 0.01$; ***$p < 0.001$.

Table S1. List of splicing primers used in this study

Gene	Forward Primer (5'-3')	Reverse Primer (5'-3')
ACTB (Control)	GTTGTCGACGACGAGCG	GCACAGAGCCTCGCCTT
CD45	ATGCAGTTTCTTAGGGACACG	CCAGAAGGGCTCAGAGTGGT
FOXP3	GCCCAACCCCAGGCCTGGCAAGC	ATTTGGGAAGGTGCAGAGCAGT
IFNG	CTCTTGGCTGTTACTGCCAGG	TTCAAATATTGCAGGCAGGACAACC
IFNGR1	CCTTGTCATGCAGGGTGTGA	CCGCTATCATCCACAAGTAGAT
PCMT1	CTGTACCTGCTCCGAGTGTG	CCACCTGGACCACTGCTT
PDCD1	CCTGAGCAGTGGAGAAGG	TCTTCTCTCGCCACTGGAAA

Table S2. List of 3'UTR primers used in this study

Gene	Forward Primer (5'-3')	Reverse Primer (5'-3')
ACTB (Control)	GTTGTCGACGACGAGCG	GCACAGAGCCTCGCCTT
FOXP3	GCTGGAGTTCCGCAAGAAAC	TTTATTGGGGACGGTACTGTGGG
IFNG	GGAGTCAGATGCTGTTTCGAGGTC	TTTGGGTACAGTCACAGTTGT
IFNGR1	ATCTACTTGTGGATGATAGCGG	ATGCTATACCAAGGCAGAGAA
PCMT1	AAGCAGTGGTCCAGGTGG	GCTGAGTGTTTACAGGAC
PDCD1	TTTCCAGTGGCGAGAGAAGA	TTGTCCCAGCCACTCAGGTG